



**BRNO UNIVERSITY OF TECHNOLOGY**

VYSOKÉ UČENÍ TECHNICKÉ V BRNĚ

**FACULTY OF MECHANICAL ENGINEERING**

FAKULTA STROJNÍHO INŽENÝRSTVÍ

**INSTITUTE OF AEROSPACE ENGINEERING**

LETECKÝ ÚSTAV

**NUMERICAL STUDY OF PULSATING JET AT  
MODERATELY SMALL REYNOLDS NUMBERS**

NUMERICKÁ STUDIE PULZAČNÍ TRYSKY PŘI NÍZKÝCH REYNOLDSOVÝCH ČÍSLECH

**MASTER'S THESIS**

DIPLOMOVÁ PRÁCE

**AUTHOR**

AUTOR PRÁCE

**Bc. JIŘÍ DOLINSKÝ**

**SUPERVISOR**

VEDOUCÍ PRÁCE

**Ing. ROBERT POPELA, PhD.**

**BRNO 2019**

## Summary

This numerical study is focused on axisymmetric pulsatile jets of moderately small Reynolds numbers and their physics which has not been fully understood so far. The main goal of the thesis is to investigate and assess the effect of introducing time-harmonic velocity component onto the steady velocity component. At first, the steady case was resolved and verified, afterwards the pulsation was introduced and the unsteady solution was carried out. The numerical solution for steady axisymmetric jet has been verified based on asymptotic solution obtained by Hermann Schlichting [44]. Moreover, an original Schlichting's solution was corrected according to an experimental observation obtained by Andrade and Tsien [1], which reduces solution singularity in the near-nozzle area. This correction was proven to be a first-order correction of the original asymptotic solution from a mathematical standpoint by Revuelta et al [36]. The analytical solution was developed in MATLAB while for the numerical simulation, the Ansys Fluent was used and the time-accurate integration of the Navier-Stokes equations based on pressure-correction approach was employed in order to solve the problem. The pulsatile jet was calculated for a set of different parameters in order to assess their impact on the jet evolution. Finally, the possible application in the industry with regards to elimination of pollutants emerging during the combustion process was discussed.

## Abstrakt

Tato numerická studie je zaměřená na axisymetrickou pulzní trysku při zachování relativně nízkých Reynoldsových čísel a její fyzikální podstatu, která dosud nebyla zcela vysvětlena. Hlavním cílem práce bylo prozkoumat a zhodnotit vliv přidání periodického komponentu rychlosti ke stacionární složce rychlosti. Nejdříve byl řešen stacionární případ, poté byla do simulace přidána pulzace a byla vytvořena nestacionární simulace. Numerické řešení stacionárního případu bylo ověřeno pomocí asymptotického řešení, které předložil Hermann Schlichting [44]. Přesnost tohoto analytické řešení byla opravena na základě experimentálních poznatků Andradeho a Tsiena [1]. Pomocí této korekce je zmenšena oblast singularity řešení v blízkosti počátku proudění. Z matematického pohledu se v podstatě jedná korekcí prvního řádu, což bylo dokázáno Revuelťou a spol [36]. Samotné analytické řešení bylo vytvořeno v MATLABu zatímco pro numerické řešení byl použit software Ansys Fluent. Při numerické simulaci byly Navier-Stokesovi rovnice integrovány ve své plné formě za pomoci algoritmu založeném na tzv. rovnici korekce tlaku. Pulzní tryska byla poté řešena pro různé parametry tak, aby bylo možné zhodnotit vliv jednotlivých parametrů na evoluci takto modulovaného proudu. Nakonec byla posouzena možná aplikace pulzních trysek v průmyslu s ohledem na možnost snížení emisí v průběhu spalovacího procesu.

---

## Keywords

Boundary-free shear flows, jets, wakes, mixing layers, Bickley jet, Schlichting jet, Pulsatile jet, Asymptotic solution, CFD, Direct Numerical Simulation.

## Klíčová slova

Proudění ve volném prostoru, trysky, úplavy, Bickleyho tryska, Schlichtingova tryska, pulzní tryska, asymptotické řešení, CFD, přímá numerická simulace.

DOLINSKÝ, J. *Numerical Study Of Pulsating Jet At Moderately Small Reynolds Numbers*. Brno: Vysoké učení technické v Brně, Faculty of Mechanical Engineering, 2019. 98 s. Vedoucí diplomové práce Ing. Robert Popela, Ph.D..



I hereby declare that I am the sole author of this master's thesis and that I have not used any sources other than those listed in the bibliography and identified as references. I further declare that I have not submitted this thesis at any other institution in order to obtain a degree.

Bc. Jiří Dolinský



I would like to thank my supervisor Dr. Mario Sánchez-Sanz from Fluid Mechanics Research Group of Charles III University of Madrid for his patience and help, my official supervisor Dr. Robert Popela from Institute of Aerospace of Brno University of Technology for allowing me to write my master's thesis at the foreign university and for his valuable comments on the thesis itself, my mother for supporting me through out my studies, my father for showing me a beauty of aeronautics and my grandfather for introducing me to the engineering in general. It has become my very way of life.

Bc. Jiří Dolinský

# Contents

<b>1</b>	<b>Introduction</b>	<b>10</b>
<b>2</b>	<b>Boundary-free shear flow</b>	<b>12</b>
2.1	Jets . . . . .	15
2.1.1	Bickley (planar) jet . . . . .	15
2.1.2	Schlichting (round) jet . . . . .	19
2.2	Other free-boundary shear flows . . . . .	19
2.2.1	Wakes . . . . .	20
2.2.2	Mixing layer . . . . .	21
<b>3</b>	<b>Analytical solution of round jet</b>	<b>22</b>
3.1	Schlichting's solution . . . . .	22
3.2	First-order correction - virtual orifice . . . . .	25
3.3	Comparison to Bickley jet . . . . .	26
<b>4</b>	<b>Turbulence in jets</b>	<b>28</b>
4.1	Flow classification . . . . .	28
4.1.1	Irrotational flow . . . . .	29
4.1.2	Vortex flow . . . . .	29
4.1.3	Rotational flow . . . . .	29
4.2	Laminar-Turbulent transition . . . . .	30
4.2.1	Steady planar jet . . . . .	31
4.2.2	Steady axisymmetric jet . . . . .	32
4.2.3	Pulsatile jet . . . . .	33
4.3	Direct Numerical Simulation . . . . .	33
<b>5</b>	<b>Pulsatile axisymmetric jet</b>	<b>35</b>
5.1	Boundary conditions and governing equation . . . . .	35
5.2	Strouhal number . . . . .	36
5.3	Generation of pulsation . . . . .	37
5.4	Effect of pulsation on the jet flow . . . . .	37
<b>6</b>	<b>Application of axisymmetric pulsatile jets</b>	<b>38</b>
6.1	Mixing ratio, entrainment and flame stabilization . . . . .	38
6.2	Pulsejet engine . . . . .	38
6.2.1	Valved Pulsejet . . . . .	39

6.2.2	Valveless Pulsejet . . . . .	40
6.2.3	Pulse Detonation Engine . . . . .	40
<b>7</b>	<b>Numerical method</b>	<b>43</b>
7.1	Domain . . . . .	43
7.2	Initial and boundary conditions . . . . .	44
7.2.1	Inlet . . . . .	45
7.2.2	Axis of symmetry . . . . .	45
7.2.3	Lateral boundary . . . . .	46
7.2.4	Internal cell zones . . . . .	46
7.3	Computational algorithm . . . . .	47
7.4	Pulsation . . . . .	49
7.5	Judging convergence . . . . .	50
<b>8</b>	<b>Validation and verification</b>	<b>52</b>
8.1	Impact of the boundary conditions . . . . .	52
8.2	Impact of domain geometry and discretization . . . . .	54
8.3	Impact of computational algorithm . . . . .	56
8.3.1	Steady . . . . .	57
8.3.2	Unsteady . . . . .	57
8.4	Axisymmetric jet self-similarity . . . . .	59
<b>9</b>	<b>Results of unsteady case</b>	<b>62</b>
9.1	Strouhal number and jet evolution . . . . .	64
9.2	Impact of the fluctuation magnitude . . . . .	66
9.3	Pulsation and the jet entrainment . . . . .	66
<b>10</b>	<b>Conclusion</b>	<b>71</b>
<b>11</b>	<b>Symbols and abbreviations</b>	<b>77</b>
<b>12</b>	<b>List of Figures and Tables</b>	<b>79</b>
	<b>Appendices</b>	<b>82</b>
<b>A</b>	<b>Bickley jet MATLAB code</b>	<b>83</b>
<b>B</b>	<b>Schlichting jet MATLAB code</b>	<b>89</b>
<b>C</b>	<b>Ansys Fluent settings overview</b>	<b>96</b>
<b>D</b>	<b>Axial velocity contours</b>	<b>97</b>

# 1. Introduction

The commercial aviation has evolved into the fastest, safest, and most far-reaching transportation mode. In the recent decade, with arrival of low-cost airlines, the aviation experienced enormous growth that does not seem to end. According to the statistical research conducted in 2015, nearly half of the global population has been using the world airlines to travel. Without a doubt, the world economy benefits greatly from the ability to move people and products all over the globe quickly and safely however the drawbacks of commercial aviation have been recently brought to light as well [13]. In 2016, transportation has produced 28% of total greenhouse gas emissions and so the contribution of the aviation to green house effect cannot be overlooked anymore [50]. As can be seen in Figure 1.1 the concentration of CO<sub>2</sub> has increased in the last 70 years so much that the current levels in the atmosphere are higher than they have been at any time in the past 400,000 years [28] and the CO<sub>2</sub> is just one of the greenhouse gases that are being released to the atmosphere due to our activities. These facts has resulted in concerns about the future of human species and led an increased number of scientists as well as engineers to look for possible ways to mitigate the environmental impact of different industries, including aviation as well.

Many different ways of reducing the environmental impact of the aviation have been investigated. Some of the researches have focused on possibility of employing different kinds of propulsion systems, such as hydrogen engines, electric engines, engines fueled by biomass or even engines using synthetic fuel for which the raw material is carbon dioxide. The last mentioned variant is the most interesting, but the most difficult to achieve and its feasibility has not been confirmed so far. In this case, the aviation could actually provide an incentive for the market to create ways to extract the carbon dioxide from the atmosphere that will be most likely needed anyway, because if the greenhouse gases will not be extracted from the atmosphere then the society will have a hard time meeting the requirements imposed by Paris climate agreement [23, 49]. The main problem of hydrogen is its safety, even though its specific energy is very high hence hydrogen could be a very promising alternative, its volatility and explosiveness keep aerospace engineers from implementing such propulsion systems. The main drawback related to electric engines is very low specific energy of batteries that makes it almost impossible to implement electric engines in big scale commercial aviation. The airplanes would simply be too heavy. On the other hand, probably the most feasible variant for the time being is to look for a possible ways of increasing an efficiency of current technology, especially of the combustion process of current jet engines, in order to decrease a fuel consumption and emissions. In jet engine, the unwanted pollutants which are found in the exhaust gases are created within the combustion chamber. The main pollutants are hydrocarbons, carbon monoxide, carbon dioxide and oxides of nitrogen. All of these can be reduced by cleaner combustion process [40].

One of the simplest ways to enhance combustion properties could be introducing pulsation during the fuel injection. However in order to do so, it is vital to properly understand the behaviour of pulsation jets first, which leads to the topic of this thesis. This thesis is focused on influence of modulating the steady flow by time-harmonic fluctuation.

## 1. Introduction

---

The aim is to simulate an unsteady laminar axisymmetric pulsatile jet of correspondingly low Reynolds number by a Direct Numerical Simulation, thus to provide a time-accurate solution of the problem. The most important property of jets for practical application is their ability to mix with ambient fluid, especially in combustion chambers and ejectors. In recent years, many new techniques to ensure better mixing were introduced. One of them is a use of swirls that improves mixing properties of the jets and contribute to stabilizing the flame. They also reduce the length of the flame as a consequence of the good mixing of the fluid. Even though some literature [24, 25] suggest that the same could be achieved by introducing the pulsation, which improves the entrainment of the ambient fluid in the near-nozzle region compared to the steady jet, thus also improves mixing and decrease the flame length, this has been poorly investigated and never actually used in practice. Also, pulsatile jets are a fundamental source of trust in Pulse Detonation Engines that are currently being investigated by several leading companies doing business in aerospace propulsion systems. These engines could become a cleaner and more efficient propulsion system available for very high velocities as well. For all these reasons, an understanding of pulsatile jet behaviour is nowadays gaining on importance.

In this thesis, particularly the influence of pulsation on the propagation of axisymmetric jet will be investigated. The pulsating jet will be modulated in order to determine the effect on the jet entrainment and its propagation. The dynamics and behaviour of the jet are examined while varying Reynolds number, fluctuation and Strouhal number of the jet.

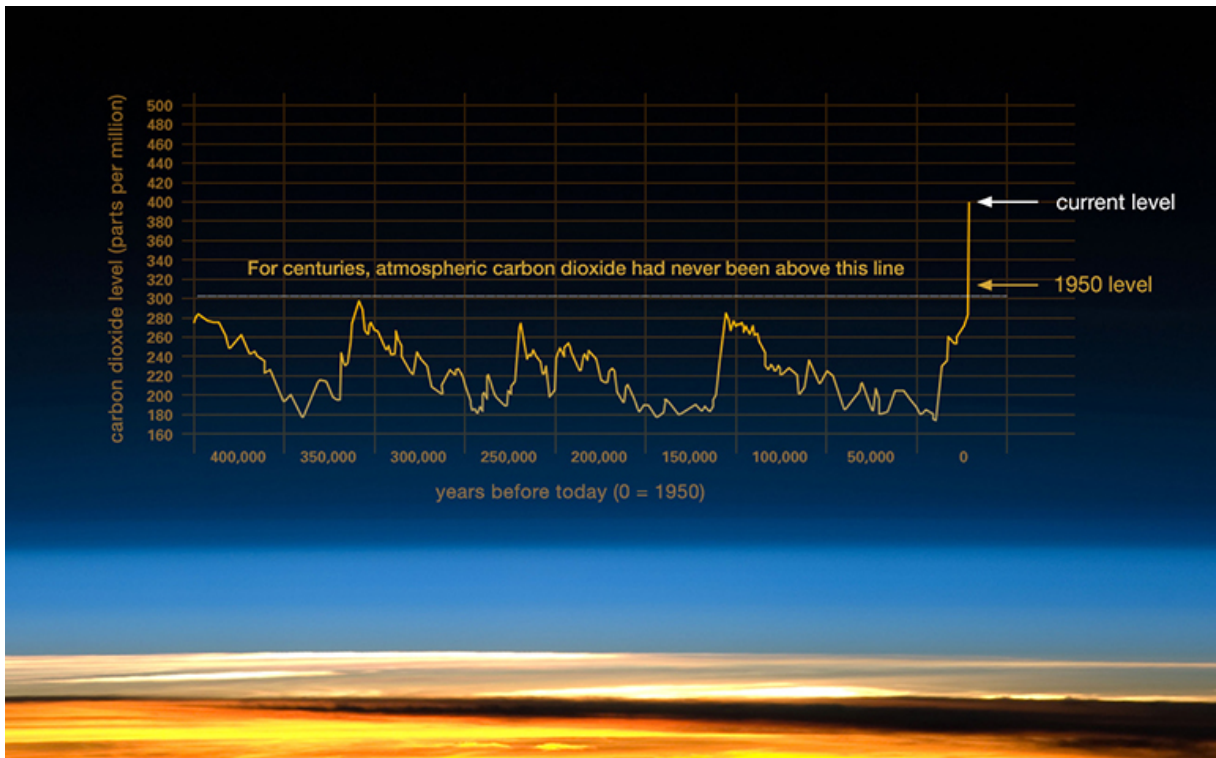


**Figure 1.1:** The rise of carbon dioxide in the atmosphere [28].

## 2. Boundary-free shear flow

In this chapter, different kinds of free shear flows will be defined. In order to introduce this group of flows, the practical examples of the most common boundary-free shear flows are the wakes behind moving bodies, the exhausts from jet engines or the most of combustion and mixing processes. [15].



**Figure 2.1:** Pratt & Whitney F119 thrust-vectoring jet aircraft engine that powers F-22 Raptor fighter aircraft during a operational test and evaluation run up.

As the name implies boundary-free shear flows are flows remote from walls. They are usually evolving which means that the structure of the flow is changing in the flow direction. The change is either due to external influences (pressure or temperature gradients) or due only to evolutionary influences inherent within the turbulence. In consequence of evolutionary character, even if generated as laminar, these flows tend to become turbulent very quickly. Moreover, the transition from laminar into turbulent flow is much faster than in wall-bounded flows. This is caused by the fact that three-dimensional vorticity necessary for the transition to turbulence can develop much more rapidly in the absence of wall which prevents the vortex from growing in the direction perpendicular to the surface [15, 31, 48].

The free shear flows in nature and in engineering environments can be divided into four categories jets, wakes, mixing layer and thermal plumes that can be either two-dimensional

or three-dimensional. In the category of two-dimensional flows, the mean velocity field is confined to planes and two categories are distinguished - planar case and axisymmetric case. In the planar flows, mean flow in planes parallel to given plane is identical while in the axisymmetric flows, that are in fact special instance of three-dimensional case that can be resolved as a two-dimensional problem, the mean flow in planes through the axis of symmetry is identical [31, 48]. The rationale for considering the axisymmetric case to be a two-dimensional problem is the fact that the axisymmetric flow is independent of one of the space coordinate and can be resolved as a two-dimensional problem using a periodic (rotated) grid system with appropriate boundary conditions on the periodic sides of the grid [29, 41, 48]. Therefore, it is much easier to solve the flow propagation of axisymmetric case compared to the general three-dimensional cases of a boundary layer in which the three velocity components depend on all three coordinates hence exhibit enormous mathematical difficulties associated with the problem [44].

Also, since the jets, wakes and mixing layers generally propagate for distances which are large compared to scales on which they are generated, it seems very natural to look for a self-similarity (sometimes also called self-perseverance) of the problems. In fact only self-similar boundary layer flows can be solved analytically. This means that scale symmetry of the problem allows to reduce the number of independent variables to number that can be analytically resolved and does not require iterative approach. This is possible, because the solution is similar to itself if the variables are conveniently scaled. In fluid dynamics, physics of waves as well as in many other fields of physics, many instances of self-similarity can be found. The self-similarity is applied to solutions of boundary layer equation in several cases, including planar as well as axisymmetric jet [12, 16].

In following chapters, the analytical solution of planar and axisymmetric jets will be shown, in both of these cases the self-similarity reside in the fact that velocity profiles are identical when appropriate scale factors are introduced. Consequence of this fact, is a reduction of governing partial differential equations of boundary layer flow to ordinary differential equation form that can be resolved using matched asymptotic expansion<sup>1</sup>. It is also worth noticing that the boundary layer problem was firstly introduced by Ludwig Prandtl at the Third International Congress of Mathematicians in Heidelberg in 1904 when he spoke on fluid motion with small friction. Ludwig Prandtl stated following: "The physical processes in the boundary layer between fluid and solid body can be calculated in a sufficiently satisfactory way if it is assumed that the fluid adheres to the walls, so that the total velocity there is zero or equal to the velocity of the body. If the viscosity is very small and the path of the fluid along the wall is not too long, the velocity will have again its usual value very near to the wall. In the thin transition layer the sharp changes of velocity, in spite of the small viscosity coefficient, produce noticeable effects" [30]. This means that from the mathematical point of view, the boundary layer is actually a singular perturbation problem [26].

There are two cases of singular perturbation, the most apparent one is when the solution of unperturbed case ( $\epsilon = 0$ ) does not exist and the second one when the exact

---

<sup>1</sup> Solution of this problem was originally known as boundary-layer technique [30].

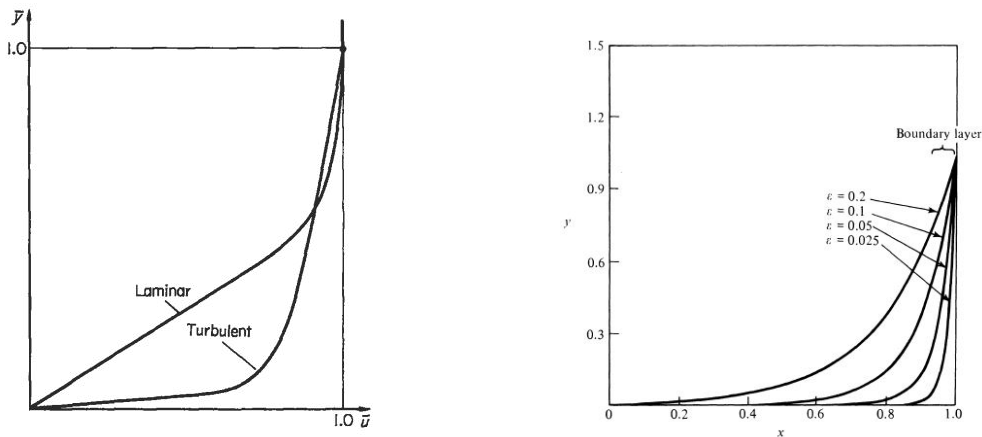
solution for arbitrarily small but nonzero  $\epsilon$  significantly differs from the neighboring solutions obtained in the limit  $\epsilon = 0$ . This will be always the cause in fluids, because of the nature of boundary layers in general. The very small viscosity value causes a significant difference in velocity close to boundaries. Moreover, it can be said that the exact solution for  $\epsilon = 0$  does not exist. The boundary value problem is defined as follows

$$\epsilon y'' - y' = 0, \quad y(0) = 0, \quad y(1) = 1 \quad (2.1)$$

and has to be a singular perturbation, because the associated unperturbed problem ( $\epsilon = 0$ )

$$-y' = 0, \quad y(0) = 0, \quad y(1) = 1, \quad (2.2)$$

does not have a solution - the solution to this first-order differential equation cannot satisfy both boundary conditions  $y(0)$  and  $y(1)$  [5]. In Figure 2.2, two types of boundary layers that exist in fluid mechanics can be seen in comparison to the influence of very small  $\epsilon$  in perturbation theory. The region of rapid variation is called a boundary layer and the resemblance can be seen at first glance, even though in laminar case the picture could be a bit confusing, suggesting that the variance is not so rapid, it actually is. In both cases boundary layer is a singular perturbation problem.



(a) Two types of boundary layers in fluid mechanics [9].

(b) General case of boundary layer problem for different values of  $\epsilon$  [5].

**Figure 2.2:** Perturbation theory and boundary layer problem.

Later this concept along with scaling and similarity theory was further used in fluid mechanics field by many including Prandtl's student Herman Schlichting who gave an analytical solution to axisymmetric jet (1933) [45] and put also the base for analytical solution of the planar jet that was finished by W. G. Bickley (1937) [6].

## 2.1. Jets

The two main kinds of the jet that can be simulated in two-dimensional space are planar jet and axisymmetric jet. Both of them have a analytical solution that was provided in case of planar jet by Bickley [6] and in case of axisymmetric jet by Schlichting. Both of these solutions expect the steady flow emerging into fluid at rest, assuming the motion to be laminar at the orifice [41].

### 2.1.1. Bickley (planar) jet

In Bickley's solution, the steady two-dimensional laminar motion of an incompressible viscous fluid issues from a long narrow orifice, which ensures only two-dimensional motion, into quiescent atmosphere. The analytical solution for this specific case that is applicable only at sufficient distance downstream from the orifice is quite straightforward. However, it shall be mentioned that this solution cannot be used in close distance to the orifice. The reason for this is the fact that the condition  $x = 0$  is a line of a singularity. Occurrence of such a line is a common feature of the solutions of the boundary layer equations [6].

The Reynolds number of Bickley jet can be calculated as

$$Re = \frac{U_j h}{\nu} \quad (2.3)$$

where  $h$  is a nozzle height,  $U_j$  is the inlet velocity and  $\nu$  is a kinematic viscosity.

In order to produce planar jet experimentally, it is necessary to ensure that the height of the orifice is significantly bigger than its width.

For the solution, the coordinates  $x$  and  $y$  are used in the plane of motion, the  $x$ -axis is in the plane of symmetry of the jet. The longitudinal velocity is denoted as  $u$  while the transverse velocity is denoted as  $v$ . It is assumed that the Prandtl boundary layer equations give a sufficiently good approximation, and that the pressure is independent of  $x$  as well as of  $y$ . Therefore the boundary layer equation of momentum can be written as

$$u \frac{\partial u}{\partial x} + v \frac{\partial u}{\partial y} = \nu \frac{\partial^2 u}{\partial y^2} \quad (2.4)$$

$$\frac{\partial u}{\partial x} + \frac{\partial v}{\partial y} = 0 \quad (2.5)$$

The boundary conditions in this case are

$$\left. \begin{array}{l} v = 0, \quad \frac{\partial u}{\partial y} = 0 \quad \text{at} \quad y = 0, \quad x > 0 \\ u \rightarrow 0 \quad \text{as} \quad y \rightarrow \infty \end{array} \right\}$$

The first boundary condition comes from the fact that the motion is symmetrical about x-axis.

Since the pressure is constant and no solid boundary is present, the total x-component of the fluid momentum must also be constant, thus

$$M = 2\rho \int_{-\infty}^{+\infty} u^2 dy = \text{constant} \quad (2.6)$$

which can be for the plug flow<sup>2</sup> integrated as follows

$$M = 2\rho u^2 \int_{-a}^{+a} dy = 2\rho u^2 [a - (-a)] = 4\rho u^2 a \quad (2.7)$$

where  $a = d/2$  and  $d$  denotes the nozzle diameter.

The solution of the equation 2.4 can be determined by writing

$$\psi = 6\nu x^{1/3} F(\eta), \quad (2.8)$$

$$\eta = yx^{-2/3}, \quad (2.9)$$

$$u = 6\nu x^{1/3} F'(\eta), \quad (2.10)$$

$$v = 2\nu x^{-2/3} (2\nu F' - F), \quad (2.11)$$

where  $\psi$  is a stream function,  $\eta$  is similarity variable,  $u$  is longitudinal velocity and  $v$  is transverse velocity. Employing terms 2.8, 2.9, 2.10, 2.11 reduces the equation 2.4 to

$$F''' + 2FF'' + 2F'^2 = 0. \quad (2.12)$$

Now the solution of equation 2.4 is obtained, by introducing the boundary conditions, in the following form

$$F(\eta) = \alpha \tanh(\alpha\eta), \quad (2.13)$$

where  $\alpha$  is an integration constant given by

$$M = 72\nu^2 \alpha^3 \int_{-\infty}^{+\infty} \text{sech}^4 \xi d\xi = 48\nu^2 \rho \alpha^3. \quad (2.14)$$

---

<sup>2</sup> The velocity of the fluid is assumed to be constant across the cross-section, perpendicular to the longitudinal axis.

## 2. Boundary-free shear flow

---

The final formulae for stream function, velocity in longitudinal direction and velocity in transverse direction can be defined as

$$\psi = 3 \left( \frac{M\nu x}{6\rho} \right)^{1/3} \tanh\xi, \quad (2.15)$$

$$u = \frac{1}{4} \left( \frac{6M^2}{\nu\rho^2 x} \right)^{1/3} \operatorname{sech}^2\xi, \quad (2.16)$$

$$v = \left( \frac{M\nu}{6\rho x^2} \right)^{1/3} (2\xi \operatorname{sech}^2\xi - \tanh\xi), \quad (2.17)$$

where similarity variable  $\xi$  can be determined as

$$\xi = \alpha\eta = \frac{1}{2} \left( \frac{M}{6\nu^2\rho x^2} \right)^{1/3} y. \quad (2.18)$$

The mass flow rate across a plane at a distance  $x$  from the orifice normal to the jet can be obtained as follows

$$\dot{m} = 2\rho \int_0^{+\infty} u \, dy = (36M\nu\rho^2 x)^{1/3}. \quad (2.19)$$

In this thesis, the mass flow rate is designated as  $\dot{m}$ , even though Bickley in his original paper designates mass flow as  $Q$  [6]. This is done in order to avoid any confusion since the  $Q$  is nowadays used for designating volume flow rate. The volume flow rate then can be readily obtained as follows

$$\dot{m} = \rho \cdot v \cdot A \quad (2.20)$$

where  $A$  is area of the inlet. The volume flow rate is defined as

$$Q = \dot{V} = v \cdot A, \quad (2.21)$$

where  $v$  is velocity of the fluid and in this case  $u = v$ ,  $A$  is again area of the inlet, thus the volume flow rate can be determined from equation 2.19 as follows

$$\frac{\dot{m}}{\rho} = Q = u \cdot A = 2 \int_0^{+\infty} u \, dy. \quad (2.22)$$

Also from the equation 2.19, the initial singularity at the orifice can be seen. For  $x = 0$ , the mass flow across a plane is equal to zero, which is obviously not true. The

actual flow from the jet orifice cannot be found by using this solution, which only involves the momentum flux  $M$  produced by the jet [6, 41].

Alternatively, the longitudinal velocity of the planar jet at a certain distance downstream  $x$  can be determined also according following formula

$$u = \frac{U}{\cosh^2(y/\delta_0)}, \quad (2.23)$$

where  $U(x)$  is the velocity at the center of the jet, and  $\delta_0$  is a characteristic width. Interestingly the same expression holds approximately for a turbulent plane jet as well. This observation has been well verified experimentally [22].

The progress of plane jet is accompanied by progressively increasing mass of fluid, which results in a decrease of velocity so that the total momentum of the moving fluid remains constant [6]. This is schematically shown in Figure 2.3.

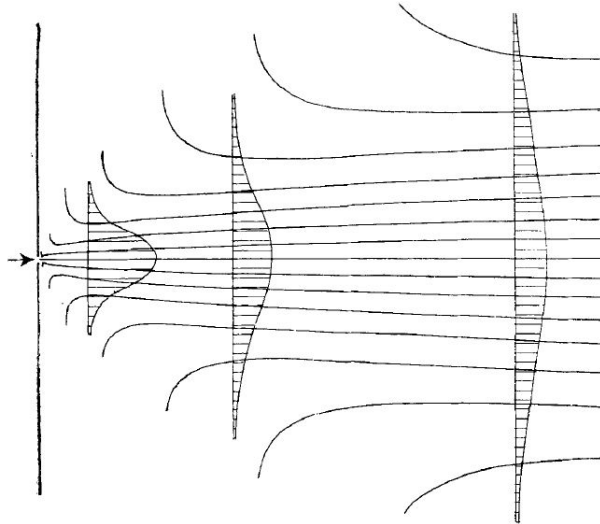


**Figure 2.3:** Stream-lines and velocity profile of the laminar plane jet [6].

Finally, it should be mentioned that two-dimensional planar jets are not very often found in the nature or engineering practice. Planar jets are very commonly used for research since they can be solved in two-dimensional space and does not require so extensive computational power. However, also in planar cases, it has been observed that there are numerous three-dimensional instabilities associated with the transition of plane jets into developed turbulence. The experiments has showed the formation of longitudinal hairpins, but these are usually being neglected in the simulations [22].

### 2.1.2. Schlichting (round) jet

Much more common in nature and engineering practice are so called round jets. The round jets are axisymmetric jets issuing from a circular hole into quiescent or moving atmosphere. The analytical solution to these jets was given, as previously mentioned, by Herman Schlichting and will be described in chapter 3.

In most practical cases the round jet is turbulent, especially turbulent round jets issuing into environment through a circular nozzle are very common and widely used in engineering applications such as combustion, propulsion and reaction flows etc. Although many works had been done focusing on this fundamental turbulence flow patterns by means of experiment, theory analysis and numerical simulation, there are still some unclear points such as micro-scale turbulence behaviors, high order turbulence statistics etc. needing further investigation [44, 51].



**Figure 2.4:** Exhaust of rocket engine [15].

The flows with rotational symmetry provide simplified examples of three-dimensional flow, because, as mentioned before, they are independent of one of the space coordinates [41].

## 2.2. Other free-boundary shear flows

Let us also briefly describe the other free shear flows that can be commonly seen in the nature - the wakes and mixing layer. Especially mixing layer plays a fundamental role in jets as well, especially in their laminar-turbulent transition.

### 2.2.1. Wakes

Even though the wakes can at first glance look pretty similar to the jets they are not. The main difference between the jets and the wakes lie in whether momentum is being added to the flow at the source as in jets or taken out by drag as in wakes [15]. The wakes can be very often observed behind the bodies passing through the fluid, such as airplanes or cars and they are used, in engineering field, for calculating drag of the body.

At the trailing edge of a body immersed in a fluid flow, there will exist the boundary layers from the surfaces on both sides. These boundary layers will merge and move downstream in the form of a wake of reduced velocity. The mean velocity will decrease with distance downstream and the wake cross-section will increase relatively. At sufficient distance downstream, the streamlines will all be parallel and the static pressure across the wake will be equal to the free stream value. By comparing conditions at this state with those in the undisturbed stream ahead of the body, the drag force on the body can be calculated from the rate at which the momentum was lost. [9]

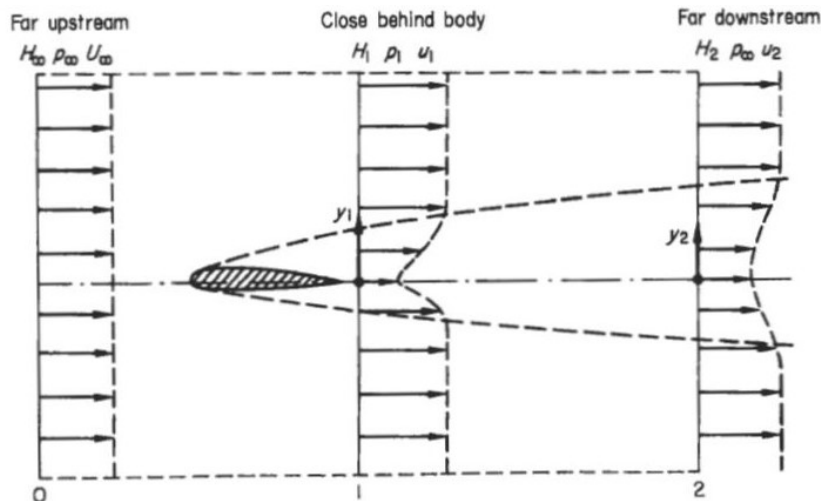


**Figure 2.5:** Wake behind the airfoil [9].

Wakes can be also divided into two groups, the plane and axisymmetric wakes according to the way they were initialized. A plane wake is formed when a uniform stream (of velocity  $U$ , in the  $x$  direction) flows over a cylinder that is aligned with the  $z$  axis. The flow is statistically stationary, two-dimensional, and symmetric about the plane  $y = 0$ . An axisymmetric wake forms behind a round object - a sphere, spheroid, or disk, for example - held in a uniform stream, flowing with velocity  $U$ , in the  $x$  direction. The flow is statistically axisymmetric, with statistics depending on two axis direction, but being independent of third [31].

The velocity profile of the plane turbulent wake is shown in Figure 2.6. It can be seen that the velocity profile is similar to the velocity profile of the jet, only the parabola is overturned.

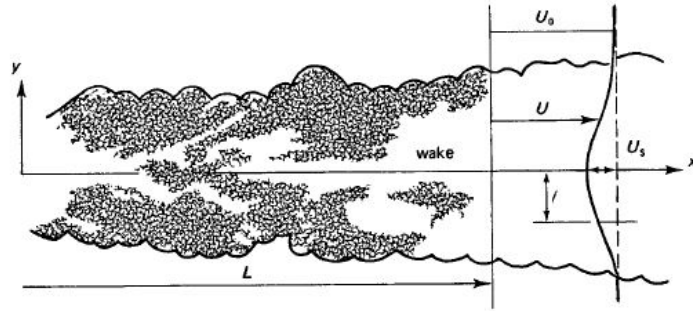


**Figure 2.6:** Plane turbulent wake [48].

### 2.2.2. Mixing layer

The mixing layer is the turbulent flow where the two uniform, nearly parallel streams of different velocities of the same sign mixes together. The resulting velocity profile of such flow is shown in Figure 2.7. Alternatively the flow can be created in a wind tunnel, with a splitter plate separating the two streams at initial stage. When the flows merge, the mixing layer develops [22, 31].

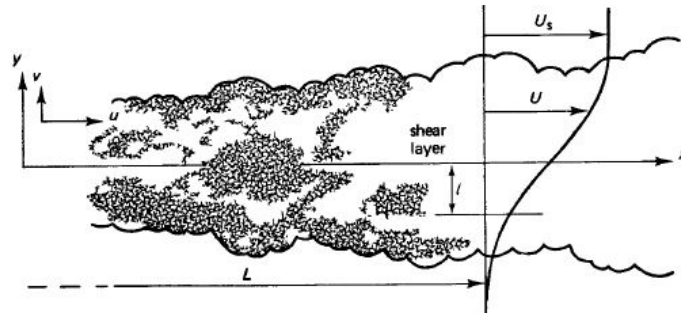


**Figure 2.7:** Plane turbulent mixing layer [48].

The mixing layers are very important in process of laminar-turbulent transition of the jets as well as in many mixing processes.

### 3. Analytical solution of round jet

In this chapter, solution of axisymmetric (Schlichting) jet that issues from a small circular opening and mixes with the surrounding fluid of the same kind is given. A sketch of typical origin of round jet is shown in Figure 3.1. As described in section 2.1.2, this is in fact three-dimensional case that can be resolved in two-dimensional space.

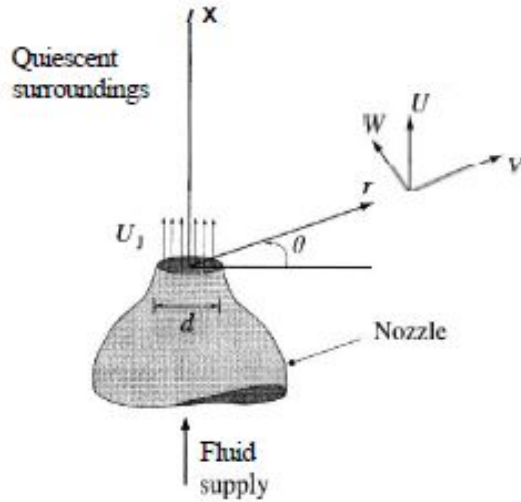


**Figure 3.1:** A sketch of a axisymmetric jet with polar-cylindrical coordinate system [31]

In the ideal case, the flow is completely defined by  $U_j$ ,  $d$ , and  $\nu$ , and hence the only non-dimensional parameter is the Reynolds number, defined as follow

$$Re = \frac{U_j \cdot d}{\nu}, \tag{3.1}$$

where  $d$  is a nozzle diameter,  $U_j$  is the inlet velocity and  $\nu$  is a kinematic viscosity.

#### 3.1. Schlichting's solution

The solution of the laminar round jet is analogous to the one for a two-dimensional jet given in section 2.1.1. The momentum of the jet is defined as

$$M = 2\pi\rho \int_0^a u^2 y \, dy, \tag{3.2}$$

that can be again readily integrated for the plug flow as follows

### 3. Analytical solution of round jet

---

$$M = 2\pi\rho u^2 \int_0^a dy = 2\pi\rho u^2 \left[ \frac{y^2}{2} \right]_0^a = 2\pi\rho u^2 \left[ \frac{a^2}{2} - 0 \right] = \pi\rho u^2 a^2, \quad (3.3)$$

and the boundary-layer equation is given as follows

$$u \frac{\partial u}{\partial x} + v \frac{\partial u}{\partial y} = \nu \frac{\partial}{\partial y} \left( y \frac{\partial u}{\partial y} \right). \quad (3.4)$$

It is obvious that the boundary conditions must be also analogues to the boundary conditions of planar case

$$\left. \begin{array}{l} v = 0, \frac{\partial u}{\partial y} = 0 \quad \text{at} \quad y = 0, \quad x > 0 \\ u \rightarrow 0 \quad \text{as} \quad y \rightarrow \infty \end{array} \right\}$$

This problem can be resolved again by means of stream function and similarity variable that in case of axisymmetric jet were determined as follows

$$\psi = \nu x F(\eta), \quad (3.5)$$

$$\eta = \frac{y}{x}. \quad (3.6)$$

Now the velocity components are determined as

$$u = \frac{\nu F'}{x \eta}, \quad (3.7)$$

$$v = \frac{\nu}{x} \left( F' - \frac{F}{\eta} \right). \quad (3.8)$$

By inserting these terms into equation 3.4, the equation for stream function can be written in following form

$$\frac{FF'}{\eta^2} - \frac{F'^2}{\eta} - \frac{FF''}{\eta} = \frac{d}{d\eta} \left( F'' - \frac{F'}{\eta} \right). \quad (3.9)$$

By integrating the equation 3.9, following differential equation is obtained

$$FF' = F' - \eta F''. \quad (3.10)$$

Now, by employing boundary conditions we obtain a differential equation

$$F \frac{dF}{d\xi} = \frac{dF}{d\xi} - \xi \frac{d^2 F}{d\xi^2}, \quad (3.11)$$

which solution is given as

$$F = \frac{\xi^2}{1 + \frac{1}{4}\xi^2}. \quad (3.12)$$

By introducing this solution to equations 3.7 and 3.8, following terms are obtained

$$u = \frac{\nu}{x} \frac{2\gamma^2}{\left(1 + \frac{1}{4}\xi^2\right)^2}, \quad (3.13)$$

$$v = \frac{\nu}{x} \gamma \frac{\xi - \frac{1}{4}\xi^2}{\left(1 + \frac{1}{4}\xi^2\right)^2}, \quad (3.14)$$

where similarity variable is defined as  $\xi = \gamma \frac{y}{x}$  and  $\gamma$  is the constant of integration which can be obtained from momentum equation

$$M = 2\pi\rho \int_0^\infty u^2 y dy = \frac{16}{3} \pi \rho \gamma^2 \nu^2. \quad (3.15)$$

So finally the formulae for longitudinal velocity, transverse velocity and similarity variable  $\xi$  are

$$u = \frac{3}{8\pi} \frac{M/\rho}{\nu x} \frac{1}{\left(1 + \frac{1}{4}\xi^2\right)^2}, \quad (3.16)$$

$$v = \frac{1}{4} \sqrt{\frac{3}{\pi}} \frac{\sqrt{M/\rho}}{x} \frac{\xi - \frac{1}{4}\xi^2}{\left(1 + \frac{1}{4}\xi^2\right)^2}, \quad (3.17)$$

$$\xi = \sqrt{\frac{3}{16\pi}} \frac{\sqrt{M/\rho}}{\nu} \frac{y}{x}. \quad (3.18)$$

Just for the clarity and convenience, Schlichting in his original solution [44, 45] calls the ratio of momentum and density a kinematic momentum and denotes it as  $K$ . Since, in

### 3. Analytical solution of round jet

---

the chapter 2.1.1, kinematic momentum  $K$  was not used in solution of planar jet, it is not used here either for the sake of unity.

Finally the volume flow rate can be calculated as

$$Q = 8\pi\nu x. \quad (3.19)$$

The singularity of the solution can be seen again when calculating the volume flow rate that will, using this analytical solution, equal to zero at the orifice. In reality, this is obviously not true.

The streamline pattern for a circular laminar jet is shown in Figure 3.2.

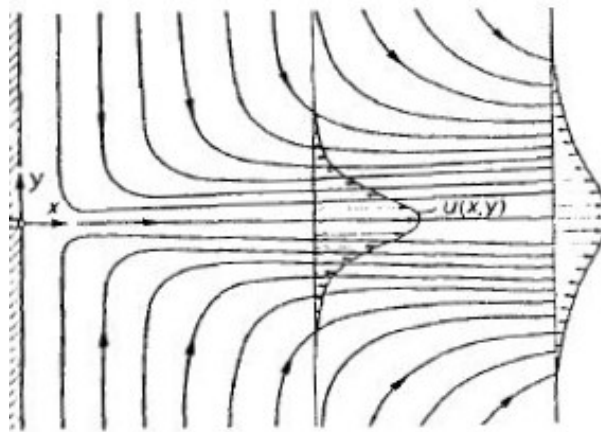


**Figure 3.2:** Streamline pattern for a circular laminar jet [44].

## 3.2. First-order correction - virtual orifice

The Schlichting solution is based on simplifying assumption that the jet issues from a point. The consequence of this assumption is that the solution exhibit a singularity at the orifice, hence the results close to the orifice are corrupted. Even though, the jet far from the orifice is described very accurately, the solution does not give any valuable results near the jet orifice. By introducing the virtual orifice, this singular behavior of the self-similar solution close to the jet origin can be remedied.[1, 36].

Virtual origin coordinate can be determined according to [1]. For the parabolic velocity profile  $x_0$  is

$$x_0^p = \frac{1}{5\pi\nu} Q \quad (3.20)$$

and for the rectangular profile

$$x_0^r = \frac{9}{40\pi\nu}Q. \quad (3.21)$$

By simple division of equation 3.20 and 3.21

$$\frac{x_0^p}{x_0^r} = \frac{\frac{1}{5\pi\nu}Q}{\frac{9}{40\pi\nu}Q} = 8 \quad (3.22)$$

$$x_0^p = 8 \cdot x_0^r \quad (3.23)$$

It can be determined that for similar volume flow rate, the value of  $x_0$  for parabolic profile is 8 times lower than for rectangular.

Now, by employing the virtual origin into the equation 3.16, 3.17 and 3.18, the final form of the corrected velocities is obtained

$$u = \frac{3}{8\pi} \frac{M/\rho}{\nu(x+x_0)} \frac{1}{\left(1 + \frac{1}{4}\xi^2\right)^2} \quad (3.24)$$

$$v = \frac{1}{4} \sqrt{\frac{3}{\pi}} \frac{\sqrt{M/\rho}}{(x+x_0)} \frac{\xi - \frac{1}{4}\xi^3}{\left(1 + \frac{1}{4}\xi^2\right)^2} \quad (3.25)$$

$$\xi = \sqrt{\frac{3}{16\pi}} \frac{\sqrt{M/\rho}}{\nu} \frac{y}{(x+x_0)} \quad (3.26)$$

$$Q = 8\pi\nu(x+x_0) \quad (3.27)$$

This solution was based on experiments, but was lately verified to be a first-order correction of the Schlichting solution [1, 36].

### 3.3. Comparison to Bickley jet

In Figure 3.3, the comparison of decay rate of Bickley and Schlichting jet can be seen. In case of Bickley jet  $d$  designates height of the orifice, for Schlichting jet it is a nozzle diameter.

The comparison was made for an air issuing from the orifice to the quiescent atmosphere of exactly the same fluid. In both cases with initial speed 1 m/s. The propagation

### 3. Analytical solution of round jet

---

of the jets was solved by analytical solution described earlier and the first-order correction was not introduced into the calculation, so the singularity close to the jet orifice is very obvious. In the graph, the velocity at the center of the jet is plotted so the  $y = 0$  and the  $x \rightarrow \infty$ . It can be very clearly seen that the round jet decays much faster than planar jet, thus application of axisymmetric jet is much more appropriate when the quick decay of the jet is required. The decay of both jets based on asymptotic solutions can be seen in Figure 3.3.

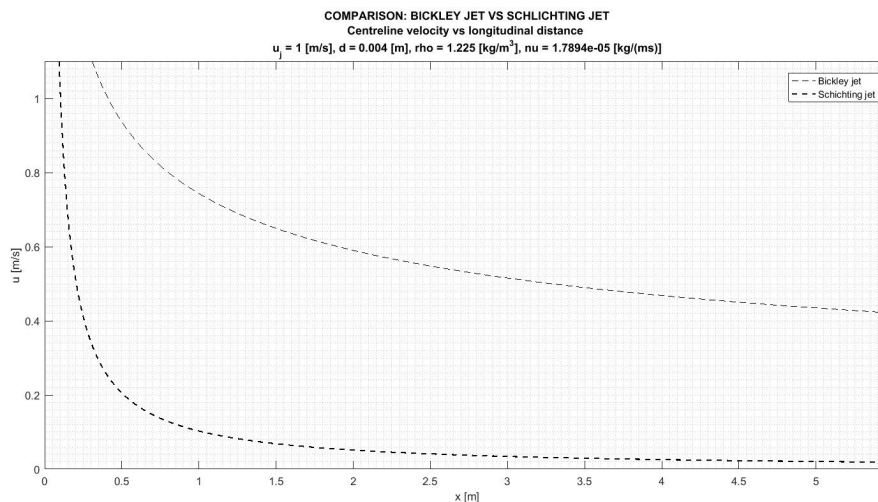


**Figure 3.3:** Comparison of decay speed of Schlichting jet and Bickley jet issuing from the orifice with similar characteristic dimension.

## 4. Turbulence in jets

”When I meet God, I am going to ask him two questions: Why relativity? And why turbulence? I really believe he will have an answer for the first.”

Werner Heisenberg [10]

As was mentioned before, the laminar free flows tend to transform into turbulent flows much more rapidly compared to wall-bounded flows. This is caused by the absence of the wall that restricts three-dimensional vorticity necessary for the transition from developing in the direction perpendicular to the surface [15]. Turbulence can only develop in rotational flow [22], so the flow classification has to be introduced. A characteristic sign of a turbulent flow is the strongly increased diffusion, three-dimensionality and unsteadiness [47].

Fluid motion can be described using the mean-velocity that is for-simplicity defined considering a homogeneous fluid parcel consisting of a large collection of identical molecules. The vector form of mean-velocity is then defined as follows

$$\bar{\mathbf{v}} = \frac{1}{N} \sum_{i=1}^N \mathbf{v}^{(i)}, \quad (4.1)$$

where  $N$  stands for number of molecules and  $i$  is an integer index,  $i = 1, \dots, N$ .

As the size of the fluid parcel becomes decreasingly small, the parcel tends to occupy an infinitesimal volume in space containing the point  $\mathbf{x}$ . In this limit, the components of the parcel velocity defined in equation 4.1 can be reduced to following form

$$u = (u_x, u_y, u_z). \quad (4.2)$$

The fluid parcels and their motion plays a fundamental role in classifying flows [34].

### 4.1. Flow classification

The flows can be divided into three categories based on kinematic properties of the flow, irrotational, vortex and rotational flows. Whether the flow is irrotational, vortex or rotational can be in a simplified way decided based on vorticity distribution in the flow and more specifically on the behaviour of small spherical fluid parcels in case of three-dimensional flow and discoidal fluid parcels in case of two-dimensional flow [34].

### 4.1.1. Irrotational flow

The first category that is also computationally the simplest is an irrotational flow. It is a flow in which the vorticity vector vanishes, and the magnitude of the vorticity is zero throughout the domain of flow. The spherical parcels in a three-dimensional irrotational flow and discoidal fluid parcels in a two-dimensional irrotational flow translate, deform, expand or contract, but do not rotate. Expansion, rotation and deformation of discoidal parcel is shown in Figure 4.1 [34].

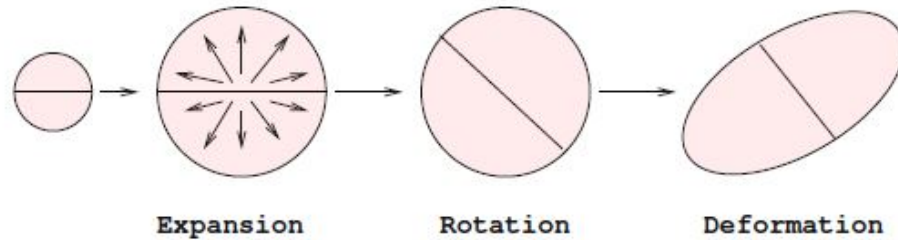


**Figure 4.1:** Expansion, rotation and deformation of small discoidal fluid parcel that occurs during infinitesimal period of time in a two-dimensional flow [34].

### 4.1.2. Vortex flow

Vortex flows contain well-defined compact regions where the magnitude of the vorticity is significant, embedded in an otherwise irrotational fluid. In practice, regions of intense vorticity appear in the form of narrow layers, thin filaments, wakes behind bluff bodies, tornadoes and swirls. When it comes to aeronautics, typical vortex flow is the flow associated with a high-speed jet emerging from a turbine engine [34].

### 4.1.3. Rotational flow

The last category includes the flow where the vorticity is significant throughout the domain of flow. The difference between vortex and rotational flows is sometimes hard to define however the simplest way is to look at the problem from computational point of view. In case of vortex flows, the vortex numerical methods can be employed in order to resolve flow motion. This is not possible in pure rotational flows, thus the availability of these methods provide a practical criterion of the distinction between vortex and rotational flow [34].

## 4.2. Laminar-Turbulent transition

In general, it is widely accepted that the transition to turbulent flow depends on the Reynolds number. This definitely holds true in case of simple circular Hagen-Poiseuille flow<sup>1</sup>, where the critical Reynolds number is approximately 2300. Below this number all small disturbances in the flow just die away and the laminar flow motion is seen. Above this value the flow inside the tube become turbulent. Of course, the transition to the turbulent flow does not only occur in pipe flows but in all laminar flows, particularly laminar boundary layers. Here it is important to mention that the analytical solution of Navier-Stokes equation given in the chapters 2 and 3 hold in principle only for arbitrarily large Reynolds number. For these solution, not only Navier-Stokes equations has to be satisfied, but the flows must also be stable with respect to small disturbances and this is not the case above the critical Reynolds number, where even an exceedingly small disturbance is enough to induce the transition to the turbulent flow [22, 47]. Above the critical number, different approaches to determine the flow propagation has to be employed and of course, the difficulty of computing the structure or evolution of a flow increases sharply as the flow transition from irrotational, to vortex, to rotational and to turbulent [34].

It has been also observed that there are two critical Reynolds numbers. The first one is the Reynolds number at which the flow becomes unstable for the first time, but this does not meant the flow will become turbulent. The Reynolds number when the flow becomes turbulent is in general different from the one at which the first instabilities occurs. Very commonly are both of these numbers called critical, but the difference between them is vital. In general a new, more complicated but still laminar flow evolves as the Reynolds number increase. As a great example of the laminar flow with large difference between mentioned two Reynolds numbers is the flow between two rotating cylinders. In this case the Reynolds number of transition to turbulence is approximately 50 time greater than the Reynolds number at which stability is lost [47]. Also for free jets, these two Reynolds numbers differ significantly. Transition behavior of jets is more described in following sections.

The transition itself has until now only been accessible by direct numerical simulation (DNS) and it is in fact questionable whether the results of DNS or experiments are more valid. The experimental investigation is very difficult, because the flow is particularly sensitive to unavoidable and often unknown disturbing influences which can still decisively change the transition behaviour [47]. For example, this thesis has been written at the department of thermal and fluids engineering of Charles III University of Madrid at the time when there were experiments conducted on this topic. One of the problem that researchers encountered while trying to investigate the laminar jet was the fact that there were trains passing several hundreds meters away from the laboratory. Vibration caused by these trains had an influence on the jet behaviour. These observations led some of the researchers to conclusion that the direct numerical simulation might, in fact, give

---

<sup>1</sup> Flow in a circular tube.

much more accurate results from the physical point of view, because the calculation is not exposed to any external influence and the researcher has a control over all the aspects of the experiment.

### 4.2.1. Steady planar jet

The steady planar jets tend to transition to turbulent flow quite quickly. This is caused by the fact that they are very prone to instabilities, significantly more than the axisymmetric jet. This is the reason why plane jets in the nature are very often turbulent, the turbulent flow developed from the plane jet, laminar at the orifice, with characteristic velocity profile is shown in Figure 4.2. The Bickley's analytical solution given in chapter 2.

The solution given in chapter 2 cannot be applied to purely turbulent flow however it can be applied to some extent to very light turbulent gas jets [43].

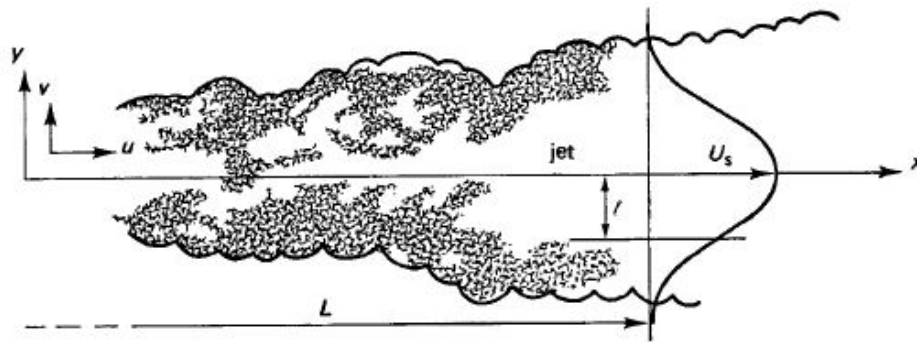


**Figure 4.2:** Plane turbulent jet [48] and its velocity profile that has the same shape as the laminar case.

The jet evolves and spreads downstream by entraining mass from the surroundings which are at most in irrotational motion induced by the vortical fluid within the jet. However, the momentum remains constant to the flow downstream of the source, and it is this fact that distinguishes the jet from all other flows. In its initial stage of development of the turbulent jet, the plane jet consists of two plane mixing layers, separated by a core of irrotational flow. After the two mixing layers have merged, the jet becomes a fully developed, self-preserving turbulent flow [15, 48]. This process is shown in Figure 4.3.

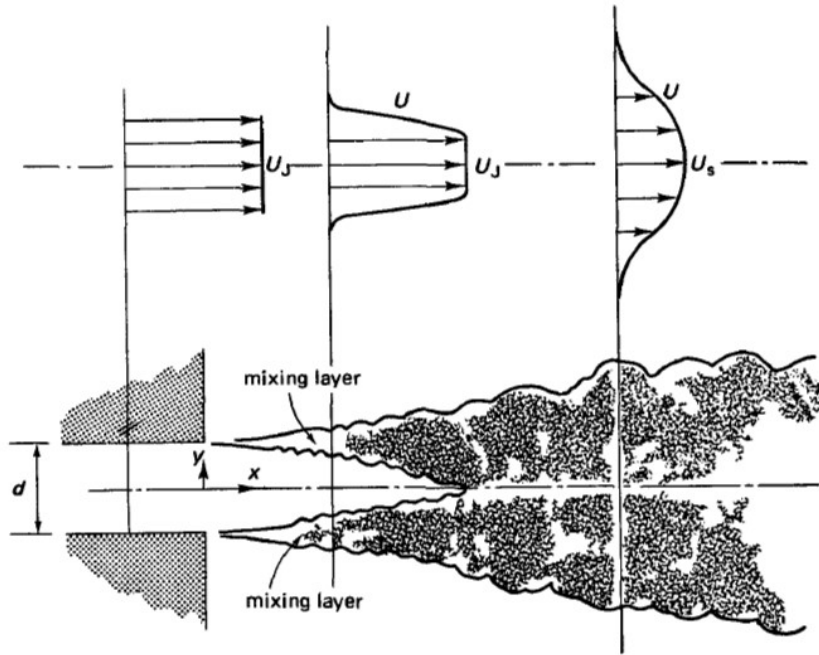


**Figure 4.3:** Development of a turbulent plane jet [48] with the plug velocity profile at the orifice.

#### 4.2.2. Steady axisymmetric jet

The axisymmetric jets exhibit much more stable behaviour compared to planar jets. Even though the analysis of the stability suggests that the free axisymmetric jet should transform into turbulent at a very low critical Reynolds number, the experiments have proved that the small-disturbance theory is unlikely to be able to account completely for the behaviour of a real jet, so whether the jet will be laminar or turbulent cannot be assessed simply by using these theories. Experiments have shown that while it is difficult to obtain a long steady jet at relatively low Reynolds numbers ( $10 < Re < 30$ ), progressively longer jets can be maintained as  $Re$  increases towards 150. For higher Reynolds numbers ( $150 < Re < 300$ ) still longer simple jets can exist. This is caused by the fact that in the viscous fluid, the axisymmetric disturbances do not grow. On the other hand, a complex breakdown can also occur, with a reduction in length of simple jet as  $Re$  increases towards 300. For  $Re > 300$  jets become disordered near the nozzle, although not so near as in the range  $10 < Re < 30$  [8, 4, 37, 48].

Lately, it was discovered that the steady laminar jet can be maintained even for much larger Reynolds number, exceeding  $Re = 600$  and even  $Re = 1000$ . In addition, the experimental results compares quite favourably with the analytical solution. It is generally agreed that the development of the instability is slow, so that for values of the Reynolds number on the order of a few hundred unsteadiness is only noticeable far downstream, at very large distances on the order of a few hundred nozzle diameters, whereas the laminar steady solution remains valid at smaller distances from the jet exit [35, 43].

### 4.2.3. Pulsatile jet

When it comes to unsteady jets, either planar or axisymmetric, the problem gets even more complicated. In case of pulsatile flow, neither the mean nor the instantaneous Reynolds number is a sufficient criterion for determining transition of laminar to turbulent flow. It was clearly shown that for the various cases studied, a pulsation of low amplitude produces a comparable flow in the steady jet case. Some papers also indicates that slowly oscillating flows of large amplitude tend to suppress or destroy turbulence downstream from sources of disturbance and so the turbulent flow is not developed. Therefore it is assumed that the jet will not become turbulent for the Reynolds number on the order of a few hundred and the solution of pulsatile system of low amplitude will produce comparable flow to the steady case [7, 25, 39, 52]. This assumption will be further computationally verified.

## 4.3. Direct Numerical Simulation

Direct Numerical Simulation (DNS) is a term used to call a computational method when the full unsteady Navier-Stokes equation are solved without any turbulence model, meaning that the equations are numerically integrated without any simplification. In this way, it is possible, if the mesh is fine enough, to resolve the smallest details of the problem. Even though the Direct Numerical Simulation can be used as a powerful tool in a turbulence research or to describe unsteady problems, it is not a brute-force solution of the Navier-Stokes equation, because this kind of simulation is so computationally demanding that it is generally limited to incompressible flow, simple flow geometries, and Reynolds numbers much lower than those typical of practical applications [26, 27]. The reason of this is that when resolving turbulent flow the mesh size has to be taken small enough to capture the finest scales. Eddies in a turbulent flow carry turbulent kinetic energy that is disturbed over a broad range of scales from the external scale, to the energy dissipating Kolmogorov scale. Energy is transferred across the scales, forward and backward, from large to small and vice versa [22, 34] and so a need of resolving all of the scales to be able properly describe the fluid motion is apparent.

DNS is very often used in research of boundary layers, jets, wakes and other shear layers. Also laminar-turbulent transition have been investigated using DNS. At some point, this was very promising method and researchers were waiting for computing power to get to the point when the DNS can be applied to the real life problems yet as Spalart pointed out in [46], the growth of computing power is slowing down, the Moore's law<sup>2</sup> encountered an apparent ceiling for chips around 2012 and besides this the growth of computing power is accompanied with increase of electricity consumption and so significant increase in cost. Just to give some example, in order to resolve flow around a non-rotating golf ball, 1 billion grid points were required.

---

<sup>2</sup> An observation that the number of transistors on a chip doubles every two years while the costs are halved.

DNS is assumed to be definitely accurate yet the limitations are significant. For example for a simple regular tennis ball, the DNS is not possible, because of the hair on it that could not be resolved directly. Treating it requires a model of rough-wall turbulence, thus empiricism. However, the application to the jets can be possible when enough computing power is available. For this purpose, usually a spectral-element methods (SEM) are used to solve differential equations. Although some consider DNS to be prohibited by pragmatic constraints associated with the grid size [34], Hosseini et al. proved opposite when they used DNS even for aerospace application [18]. They have performed three-dimensional DNS to resolve the flow over the wing with airfoil NACA 4412. The simulation was initiated using RANS in order to determine the velocity distribution around the wing and afterwards incompressible SEM solver Nek5000 was used to resolve finest scales. The chord Reynolds number<sup>3</sup> was 400 000 and the angle of attack  $5^\circ$ . The grid was enormous, using 3.2 billion grid points. This is the first time well resolved direct numerical simulations of this kind ever performed.

The application of DNS to the free planar jet is shown in Figure 4.4. In this case the jet creates Karman-like street after breakdown. This evolution corresponds to sinuous mode however jets can also break down in varicose mode and remain approximately axisymmetrical [22].



**Figure 4.4:** DNS of a two-dimensional spatially growing Bickley jet [22].

In this thesis, we will stick to laminar pulsatile flow, so the unsteady NS equations will be integrated directly however without a need to resolve finest Kolmogorov scales. Analysis of turbulent axisymmetric jet would require employing spectral-element methods and most likely creating in-house code and access to enormous computing power. Even when possessing all mentioned, the computation would take a lot of time.

---

<sup>3</sup> For calculation of Reynolds number of flow around the airfoil, chord width of the airfoil is used as the characteristic length.

# 5. Pulsatile axisymmetric jet

The main topic of this thesis is the pulsatile axisymmetric jet. The principle of the pulse jet is imposing unsteady component to the jet velocity at the nozzle exit plane. The source of the jet flow basically comprises a mean-flow component with a superposed temporally periodic pulsation. The most common case is where the unsteady component is a small fraction of the mean component. This case is often referred as forced jet. The limiting case when the jet velocity returns to zero between pulses is known as a fully-pulsed jet [21, 17, 39].

The application of the pulsatile jets will be discussed in the following chapter. There are several application in aerospace propulsion where applying pulsatile flow can enhance the efficiency of the combustion or even serve as the thrust generator. The pulsatile flow is also inherently related to medicine. Medical application will be mentioned, but will not be further investigated since the solution of the pulsatile jet in this thesis cannot be applied to the arterial blood system.

In this thesis, a solution is given for the axisymmetric pulsatile jet of moderately low Reynolds numbers and rather small fluctuation magnitudes issuing to the quiescent atmosphere. The range of tested Reynolds numbers was based on the facts summarized in chapter 4. It was ensured that the jet will be in laminar mode at the orifice and thus it is possible to create a time-accurate solution of the problem without a need of extensive computational power as long as the jet remains in laminar mode. However, solving pulsatile flow of course requires employment of transient simulation and integration of Navier-Stokes equation with respect to time. This makes the whole simulation much more time consuming.

## 5.1. Boundary conditions and governing equation

The initial conditions of the pulsatile axisymmetric jet issuing into the quiescent atmosphere/environment can be defined as follows

$$u \begin{cases} U_j \cdot (1 + \epsilon \cdot \cos(2\pi \cdot f \cdot t)), & |y| < a \\ 0, & |y| > a \end{cases} \quad (5.1)$$

$$(5.2)$$

where  $U_j$  is initial velocity of the jet,  $a$  is the radius of the nozzle,  $\epsilon$  defines the fluctuation of the velocity,  $f$  is the frequency and  $t$  is the time. As can be seen, herein a time-harmonic function is used to define an unsteady component of the jet velocity. The unsteady component might be defined using different functions, yet using cosine or sine function is very neat considering the ease of calculation of period based on the frequency. This also means that the time when the unsteady component of the velocity is null can

be found by simple determination of the period and comparing it to the time-step of the calculation.

The boundary conditions for the case of unrestricted flow are defined as follow

$$\left. \begin{array}{l} v = 0, \frac{\partial u}{\partial y} = 0 \quad \text{at} \quad y = 0, \quad x > 0 \\ u \rightarrow 0 \quad \text{as} \quad y \rightarrow \infty, \quad x > 0 \end{array} \right\}$$

Once the initial and the boundary conditions are define, the governing equation can be written in the following form [39]

$$St \frac{\partial u}{\partial t} + u \frac{\partial u}{\partial x} + v \frac{\partial u}{\partial y} = \frac{\partial u^2}{\partial y^2} \quad (5.3)$$

$$\frac{\partial u}{\partial x} + \frac{\partial v}{\partial y} = 0 \quad (5.4)$$

where  $St$  designates the Strouhal number that will be defined in following section. This problem cannot be approximated by analytical solution and so the only way is to employ the numerical/iterative approach.

## 5.2. Strouhal number

Strouhal number, sometimes also called Stokes number, is the dimensionless number describing oscillating flow mechanism. It is mostly known for its relation with frequency of vortex shedding however any unsteady behaviour of fluid is affected by Strouhal number, and the jets are not an exception.

It can be defined using many different variables however the most appropriate for our case is the following form

$$St = \frac{\omega \cdot d}{u_j}, \quad (5.5)$$

where  $\omega = 2\pi f$ . As results of previous studies suggested, the Strouhal number has a significant influence on the behaviour of pulsatile jet, especially on the decay of the time-harmonic fluctuation that is imposed upon the mean velocity. Not only because the Strouhal number actually appear in equation describing pulsatile flow, also due to physical meaning of Strouhal number it is more appropriate to use it when defining the unsteadiness of the flow.

### 5.3. Generation of pulsation

In the reality, a pulsation can be imposed on the flow in several ways. The pulsation of forced jet where the velocity does not reach zero can be generated in principle by two main methods. By periodically varying the area of the pipe through which the flow is passing on its way to the nozzle exit using a control valve directed by a controller or by using a pump/blower with a variable flow rate. Much easier solution out of these two is of course applying a control valve to the system. It is also the most commonly used method.

In numerical experiments, there are several ways to impose the pulsation on the jet. In these cases a pulsatile velocity profile was used. This method will be further discussed in Chapter 7.

### 5.4. Effect of pulsation on the jet flow

As reported by Hewitt and Duck [17], the numerical results for a planar case indicate that the effect of jet pulsation triggers a spatially growing instability that increases rapidly downstream, which is in striking contrast with the conclusion of Riley, Sanchez-Sanz and Watson [39] as well as with the conclusion of Binder [7] and Marzouk [25] for axisymmetric jets who have reported that the time-dependent part of the solution decays exponentially with downstream axial distance while the time-averaged solution decays more slowly, thus developing into a steady jet that decays algebraically with axial distance.

It is assumed that the planar and axisymmetric jets react to the introduction of an unsteady component to the jet velocity at the exit plane in the same way. The mentioned disagreement between Riley and Hewitt in the case of a planar jet might be caused by a usage of different Reynolds numbers or fluctuation magnitudes. Due to this disagreement and lack of experimental data, it is hard to predict how the pulsation affects the flow.

Nevertheless, for pulsations of low amplitude and low Reynolds number, the perturbation imposed on the axisymmetric jet is expected to disappear after some distance from the nozzle yielding a classical asymptotic solution of Schlichting as was reported by [7] and [25]. Since the problem is solved by time-accurate integration of the Navier-Stokes equations the perturbation growth would strongly affect the results as well as the convergence, thus the instabilities indicating laminar-turbulent transition could be identified.

# 6. Application of axisymmetric pulsatile jets

There are several applications of pulsatile flow in the aerospace engineering field related to combustion and the propulsion itself, specifically some athodyd<sup>1</sup> engines generate thrust utilizing mechanics of pulsatile flow. All these will be discussed further. Another application that is not a topic of this thesis can be found in medicine. The pulsatile flow restricted in circular tube can simulate the arterial blood flow. However it is important to note here that arterial blood flow differs significantly from sinusoidal flow investigated in this thesis. In a typical in-vivo flow the systolic phase occupies only one-third of the cycle and is characterized by extremely large accelerations to a peak flow which is much greater than mean flow. The diastolic phase occupies remaining two thirds of the cycle and is accompanied by a small amount of net back-flow [52]. In this thesis, rather small values of fluctuation are used and moreover the flow issues into the quiescent atmosphere, not into a flexible tube, thus this application is not considered in this thesis.

## 6.1. Mixing ratio, entrainment and flame stabilization

Many practical applications of jets, as for instance diffusion flames or ejectors, depend crucially upon their mixing and entrainment rate. In order to improve the efficiency of the combustion, it has been attempted to control these properties in various ways. One of them is forcing the velocity of injection of the fuel. It was proved that enhanced entrainment, diffusion and development of the jet can be achieved near the nozzle by forcing, hence it could improve the efficiency of combustion chamber while maintaining simple design by avoiding a usage of mechanical swirls. In addition, pulsation of the fuel supply can also enhance stabilization of the flame and reduce its length [7, 25, 24].

## 6.2. Pulsejet engine

Probably the most obvious application of pulsatile jets is the thrust creation/propulsion. Creation of thrust can be achieved by using both the fully-pulsed and the forced jet (i. e., a periodic series of starting jets or pulses). The first man-made propulsion system utilizing pulsatile jet for generating a thrust was a concept known as pulsejet. Even though, these engines have found very limited applications as there are great difficulties of its integration onto manned aircraft [21, 40, 11], they paved a path to much more promising concept called Pulsed Detonation Engines, thus they will be also briefly mentioned.

---

<sup>1</sup> Aero THERMODYNAMICS Duct engines has no major rotating parts such as fans/compressors or turbine [11].

## 6. Application of axisymmetric pulsatile jets

The pulsejets are very simple jet engines that can be made with a few or no moving parts. The main parts are air intake, a combustion chamber, and an exhaust pipe. Intake of air is not continuous, thus combustion occurs in pulses creating a pulsating thrust [40]. The main advantages of pulsejet engine are its capability to run statically, low weight, simple construction and the use of atmospheric oxygen and cheap fuels. On the other hand, the main disadvantages are poor reliability and fuel economy accompanied with low specific impulse, very high noise levels and severe vibrations.

There are three types of pulsejets that will be discussed in the following sections - valved pulsejet, valveless pulsejet and relatively new concept designated as Pulse Detonation Engine (PDE). All of them are based on Humphrey cycle shown in Figure 6.1.

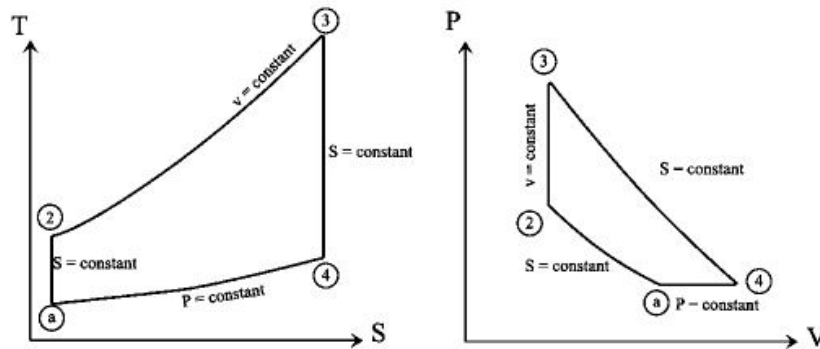


Figure 6.1: Humphrey cycle [11]

### 6.2.1. Valved Pulsejet

The valved pulsejet uses a set of one-way valves through which the incoming air passes. Fuel in the form of a gas or liquid aerosol can be either mixed with the air in the intake or injected in to the combustion chamber. When the fuel mixture is ignited, the valves shut so hot gases leave through the exhaust pipe creating forward thrust. Once the engine is running, it requires only an input of fuel, but it usually requires forced air and an ignition method for the fuel-air mix. The main drawback of this concept is a need of regular replacement of the valves which causes a very low reliability of the engine [11].

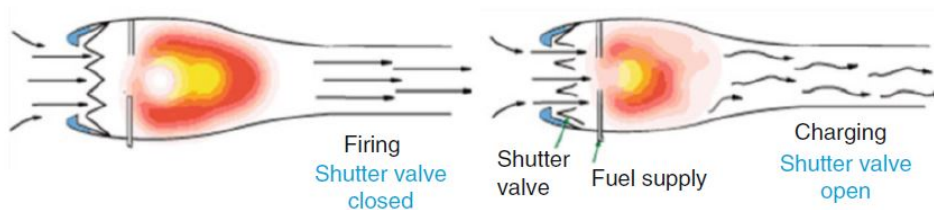
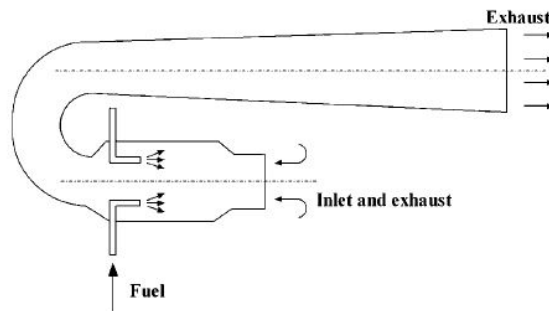


Figure 6.2: Valved pulsejet [11]

### 6.2.2. Valveless Pulsejet

The significant improvement in reliability is achieved by elimination of valves. The valveless pulsejet uses so called aerodynamic valve instead, thus in fact it uses the mass of air in the intake tube as the valve, but there are no mechanical parts to stop fuel mixture to escape to the wrong direction. This adjustment makes valveless pulse jet one of the simplest engines in the world. In valveless pulse jet, the main problems are again noise level and excessively high fuel consumption. Moreover, the intake and exhaust pipe usually face the same direction which results in a need to bend the engine into a "U" shape as is shown in Figure 6.3. Nevertheless, it is important to mention that deflagration nature of pulsejet combustion is very beneficial when it comes to environmental impact, these engines produce practically no hazardous pollutants even when using hydrocarbon fuels [11] and that is the reason for researchers and engineers to investigating them again at this time in which the environmental impact of mankind is of the greatest concerns of the society. The most promising concept of pulsed propulsion system that recently experienced a great come back into the limelight will be described in following section.



**Figure 6.3:** Valveless pulsejet [11]

### 6.2.3. Pulse Detonation Engine

In order to achieve a high-speed cruise capability in the atmosphere that would be sustainable, a revolutionary concept in propulsion is required. A need of clean and highly efficient propulsion system is vital to achieve a high-speed cruise [33]. This is obvious since the end of Concorde, the only commercial airplane that was able to fly at supersonic speed and transport passengers around the world.

One of such revolutionary concept could be the Pulse Detonation Engine (PDE) that marks a new approach towards non-continuous combustion jet engines. It is a constant-volume combustion ramjet that is capable of producing static thrust. The operation of a PDE is similar to a pulsejet except combustion in pulse jet is based on the principle of deflagration that is, the rapid but relatively gentle subsonic combustion of fuel driven by the transfer of heat while the PDE creates a detonation wave, which is akin to an explosion that creates high pressure shock waves. These explosions occur approximately 60 detonations per second. In other words, PDEs detonate, rather than deflagrate, their fuel.

Detonation of fuel is a sudden and violent supersonic combustion involving a supersonic exothermic front accelerating through a medium driving a shock wave directly in front of it, this results in immense pressure which in turn is used as thrust. Combustion process in PDE resembles perfectly constant volume combustion, while combustion process in valveless and valved pulsejets is approximated only as a constant volume process [14, 11]. PDE is being developed along two avenues, the first uses conventional hydrocarbon fuel reacted with air with, in some cases, a small, localized, oxygen addition to promote the rapid formation of a detonation wave, while the other approach employs oxygen as the oxidant in conjunction with a specialized fuel such as hydrogen [20].

The PDEs share the same advantages with classical pulsejets, they are light, easy to manufacture, and moreover promises higher fuel efficiency compared to turbofan engines. Until now, no practical PDE engine has been put into production, but several companies and institutions are working on development of these engines. Test engines have been built by Pratt & Whitney, General Electric and research in this fields is also being carried out by NASA [32, 11].

The most promising type is a combined-cycle PDE. Since a PDE has an ability to provide thrust at static conditions, the possibility of combined-cycle propulsion system capable of flight from to the high Mach number required for scramjets might be possible by adding a PDE to the flowpath of a ramjet or scramjet. These engines would seem initially suitable for high altitude, high-speed aircraft and hence allow a revolution in commercial aviation [11, 33].

Especially Povinelli<sup>2</sup> and Yungster<sup>3</sup> [32, 33] have computationally investigated behaviour of pulsed combustion of airbreathing PDE that uses hydrogen-air mixture. They focused on creation and propagation of detonation waves. The growth of the detonation wave in the PDE can be seen in Figure 6.4. The detonation creates a short duration thrust spike that is followed by longer plateau region of 2 msec and subsequently vanishes quickly as the flow decays. The flow decay is rapid, within the mentioned 2 msec. The current problem of PDE is that, in spite of the promise of significantly higher performance, it suffers from a low specific thrust caused by losses during the detonation process and other imperfections. Using CFD, it was found that the PDE performance is improved by operation at off-stoichiometric conditions, which suggest operation of a PDE on the lean side could produce sufficient thrust yet there is still a lot to be investigated when it comes to a behaviour of detonation waves or actual engine design in order to achieve sustainable PD propulsion superior to conventional propulsion systems.

---

<sup>2</sup> Former Chief Scientist and current Project Scientist, Turbomachinery and Propulsion Systems Division at Glenn Research Center Cleveland, Ohio 44135

<sup>3</sup> Senior Scientist at Ohio Aerospace Institute Cleveland, Ohio 44142

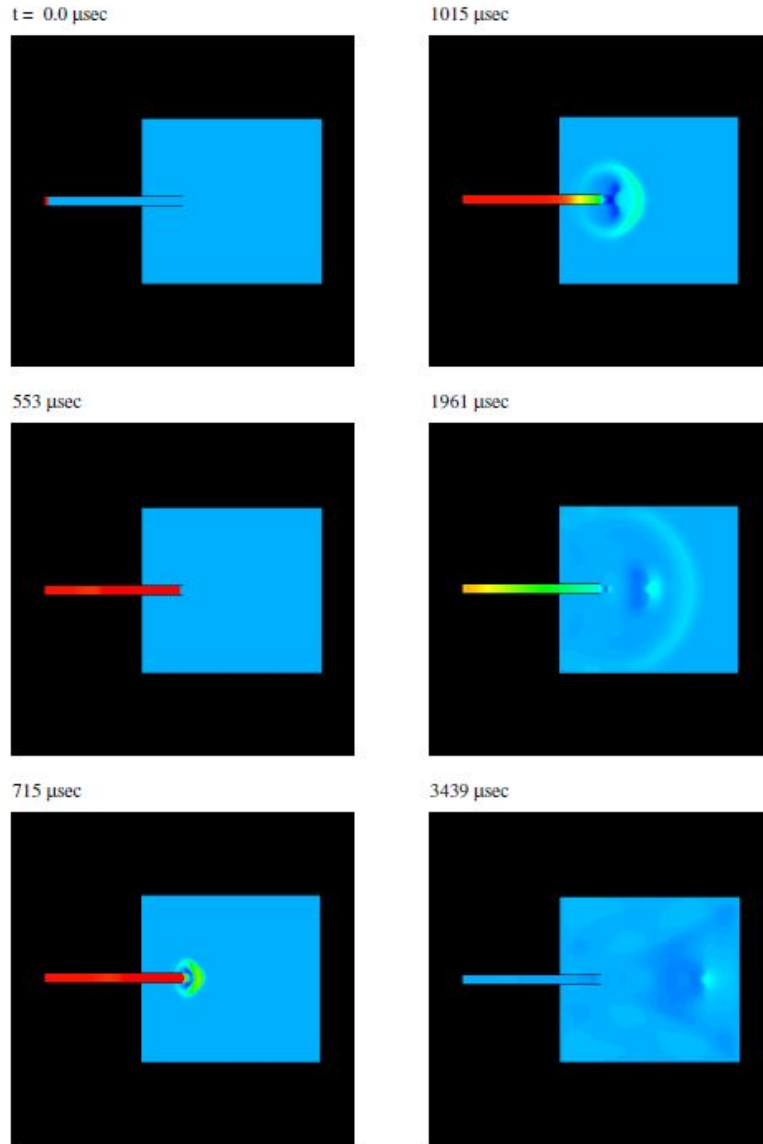


**Figure 6.4:** Pressure contours showing the growth of the detonation wave [32]

Even though this thesis is focused on the jet of low Reynolds number, all mentioned applications produce jets that can be described based on the same principles, so if the Reynolds number and mesh refinement were increased sufficiently, the numerical simulation of jets involved in these propulsion could be performed. However it is important to note that in case of so high Reynolds numbers, it is being dealt with turbulent flow and so creating time-accurate solution of such problem involves extensive computational power as well as enormous computational time, thus it is not possible to investigate these flows using conventional clusters. This is the reason why the Reynolds numbers used in simulations performed in this thesis will not exceed 600.

# 7. Numerical method

In order to achieve a correct result of numerical solution, it is necessary to opt for a correct domain size, discretization, boundary conditions and computational algorithm. Selection of mentioned parameters was based on the throughout analysis of obtained results that are discussed in this and the following chapters.

## 7.1. Domain

The domain geometry is of a standard rectangular shape that is commonly used for numerical studies of jets [17, 39] and takes advantage of the axial symmetry of the jet. Domain is shown in Figure 7.1.

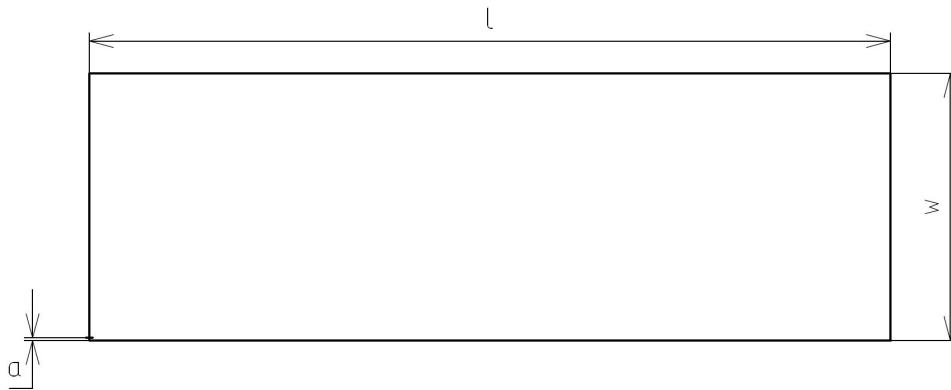
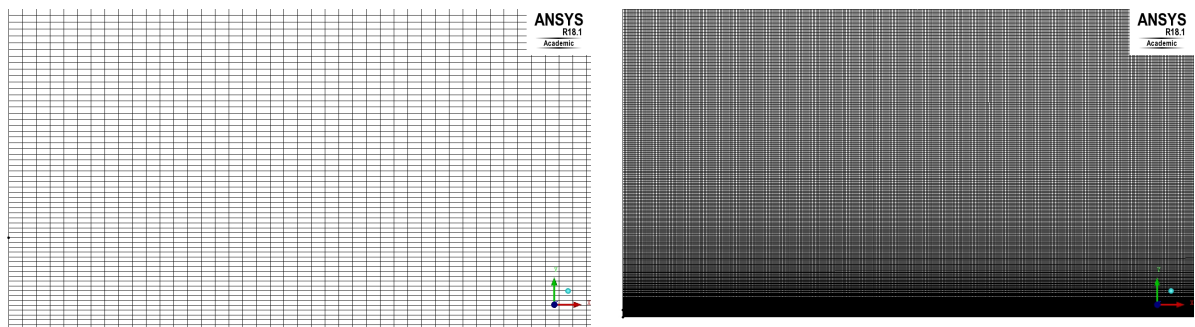


**Figure 7.1:** Domain.

In order to ensure as precise results as possible, it was important to create a very fine mesh, especially close to the inlet area. The domain discretization can be seen in Figure 7.2.



(a) Refinement at the nozzle area.

(b) Demonstration of the mesh refinement.

**Figure 7.2:** Mesh refinement.

In many cases, it is difficult to achieve sufficient quality of the grid, especially in cases of complex geometries yet this is not a problem in our case. The high quality structured grid can be achieved by fine discretization at the near-nozzle region and gradually increasing distance between nodes in transverse direction in order to reduce a computational time. The area far from the jet in transverse direction is out of interest however the mesh has to be big enough to ensure that the boundary conditions will not corrupt the results.

The correct mesh size and refinement was investigated by so-called independency study which consists in performing calculations for different grids and comparing the results. Independency is achieved when the results do not differ regarding the grid size and discretization. Grids that have been tested in order to eliminate any inaccuracies as a consequence of domain size and refinement are listed in Table 7.1.

Mesh	Length	Height	Discretization
Mesh 1	0.6	0.2	320 x 2000
Mesh 2	1	0.4	320 x 2000
Mesh 3	1	0.4	620 x 4000
Mesh 4	2	0.8	620 x 4000

**Table 7.1:** Mesh dimensions and number of nodes.

All the meshes were created using software Ansys ICEM CFD and were tested for different inlet velocities in order to evaluate not only the quality as a consequence of mesh refinement, but also whether an increase of velocity/Reynolds number requires increase of domain dimensions in order to ensure converged and precise solution.

## 7.2. Initial and boundary conditions

A correct choice of initial and boundary conditions is vital in order to achieve physically correct results, because they specify the flow and thermal variables on the boundaries of the physical model [2]. In this case, even though the geometry of the domain is very simple, obtaining sufficiently good convergence was quite difficult. Due to the problems with convergence, many different approaches have been tested in order to receive good results that are in the best match with the analytical solution.

In addition, it should be pointed out that the boundary conditions are defined in different way in Ansys Fluent. Since it is made for a wide range of engineers from different field, so for a wide range of applications, it is trying to be very user friendly, yet sometimes it is difficult to figure out what exactly is hidden under the names of boundary conditions that are available in Fluent. The boundary condition are divided into four groups:

### 1. Flow inlet and exit boundaries

pressure inlet, velocity inlet, mass flow inlet, and inlet. vent, intake fan, pressure outlet, pressure far-field, outflow, outlet vent, and exhaust fan

### 2. Wall, repeating, and pole boundaries

wall, symmetry, periodic, and axis

### 3. Internal cell zones

fluid, and solid

### 4. Internal face boundaries

fan, radiator, porous jump, wall, and interior

As can be seen, the designation of boundary conditions in Fluent is not based on its mathematical definition, but rather on their application. This can get tricky in some cases and it should be always verified that the mathematical definition of used boundary condition corresponds to the problem that is being simulated.

The initial and boundary conditions that needs to be specified in our case are inlet, axis of symmetry, lateral boundary and internal cell zones.

### 7.2.1. Inlet

The inlet of gas is defined using a boundary condition of Dirichlet type<sup>1</sup> with known velocity. For steady case, this boundary condition can be imposed in Fluent using velocity-inlet, which was intended for incompressible flows and so it is important to note that it cannot be used for compressible flows. In case of pulsatile jet and so transient simulation, the boundary condition must be defined in transient manner using UDF that ensure fluctuation of velocity magnitude, an example of such an UDF is shown in Section 7.4.

### 7.2.2. Axis of symmetry

For defining axial symmetry a boundary condition of Neumann type<sup>2</sup> with zero normal velocity gradient was used. It is very simple to set up such a boundary condition in Ansys Fluent, because it has a boundary condition for axial symmetry available directly. The boundary condition is designated as "axis" and it must be used as the centerline of an axisymmetric geometry. It can also be used for the centerline of a cylindrical-polar quadrilateral or hexahedral grid [2]. It is also important to notice the difference between

---

<sup>1</sup> The value of the variable is specified [19].

<sup>2</sup> The value of gradient of a variable is specified [19].

”symmetry” boundary condition that is applicable for cases with planar symmetry and ”axis” boundary condition that is applicable for cases with axial symmetry.

### 7.2.3. Lateral boundary

Defining boundary condition at the lateral edge of the domain was the most challenging. Since the actual boundary condition defined for lateral domain boundary is following

$$u \rightarrow 0 \quad \text{as} \quad y \rightarrow \infty, \quad x > 0. \quad (7.1)$$

As can be seen from the Equation 7.1, at the lateral boundary of the domain only known value is that at infinite distance, the impact of jet on the atmosphere vanishes, which suggests that the results could also be strongly dependent on mesh size.

The boundary condition tested were outlet pressure, outflow and also velocity inlet. Velocity inlet was tested due to the fact that some codes cannot deal with a non-moving/quiescent atmosphere properly as described by NASA [29]. Moreover using pressure outlet and outflow boundary conditions was causing backflow at the lateral boundaries that could have an impact on time required to achieve a convergence and quality of convergence itself as pointed out in Ansys Guide [3]. This flow-warning means that the air was actually entering domain and not leaving it. For this reason, a velocity inlet was also tested on upper and left boundary of the domain, imposing very small inlet velocity, expecting that the mesh is big enough and so the actual velocity of the air entrained by jet is close to zero at this distance.

The influence of different boundary condition on the numerical results is evaluated in the chapter 8.

### 7.2.4. Internal cell zones

Group of cells for which all active equations are solved. The only required input for the fluid zone is the type of fluid material [2]. In our case, the incompressible air was used. The parameters of the fluid were set up as follows

$$\begin{aligned} \rho &= 1.225 \text{ kg}/\text{m}^3 \\ \nu &= 1.7894e - 05 \text{ kg}/(\text{ms}) \\ T &= 293.15 \text{ K} \end{aligned}$$

These values correspond to the values used for the asymptotic solution.

### 7.3. Computational algorithm

Since in the cases computed in this thesis, the velocity and Reynolds numbers are rather small, the incompressible fluid can be considered. The rule of thumb for determination whether the fluid should be considered incompressible or compressible is velocity approximately 100 m/s. Below this limit, the flow is generally considered to be incompressible. In incompressible flows, the density is constant and so the governing equations in the vectorial form can be written in the following form.

Continuity equation:

$$\nabla \cdot \mathbf{u} = 0, \quad (7.2)$$

General equation to express momentum conservation can be written as follow:

$$\frac{\partial \mathbf{u}}{\partial t} + \nabla \cdot (\mathbf{u}\mathbf{u}) = g - \frac{1}{\rho} \nabla p + \nu \nabla^2 \mathbf{u}, \quad (7.3)$$

where  $\nabla$  designates divergence<sup>3</sup> that is defined for two-dimensional space in the Cartesian space as follows

$$\nabla = \left( \frac{\partial}{\partial x}, \frac{\partial}{\partial y} \right), \quad (7.4)$$

and  $\mathbf{u}$  is a velocity vector,  $\nu$  is kinematic viscosity,  $\rho$  is density,  $p$  is a pressure,  $t$  is a time and  $g$  is a gravity acceleration<sup>4</sup> [19, 34]. In our case, the influence of gravity is also assumed to be null, so the momentum conservation equation is simplified to the form

$$\frac{\partial \mathbf{u}}{\partial t} + \nabla \cdot (\mathbf{u}\mathbf{u}) = -\frac{1}{\rho} \nabla p + \nu \nabla^2 \mathbf{u}. \quad (7.5)$$

For a compressible flow without external heat addition or body forces, the governing equations are the continuity equation, the three momentum equations and the energy equation. These five scalar equations involve six unknown quantities: heat transfer, velocity in x direction, velocity in y direction, velocity in z direction, pressure and entropy. Therefore an additional equation is required to close the system of equations. This is

---

<sup>3</sup> Divergence is a vector operator used to produces a vector field.

<sup>4</sup> Assuming gravitational field to be the only possible potential field acting on the system

provided by the thermodynamic relationship which exists among the fluid properties, and is known as the equation of state.

In the incompressible case, the solution of Navier-Stokes equation is complicated by the lack of an independent equation for the pressure, which appears in each of the three momentum equations, but not in the continuity equation. This means that the continuity equation does not have a dominant variable in incompressible flows unlike in compressible flows, where it can be used to determine the density from which pressure is obtained using an equation of state. In incompressible flows, the density is constant and it therefore drops out of the continuity equation altogether as can be seen in Equation 7.2, so there is no direct relation between pressure and density. The absence of the density-enabled linkage between the continuity and the momentum equations means that methods developed for compressible flows cannot be applied to incompressible flows.

In order to overcome this problem, several approaches have been developed to solve incompressible flows - artificial compressible approach, streamfunction-vorticity approach, pressure equation approach and pressure correction approach. In our case, the solution method based on pressure correction approach has been employed. This approach is kind of extension of pressure equation approach. Since the incompressible flows show constant thermophysical properties<sup>5</sup> the momentum equations get decoupled from the energy balance equation. The continuity and the momentum balance equations need to be solved together; however, the energy balance equation, usually expressed in terms of temperature as the main variable, can be solved after the velocity field is computed. The streamfunction-vorticity approach solves the problem by eliminating pressure from the momentum equation by introducing streamfunction and vorticity so that the three equations involving velocities and pressure can be rewritten as only two coupled equations involving streamfunction and vorticity and one decoupled Poisson equation. This system satisfies the continuity and the velocity field can be obtained without explicitly solving for the pressure. If pressure needs to be evaluated, then the Poisson equation can be derived for pressure by taking divergence of the momentum equation. This approach can then provide the time accurate solution which is however applicable only to two-dimensional problems. For three-dimensional cases it is necessary to employ pressure-based approach. In this case, the velocity is again solved without explicitly computing pressure and the fact that velocity field computed from the momentum equation also satisfies the continuity equation or vice versa is the reason why one can conclude that a specific role for pressure in incompressible flow is enforcing continuity. The various pressure-based computations of incompressible Navier Stokes equations use this principle to generate a linkage between the continuity equation and pressure. [19]. In this thesis, a computational algorithm based on pressure correction approach has been used in steady as well as in unsteady case.

In Ansys Fluent there are three main pressure-based solvers. In other words solvers based on pressure-velocity coupling technique, using finite-volume method and pressure correction approach that have been developed for solving incompressible flows. These

---

<sup>5</sup> The fluid density, viscosity, specific heat and thermal conductivity.

are Semi-Implicit Method for Pressure Linked Equations (SIMPLE) algorithm, SIMPLE-Consistent (SIMPLEC) algorithm which is fundamentally similar to SIMPLE except it uses modified correction equation that involves the pressure correction under-relaxation factor and the last one is PISO (Pressure-Implicit with Splitting of Operators) method, which is also derived from SIMPLE except it involves higher degree of the approximate relation between the corrections for pressure and velocity. One of the limitations of the SIMPLE and SIMPLEC algorithms is that new velocities and corresponding fluxes do not satisfy the momentum balance after the pressure-correction equation is solved. As a result, the calculation must be repeated until the balance is satisfied. To improve the efficiency of this calculation, the PISO algorithm performs two additional corrections: neighbor correction and skewness correction.

SIMPLEC has been proved to accelerate convergence in problems where pressure-velocity coupling is the main deterrent to obtaining solution. Especially, for steady laminar flow with no additional models activated. In these cases, the convergence is limited by the pressure-velocity coupling only and the converged solution can be obtained more quickly using SIMPLEC. In transient flows PISO method in general was reported to show the most robust convergence, it takes more CPU time per iteration, but it can dramatically decrease the number of iterations required for convergence, especially for transient problems. The only case where SIMPLEC exhibits superior behaviour to PISO method is the flow where the scalar variable was weakly linked to momentum equation (e.g. free convection flows<sup>6</sup>) [3, 19].

According to the information above, it was decided to test both SIMPLE as well as SIMPLEC. When using SIMPLEC, the skewness correction was set to zero since the mesh does not require any correction of skewness. In case of steady laminar jet, SIMPLEC exhibits much quicker convergence compared to SIMPLE. Number of iterations in order to achieve convergence was decreased approximately by 30% by using SIMPLEC algorithm. For transient simulation, the PISO algorithm was employed since it exhibits much faster convergence than SIMPLEC.

### 7.4. Pulsation

Pulsation can be directly applied by modifying the velocity-inlet boundary condition by UDF. A user-defined function, or UDF, is a function that can be dynamically loaded with the Fluent solver to enhance the standard features of the code. For example, the UDF can be used to define boundary conditions, material properties, and source terms for your flow regime, as well as specify customized model parameters (e.g. multiphase models), initialize a solution, or enhance post-processing [2]. In our case, the UDF was used to modify an inlet boundary condition and introduce the pulsation. For each Reynolds

---

<sup>6</sup> Flow motion is generated by density difference in the fluid due to temperature gradient, no external source is involved.

number, different amplitudes were tested in order to assess an influence of fluctuation intensity as well as Reynolds number. The amplitude of fluctuation was kept rather small, up to 10 % of the inlet velocity.

The pulsatile axisymmetric jet can be created within Ansys Fluent by introducing pulsatile velocity-inlet. Therefore the boundary condition at the inlet is set to velocity-inlet, the UDF is loaded to solver and set up as the value of velocity. Pulsatile velocity profile in our case will be based on sinusoidal function according to the following equation

$$u = U_j + U_j \cdot \epsilon \cdot \cos(2\pi \cdot f \cdot t). \quad (7.6)$$

User Defined Function defining the pulsatile velocity in Ansys Fluent is show in Code 7.1. In this case, the UDF is written so that it defines a time-harmonic fluctuation ( $\epsilon$ ) of magnitude of 1 % of the inlet velocity that is  $u_j = 1.5 \text{ m/s}$  and Strouhal number ( $St$ ) equals to 3. In the case of fully-pulsed jet, the fluctuation equals to inlet velocity and the velocity returns to zero between pulses, thus create a flow that exhibits much more complex structure.

```

1 #include "udf.h"
2 #define PI 3.141592654
3
4 DEFINE_PROFILE(my_velocity_v1_5_fluc_0_01_St3, thread, position)
5 {
6     face_t f;
7     real t = CURRENT_TIME;
8
9     begin_f_loop(f, thread)
10    {
11        F_PROFILE(f, thread, position) = 1/100.*3/2.*cos(2*PI*3*t)+3/2.;
12    }
13    end_f_loop(f, thread)
14 }

```

**Code 7.1:** User Defined Function modulating the steady jet by imposing time-harmonic fluctuation on the jet.

## 7.5. Judging convergence

For most problems, the default convergence criterion in Fluent requires that the scaled residuals decrease to  $10^{-3}$  for all equations except the energy and P-1 equations, for which the criterion is  $10^{-6}$ . Even though this criterion is sufficient in most cases, it is not a universal metrics for judging convergence. Residual definitions that are useful for one class of problem are sometimes misleading for other classes of problems. Therefore it is not a good idea to judge convergence only by examining residual levels, but also by

monitoring relevant integrated quantities such as velocity, pressure, lift coefficient, drag coefficient or heat transfer coefficient [2].

In our case mentioned general convergence criterion is not sufficient. The scaled residuals go below defined values after several hundreds of iterations even though the calculation is far from being converged. The development of convergence can be seen in Figure 7.3.

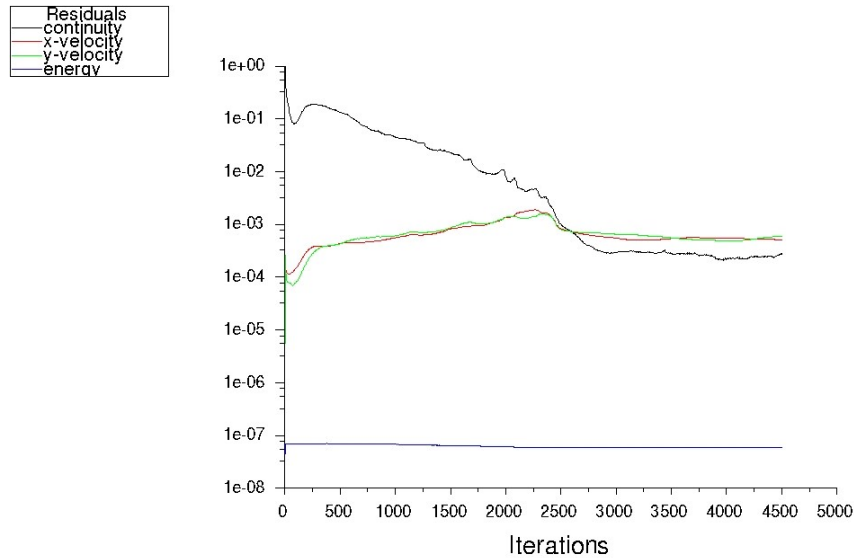


**Figure 7.3:** Residuals of calculation.

So in order to assess the convergence, a point monitor in form of vertex average was created on plane of axial symmetry far enough from the inlet. In this point, the axial velocity was tracked and once the value becomes stabilized, the axial velocity along the domain was plotted. In case, a development of axial velocity with respect to distance from the inlet was in alignment with theory, the calculation was considered converged.

In order to be able to judge convergence thoroughly, the most helpful tool was the analytical solution for steady axisymmetric jet that was developed for this purpose in MATLAB. The MATLAB code for axisymmetric jet is attached in appendix B. The explanation of the solution is given in Chapter 3. The solution is written so that it returns a value of axial velocity at required distance from the inlet. This value can be compared to the value obtained by numerical solution at this distance<sup>7</sup> even before stopping the calculation and exporting data, so one can see whether the solution gives reasonable values or not. Moreover, the code returns also expected development of axial velocity along the x-axis as well as transverse velocity in given distance from the inlet. All of this data was used to verify the convergence as well as correct.

<sup>7</sup> Using mentioned vertex average that can be created in Ansys Fluent under the tab "Setting up domain" and section "Surface"

# 8. Validation and verification

In this chapter the validation and verification process will be described. The validation and verification process was based on comparison of the asymptotic solution of steady axisymmetric jet introduced in chapter 3 to the numerical solution. Since the asymptotic solution was experimentally tested and proven to be correct [1], it can be used as the benchmark for the numerical solution that was later modified to direct solution of the unsteady Navier-Stokes equations.

## 8.1. Impact of the boundary conditions

As mentioned previously, the most challenging boundary condition was the lateral boundary of the domain. Ansys Fluent offers several different boundary conditions that can be used for simulating axisymmetric jet. One of the boundary conditions offered is a "velocity inlet". It is a boundary condition of Dirichlet type that allow air to enter the domain under defined speed. This condition was used for the area where the fluid enters the domain and has been also tested for left boundary and upper boundary of the domain. This solution was tested mostly because of the backflow warning that was received during the calculation when using a pressure-outlet boundary condition. This is caused by decrease of pressure due to the jet which consequently causes entrainment of the surrounding air.

In order to avoid any further complications, many attempts were conducted to eliminate this problem. The first idea was to decrease the velocity and increase the size mesh, so the lateral boundary is affected as less as possible. Unfortunately this did not help. The backflow warning was emerging during the solution even for Reynolds numbers around 100 and for domain width 200 jet diameters. All the tested combination are listed in the table 8.1, where V-I stands for velocity-inlet, P-O for pressure-inlet and O for outflow boundary condition.

<b>Inlet</b>	<b>Axis</b>	<b>LE</b>	<b>UE</b>	<b>RE</b>
V-I	Axis	P-O	P-O	P-O
V-I	Axis	O	O	O
V-I	Axis	V-I	P-O	P-O
V-I	Axis	V-I	V-I	P-O

**Table 8.1:** Boundary conditions combinations that have been tested.

Imposing velocity-inlet boundary condition for lateral boundary is problematic since the velocity at the boundary must be specified. If in reality the velocity at the boundary is significantly different from the velocity defined, the results will be corrupted. In fact, in order to correctly impose such boundary condition, the velocity at the boundary has to be

known or the error introduced by imposing such condition must be negligible [29]. This approach can be sufficiently accurate in cases when the upper and lower edge is far enough from the domain, so a very low velocity that will not affect the solution significantly can be introduced. Unfortunately, extending mesh so much is problematic when it comes to computational power hence less computationally demanding solution has been sought.

In this case two other options were readily available. Using "outflow" boundary condition or stick with the "pressure-outlet" and ensure the convergence is achieved. Several calculation was performed in order to assess the accuracy of both. The comparison can be seen in Figure 8.1.

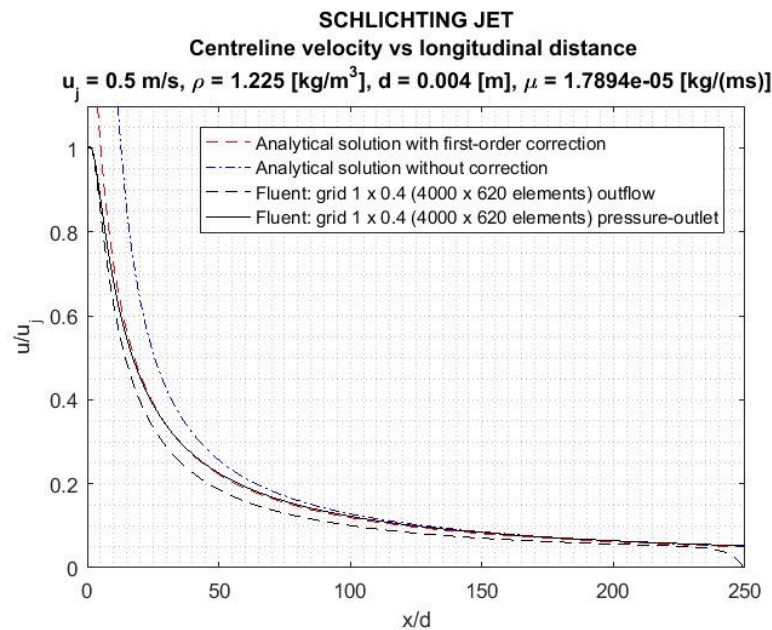


**Figure 8.1:** Comparison of boundary condition outflow and pressure-outlet.

As can be seen, when using outflow boundary condition, the results did not correspond to the analytical solution. The jet velocity was decaying too quick and the development of the centreline axial velocity did not match the expectations. Especially at the end of domain, the velocity has experienced significant decrease that is not physically correct. In addition, using outflow boundary condition caused significant increase of iterations required to achieve the convergence.

On the other hand, a use of "pressure-outlet" boundary condition has produced very accurate solution despite the backflow occurrence during the calculation. Therefore it was concluded by comparing all the results that the best boundary condition to be imposed in this case is the "pressure-outlet" for the lateral boundaries and "velocity-inlet" for the boundary that defines the orifice of the jet.

## 8.2. Impact of domain geometry and discretization

The mesh size and discretization has also a significant influence on the accuracy of the results. In order to eliminate any influence of the mesh refinement and mesh size on the results, several calculations were performed.

In Figure 8.2a and 8.2b, the comparison of different refinements can be seen as well as the influence of the inlet velocity on the centreline velocity. It can be seen that increasing grid refinement does not have any significant influence on the results that corresponds very accurately to asymptotic solution. The increase in velocity shifts the point of harmonization of both solution further from the orifice however this is expected and agrees with the theory, increasing velocity basically decreases the rate of the velocity decay.

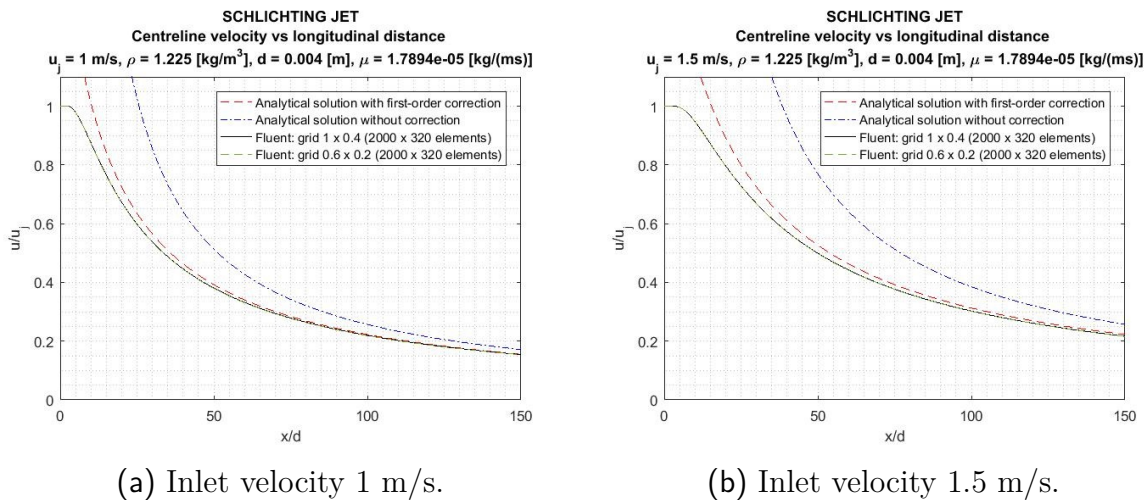


**Figure 8.2:** Development of centreline velocity with respect to inlet distance.

All the graphs are non-dimensional. The non-dimensionality is introduced by using non-dimensional variables. On vertical axis the ratio between axial velocity and the inlet velocity is used while on horizontal axis ratio between the distance and the inlet diameter is used. This helps when comparing the results since the asymptotic solution is non-dimensional and it also makes sense when considering that the jet is self-similar, due to this, there is no need to consider the actual velocities.

In Figures 8.3 and 8.4, the transverse velocity profiles at different directions are shown. These profiles were created by determining the axial velocity in direction perpendicular to jet centreline. Equally, it can be seen that the velocity profiles obtained by numerical solution match the asymptotic solution very accurately. It can be also seen that the further from the orifice the transverse velocity profiles are plotted the better the fit is. And correspondingly to Figure 8.2, when the velocity is increased, the difference between asymptotic solution and the numerical solution increases at the same location as well.

## 8. Validation and verification

As mentioned before, the point where the solutions harmonize is moved further from the orifice.

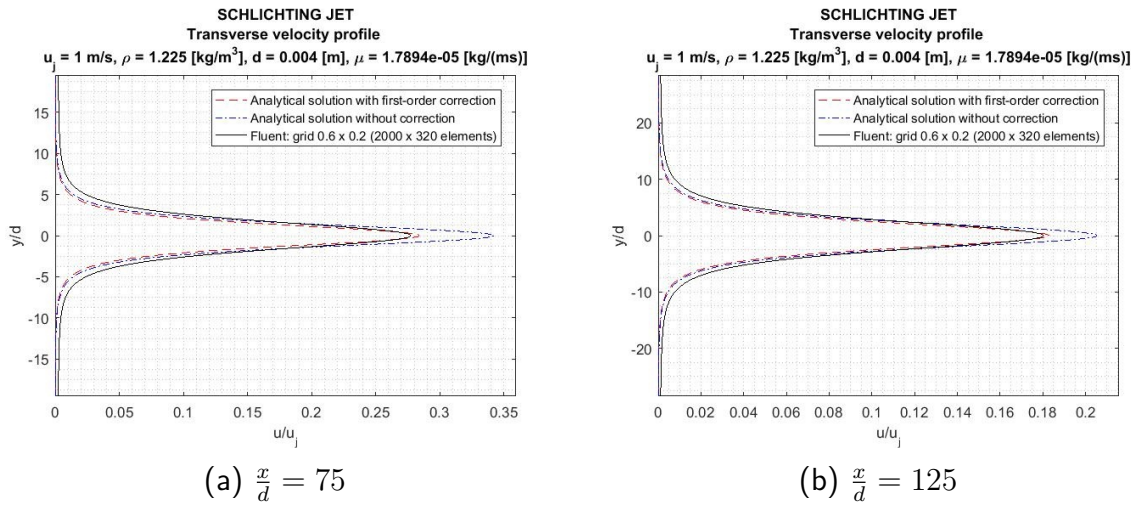


**Figure 8.3:** Transverse velocity profiles for an inlet velocity  $u_j = 1 \text{ m/s}$ .

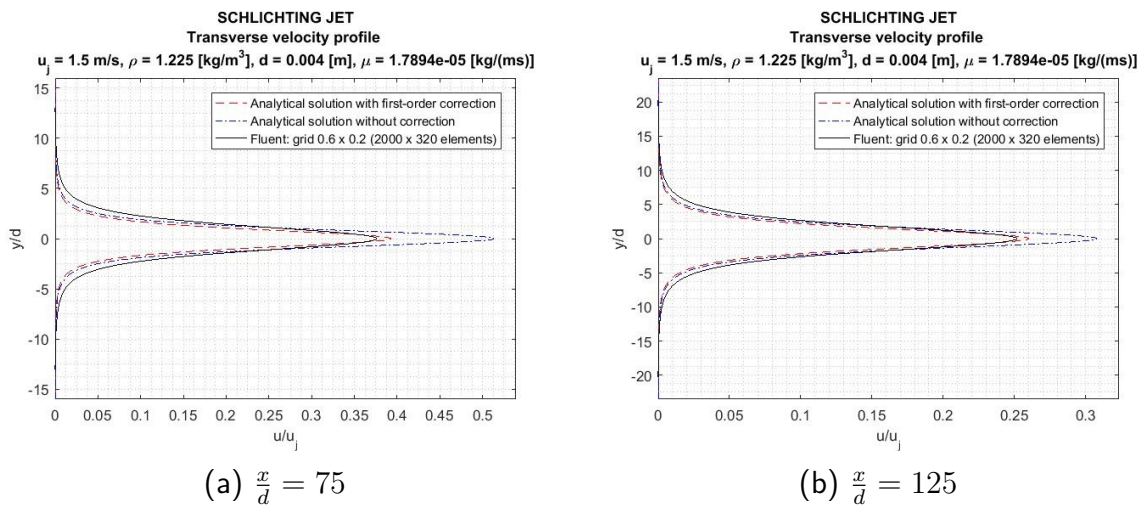


**Figure 8.4:** Transverse velocity profiles for an inlet velocity  $u_j = 1.5 \text{ m/s}$ .

The only discrepancy in the solution was found for very low Reynolds number in the region very near to the nozzle. This can be seen in Figure 8.5. First of all it is necessary to explain why the velocity increase was observed in this case. Since the velocity is very small, the pressure of surrounding air can actually decrease the width of the jet slightly and therefore cause a small increase in velocity. This is magnified in Figure 8.5b, where can be also seen that in this case of very small velocity difference, the difference in results can be seen when the mesh is refined. Nevertheless, this difference is smaller than 0.5% and so can be neglected. The decrease of jet width close to the orifice is so small that

enormously fine mesh has to be implemented to exactly determine an increase in the velocity.

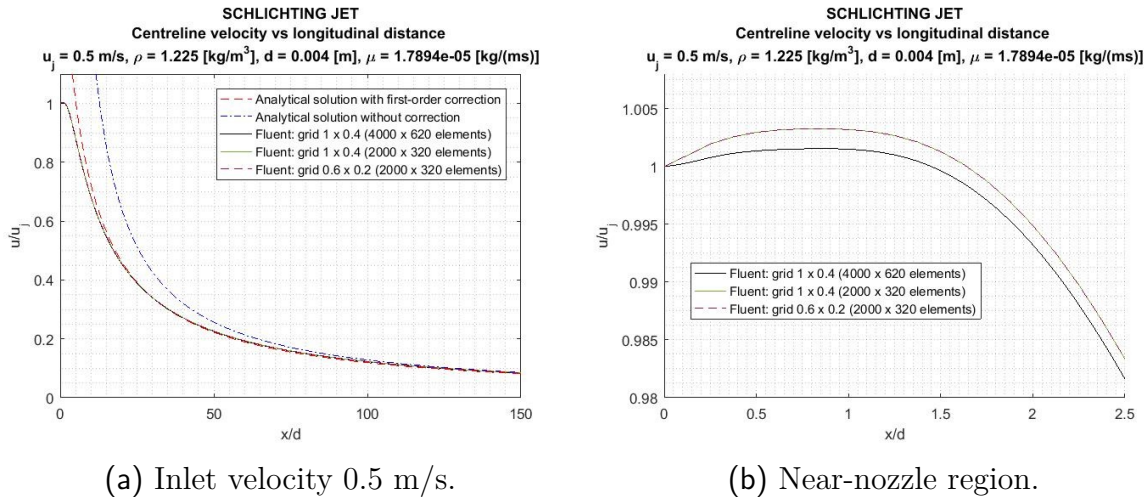


**Figure 8.5:** Development of centreline velocity with respect to inlet velocity.

The grid used for the simulation of pulsatile jet was the Mesh 1 from the Table 7.1, the exact details of the mesh, including also the boundary conditions imposed, are listed below.

---

Grid Zone Information

---

```
635682 quadrilateral cells, zone 10, binary.
1269047 2D interior faces, zone 11, binary.
  19 2D velocity-inlet faces, zone 12, binary.
 299 2D pressure-outlet faces, zone 13, binary.
1999 2D pressure-outlet faces, zone 14, binary.
 318 2D pressure-outlet faces, zone 15, binary.
1999 2D axis faces, zone 16, binary.
638000 nodes, binary.
638000 node flags, binary.
```

---

### 8.3. Impact of computational algorithm

For steady and unsteady/transient calculations were used different algorithms, but both are pressure-based algorithms using pressure-correction approach.

### 8.3.1. Steady

At the beginning, a very popular SIMPLE algorithm was implemented, yet based on the results and recommendations that can be found in literature [2] and [19], the SIMPLE-Consistent algorithm was also tested. It has been discovered that using SIMPLEC, instead of SIMPLE, significantly speed up the convergence. While the SIMPLE solver yielded the converged solution between 15 and 20 thousands iteration in case of steady flow, SIMPLEC yielded sufficiently converged solution even before 10 000 iterations. The skewness correction of the SIMPLEC solver has been set up to zero. Involving skewness correction is not necessary in case of rectangular mesh off which the skewness is equal to 1.

### 8.3.2. Unsteady

When it comes to transient simulation, the calculation gets more complex. Another parameters that have to be set in unsteady case are frequency, amplitude of fluctuation and time-step.

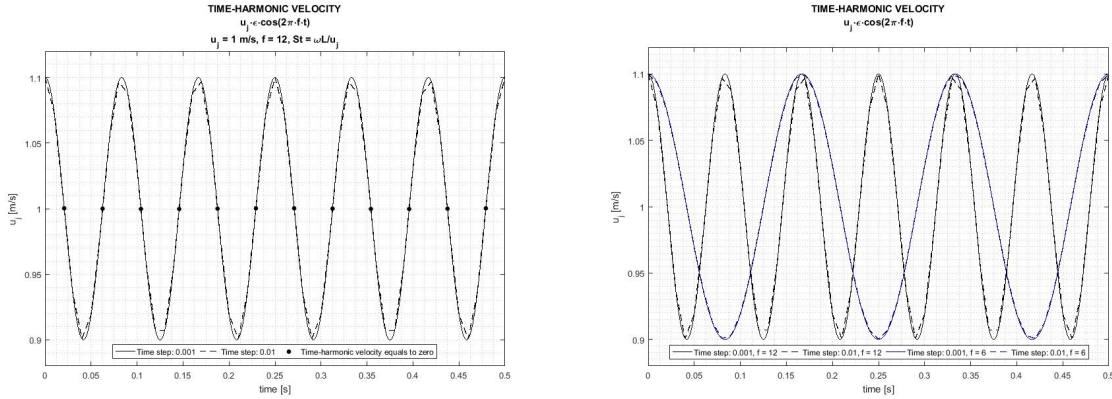
The computational algorithm used in this case is a PISO algorithm. This algorithm is using the same approach to obtain pressure and velocity corrections as in the SIMPLE method however in this case two evaluations of pressure are needed for one update of the velocity field, including the contribution of neighbouring velocity corrections. It can be said that the PISO algorithm generally shows the most robust convergence and the time-step can be set to larger values than when using different methods so the computational time can be slightly decreased [2].

#### Time-step

When setting the time-step, the problem is that the frequency is related to the domain size and the time-step as well. The higher the frequency is, the smaller time-step is required in order to precisely grasp the velocity fluctuation and simultaneously, it was found that the lower the frequency is, the longer the domain has to be since the perturbation travels further downstream. This will be further discussed later, however a consequence of this fact is that the transient computations of pulsating jets are very time-demanding. In Figure 8.6, the influence of the time-step on smoothness of the curve of time-harmonic velocity can be seen.

Based on a plot of time-step with respect to the velocity development, the correct value of time-step size can be estimated. As can be seen in Figure 8.6a, in case of frequency being 12 Hz, the time-step of 0.01 s is not sufficient. This can be clearly observed in peak areas where this time-step is too coarse to grasp the velocity change. Using so coarse time-step would lead to inaccuracies in calculated velocity, thus the smaller time-step had to be used. While in case of frequency being 6 Hz, the time-step of 0.01 s could be used,

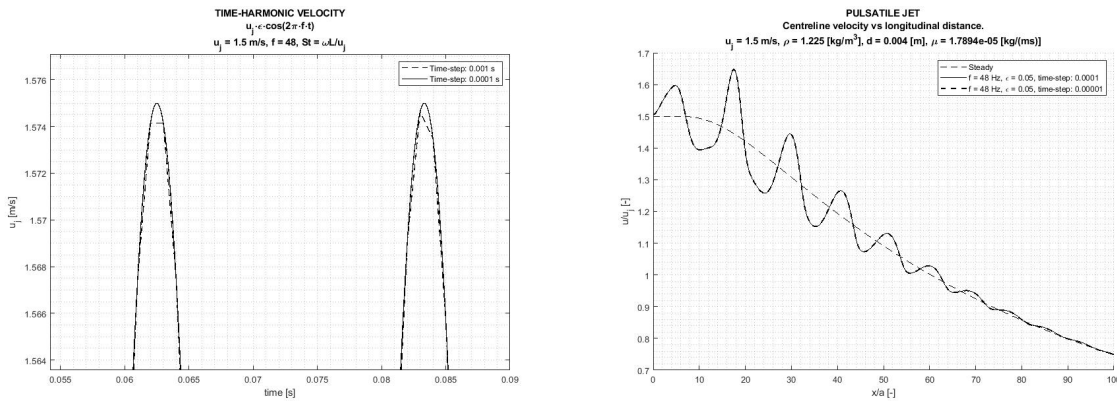
even though it is not perfect. This Figure also shows very clearly why the increase in frequency requires correspondent decrease in the time-step.



(a) Frequency 12 Hz (b) Comparison of frequency 6 Hz to 12 Hz.

**Figure 8.6:** Frequency and time-step size dependency.

This approach of estimating time-step size was verified for case of  $u = 1.5 \text{ m/s}$ ,  $f = 48 \text{ Hz}$ ,  $\epsilon = 0.05$ . in Figure 8.7a, it can be seen that time-step 0.001 is no more sufficient to actually describe the peak area of the time-harmonic fluctuation. This has been the reason to decrease the time-step size to 0.0001 s. for frequency  $f = 48 \text{ Hz}$ . The size of time-step has also been verified by performing the calculation using even one order smaller time-step 0.00001 s. Comparison of results for different time steps can be seen in Figures 8.7b. With increasing frequency and decreasing the time-step, calculations become very time demanding, thus considering available computational power, it was not possible to perform calculations for very high frequencies.



(a) Influence of time-step size on the accuracy. (b) Comparison of centreline velocity evolution for different time-steps.

**Figure 8.7:** Validation of the time-step size.

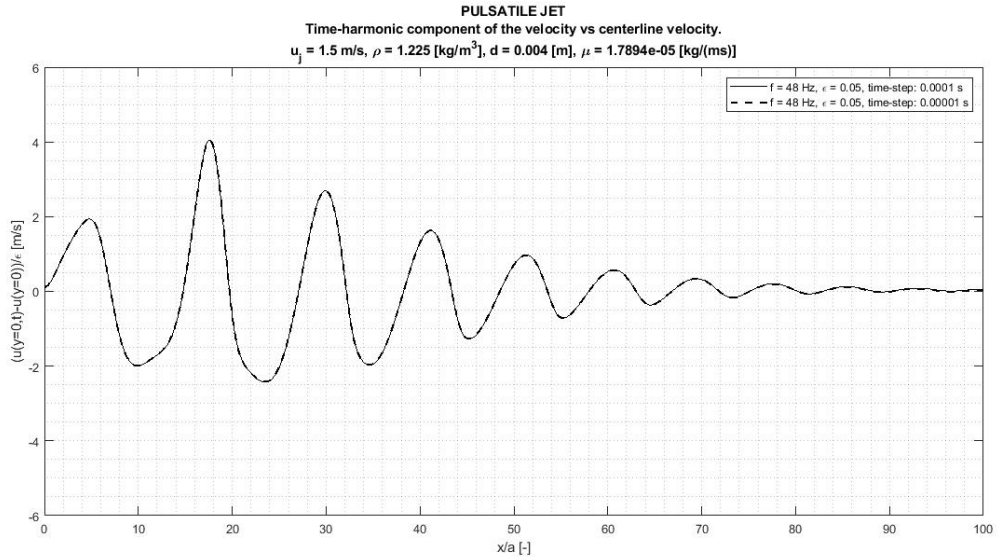


**Figure 8.8:** Evolution of time-harmonic component of the velocity.

### Number of iteration per time-step

Another variable that has a significant impact on the results of transient calculation is the number of iterations per time-step. This number must be set up based on either experience or experiments. In this case, 120 iterations per time-step was a minimum since the calculation otherwise exhibited oscillations near the end of the domain.

### Time-periodicity of the solution

In case of pulsatile flow, it is necessary to ensure that the time-periodic solution is reached, so the result for  $|\cos(k \cdot \pi)|$  are similar for different  $k$ . This eliminates the possibility of solution being corrupted by insufficient computational time, which could result in jet not being developed through the domain completely and so affecting the solution. It also eliminates possibility of any oscillation in the solution.

## 8.4. Axisymmetric jet self-similarity

As explained in chapter 2 and 3, the asymptotic solution is fundamentally based on self-similarity of the jets, because it allows reduction of PDEs to ODEs from which the exact solution arises [38]. Such self-similarity is demonstrated in Figure 8.9 and 8.10. As can be seen, when the jet is properly scaled, the shape of its velocity profiles along the longitudinal distance is similar. The profiles were scaled using jet half width designated

as  $r_{1/2}$ . This width can be determined from numerical solution by analysing a vicinity of the jet and looking for the threshold when the pressure drop approaches zero.

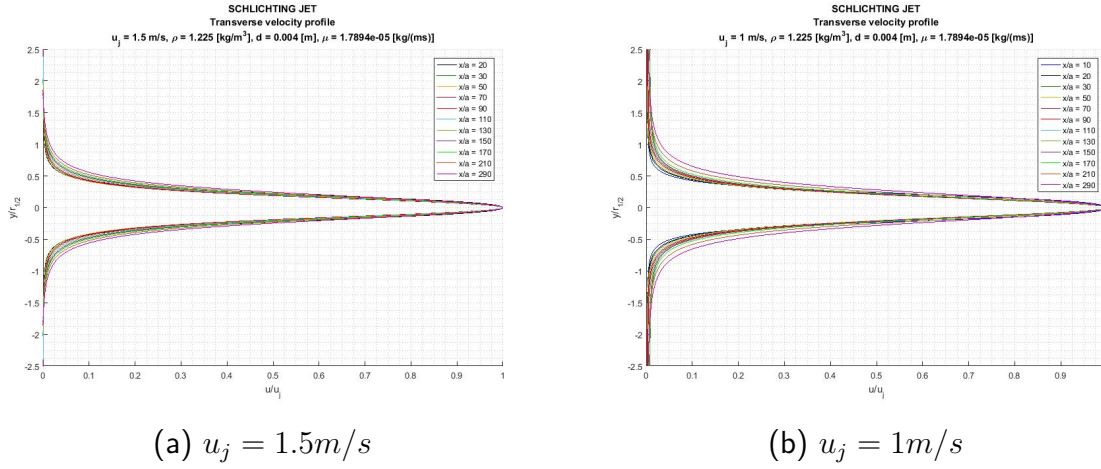


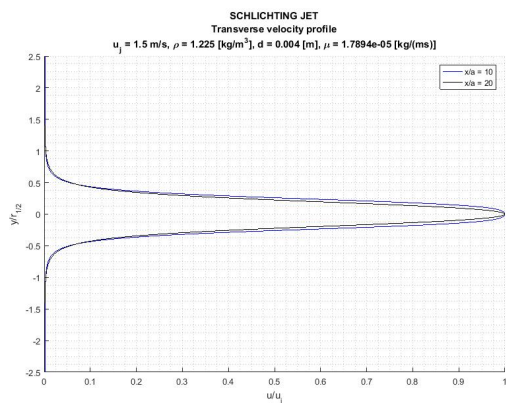
**Figure 8.9:** Numerical solution of the axisymmetric jet showing the self-similarity.

However as can be seen in Figure 8.10, the self-similarity can be considered from certain distance from the jet inlet only, the distance at which the self-similarity emerges can be seen in Figure 8.9a and 8.9b. Close to the jet, the velocity profile is not fully developed and the self-similarity does not hold true. Nevertheless, since the asymptotic solution is assuming an infinity inlet velocity and an infinitely small orifice, the solution is not valid close to the orifice anyway. This was also described in chapter 3. In addition, when the velocity decreases, it can be seen from the Figure 8.9b, the accuracy for scaling the velocity profile has to be increased in order to obtain self-similar velocity profile. This is very apparent on the shape of velocity profile for  $u_j = 1 \text{ m/s}$  for the distance  $x/a = 290$ . The shape of the velocity profile is wider compared to the one for  $u_j = 1.5 \text{ m/s}$ . This is caused by the fact that the same pressure drop threshold was used to scale the profiles. When the velocity is decreased, the actual pressure drop at the same distance is smaller thus higher accuracy is required to scale the profiles precisely.

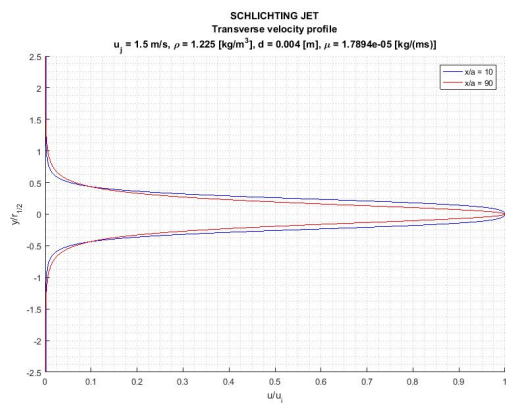
The undeveloped velocity profile can be seen in Figure 8.10a. In this case, the self-similarity cannot be considered since the jet is strongly influenced by the jet inlet. The sufficiently accurate self-similarity emerges approximately at  $x/a = 30$  in case of inlet velocity  $1.5 \text{ m/s}$ . This can be seen in Figure 8.10d. The difference between  $x/a = 30$  and  $x/a = 90$  is very small while when comparing velocity profile at  $x/a = 90$  to  $x/a = 10$  or  $20$ , the difference in shape of the curves is obvious.

Analysis of self-similarity is also a powerful tool in assessing the validity of the numerical solution of steady jet. In this case the self-similarity analysis shows very precise agreement of transverse velocity profiles along the  $x$ -direction and so the solution can be considered valid. Therefore it is possible to move forward and modify the initial velocity boundary condition by imposing the time-harmonic fluctuation, so the transient case can be calculated. In the following chapter, the results of pulsatile jets with different parameters of pulsation frequency and amplitude will be summarized and evaluated.

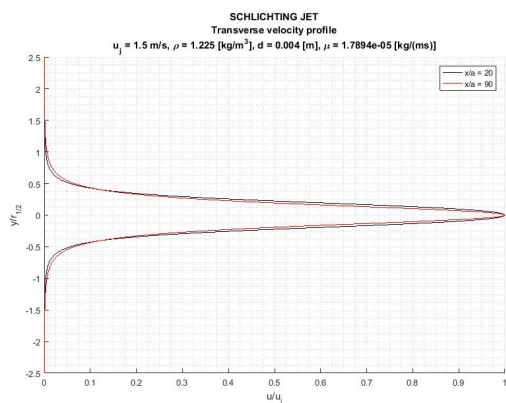
## 8. Validation and verification



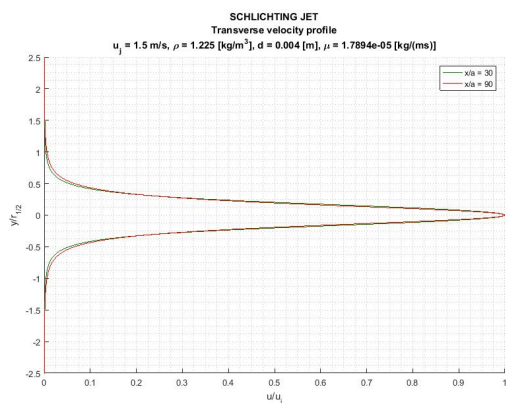
(a)  $\frac{x}{a} = 10$  vs  $\frac{x}{a} = 20$



(b)  $\frac{x}{a} = 10$  vs  $\frac{x}{a} = 90$



(c)  $\frac{x}{a} = 20$  vs  $\frac{x}{a} = 90$



(d)  $\frac{x}{a} = 30$  vs  $\frac{x}{a} = 90$

**Figure 8.10:** Comparison of transverse velocity profiles at different distances from the inlet.

# 9. Results of unsteady case

For assessing the influence of frequency and fluctuation of the jet, the numerical simulations were performed for parameters summarized in 9.1.

<b><math>u_j = 1 \text{ m/s}, \quad \text{Re} = 273.8</math></b>				
	<b>f</b>	<b><math>\epsilon</math></b>	<b>a</b>	<b>St</b>
Case 1 (time-step: 0.001)	3 Hz	1 %	0.002 mm	0.075
Case 2 (time-step: 0.001)	6 Hz	1 %	0.002 mm	0.15
 <b><math>u_j = 1 \text{ m/s}, \quad \text{Re} = 273.8</math></b>				
	<b>f</b>	<b><math>\epsilon</math></b>	<b>a</b>	<b>St</b>
Case 3 (time-step: 0.001)	6 Hz	1 %	0.002 mm	0.1
Case 4 (time-step: 0.001)	12 Hz	5 %	0.002 mm	0.2
Case 5 (time-step: 0.001)	24 Hz	5 %	0.002 mm	0.4
Case 6 (time-step: 0.0001)	48 Hz	5 %	0.002 mm	0.8
Case 7 (time-step: 0.00001)	48 Hz	5 %	0.002 mm	0.8
Case 8 (time-step: 0.0001)	96 Hz	5 %	0.002 mm	1.6
Case 9 (time-step: 0.001)	12 Hz	10 %	0.002 mm	0.2

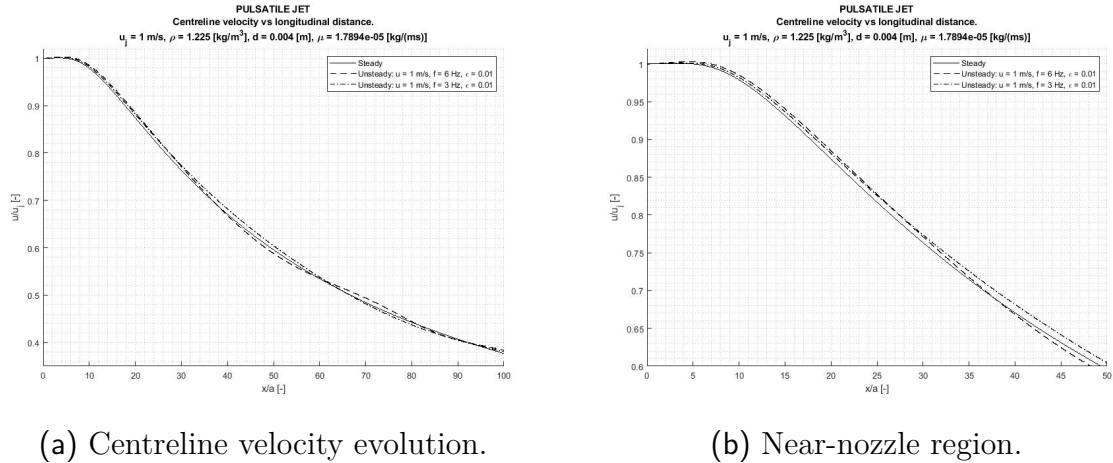
**Table 9.1:** Parameters of simulated pulsatile jets.

In order to ensure that the steady jet is stable, the Reynolds numbers were kept rather small. It was previously determined that an axisymmetric jet exhibit first instabilities around Reynolds numbers 550 which corresponds to initial velocity 2 m/s in our case. The emergence of instabilities can be seen in Figure D.3 that shows velocity contours for steady inlet velocity 2 m/s. Even though the jet stays stable near the nozzle, at some distance from it, it begins to exhibit unstable behaviour. This does not necessarily mean that the jet will transition to the turbulent, because as already reported by [8], [37] and others, the instabilities can emerge during the solution even though the jet will remain laminar. Either way, the simulation was not developed to grasp instabilities in the flow. Calculating such cases requires very complex analysis, therefore it was decided to keep the Reynolds number of the jet, with fluctuation included, below this value.

The computational itself has been performed using two meshes, the mesh 1 and mesh 3 from table 7.1. The mesh 3 has been used to calculate two cases of very small Strouhal numbers  $S = 0.075$  and  $S = 0.15$ . This calculation can be seen in Fig. 9.1 and Fig. 9.2, in both cases the  $\epsilon = 0.01$ . The calculation of both cases was very time demanding due to low initial velocity and extensive mesh size, it was primarily done as a baseline for setting up parameters so that the calculation could be performed using smaller mesh,

## 9. Results of unsteady case

thus saving computational power. As can be seen in the Fig. 9.2, for the lowest  $S = 0.075$ , the bigger mesh is really necessary in order to track the jet evolution to the point where the time-harmonic component decays entirely and the solution yields the classic Schlichting jet. However for  $S = 0.15$ , the mesh of this size is not necessary and the mesh 1 could have been used.



(a) Centreline velocity evolution. (b) Near-nozzle region.  
**Figure 9.1:** Jet evolution for Strouhal numbers 0.075 and 0.15, time-step = 0.001.

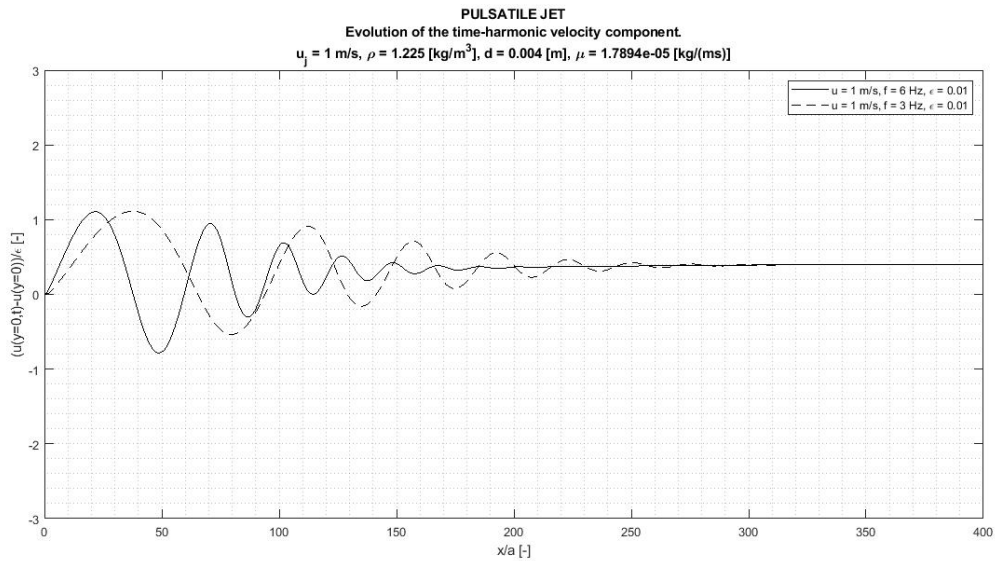


**Figure 9.2:** Results obtained for  $S = 0.075$  and  $0.15$  using mesh 3 (Tab 7.1)

It is also necessary to mention that increasing mesh size while preserving the same mesh refinement has resulted in misalignment of unsteady and steady solutions. This can be observed in Figure 9.2. The unsteady solution reached the steady state, yet it did not approach the steady solution precisely. This is the reason why the null value is not reached after the time-harmonic component of the velocity decays. This difference in velocity is negligible when considered from initial velocity point of view, since it is just 0.4 % of its

magnitude. The cause of this misalignment has not been discovered, the most probable cause are numerical errors emerging during the integration of Navier-Stokes equations as a consequence of discretization. Another possibility could be that the number of iteration was not sufficient and the solution could be made more accurate by dedicating more time for the computation. However, since this simulation was performed as a baseline only, the accuracy of the solution is sufficient for this purpose.

## 9.1. Strouhal number and jet evolution

In order to find out the influence of the Strouhal number, the simulation was performed for different frequencies while preserving the same velocity and for two different velocities while preserving the same frequency. It was found that the time-harmonic component decay depends strongly on frequency and jet velocity<sup>1</sup>. The time-harmonic component of the velocity decays more rapidly with increasing Strouhal number. This can be observed in Figures 9.3 and 9.4.

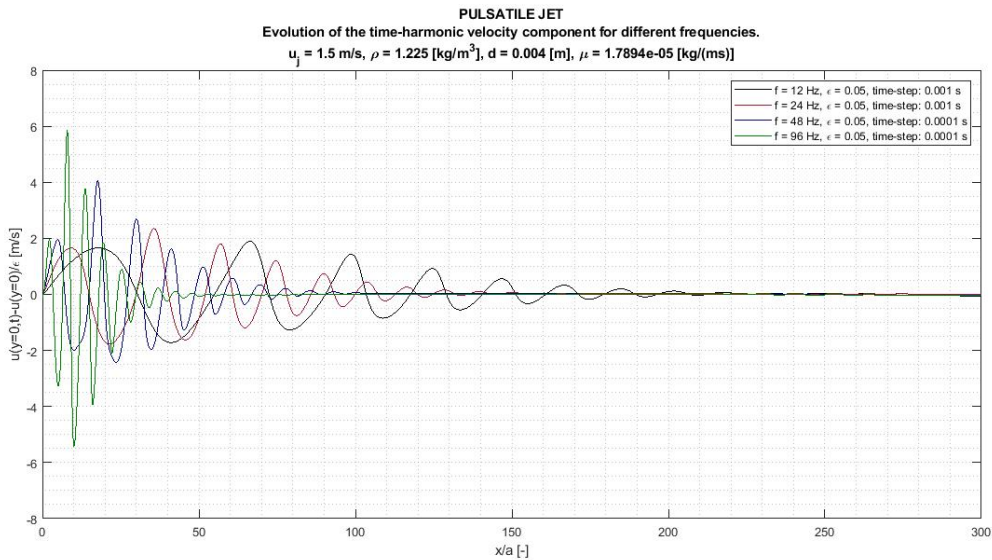


**Figure 9.3:** Evolution of the time harmonic component for different frequencies of pulsation.

Results also suggest that the increase in frequency of pulsation causes contraction of the flow in the near-nozzle region, the higher the frequency, the closer is the contraction to the nozzle. This results in a significant increase of the velocity in this region. It can be better seen in the following Figure, where only cases of  $f = 12$  Hz and  $f = 96$  Hz are

<sup>1</sup>Steady component of the velocity

## 9. Results of unsteady case

compared. The increase in velocity of the pulsatile jets forced by high frequency is quite significant.

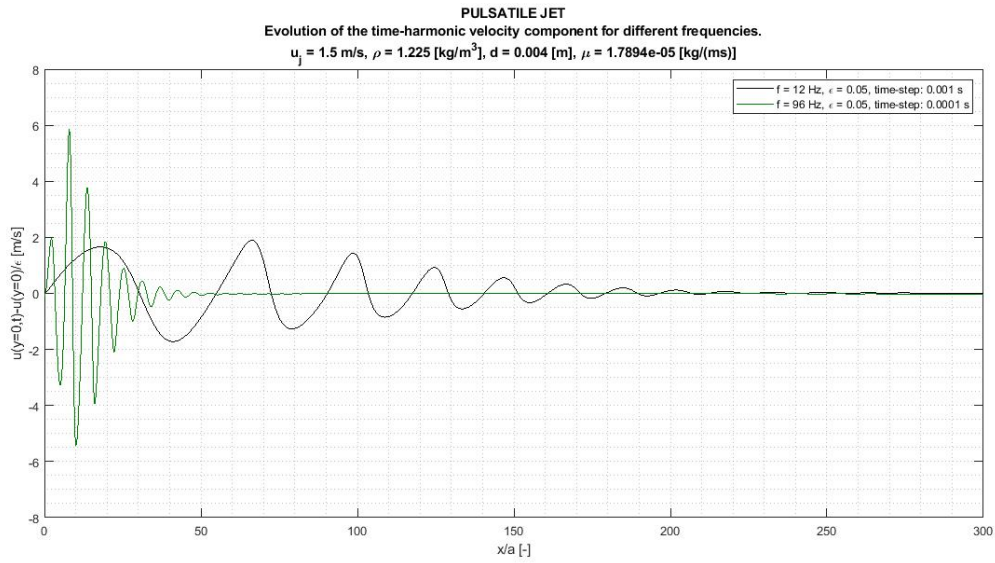


**Figure 9.4:** Evolution of the time harmonic component for  $f = 12 \text{ Hz}$  and  $f = 96 \text{ Hz}$ .

It can be also easily verified that the behaviour of the jet is not dependent only on the frequency, but on the steady velocity component as well, thus the Strouhal number is used as a key parameter when describing the behaviour of the pulsatile jets. The comparison of two pulsatile jets of the same frequency and fluctuation, but with different initial velocity can be seen in Figure 9.5.

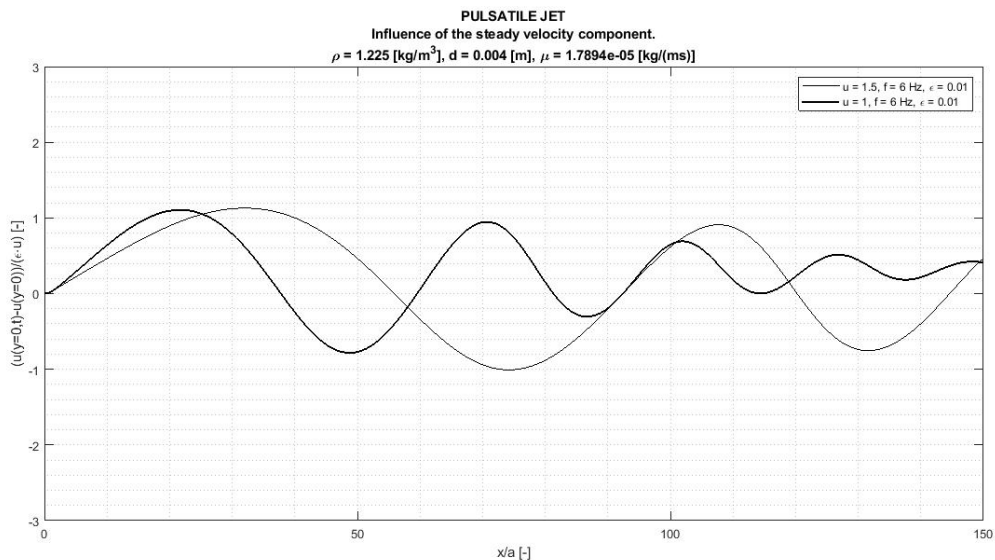


**Figure 9.5:** Influence of the steady velocity component on the disturbance propagation.

## 9.2. Impact of the fluctuation magnitude

The fluctuation itself has been also found to have a slight impact on the jet evolution. This is shown in Figure 9.6, where two pulsatile jets of the same frequency and initial velocity are compared. In the first case, a time-harmonic velocity component of 5% of the magnitude of steady velocity component was imposed onto the jet while in the second case the jet was forced using a time-harmonic velocity component of 10% of magnitude of the steady velocity component. A slight difference can be observed in the jet evolution however the decay rate of both cases is almost similar and the difference is negligible.

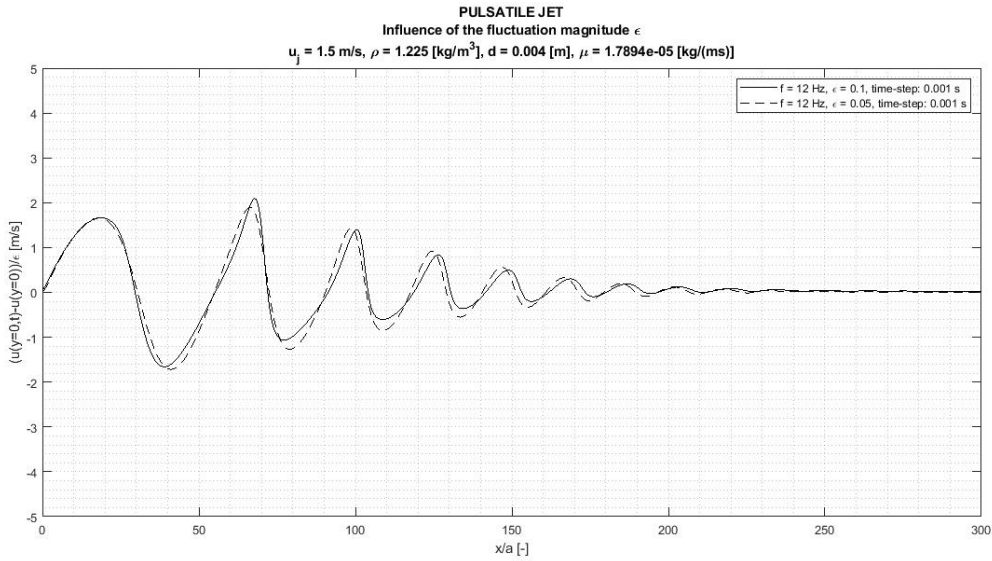


**Figure 9.6:** Influence of the fluctuation magnitude  $\epsilon$  on the jet evolution.

Moreover, the results did not suggest that the fluctuation magnitude has an impact on the laminar-transition behaviour of the jet if the maximum velocity is kept below the value of initial velocity of the steady jet for which the instabilities emerge even in steady case.

## 9.3. Pulsation and the jet entrainment

Finally, the impact of the pulsation on the jet entrainment has been investigated. The main measure of the jet entrainment is the radial velocity of the flow adjacent to the jet. In this case, the radial velocity along the whole domain has been considered and different frequencies of the same fluctuation were compared to steady jet. This comparison can be seen in Figure 9.7, where radial velocity with respect to transverse distance at different distances from inlet is shown.

## 9. Results of unsteady case

It has been anticipated that introducing pulsation should enhance the entrainment significantly. Nevertheless, the actual jet entrainment is much more complex problem. As can be seen in graphs shown below, pulsation has an influence only on the region very close to the jet, but the entrainment in this region can be affected strongly by imposing pulsation. Further away from the jet, the radial velocities align with the steady solution.

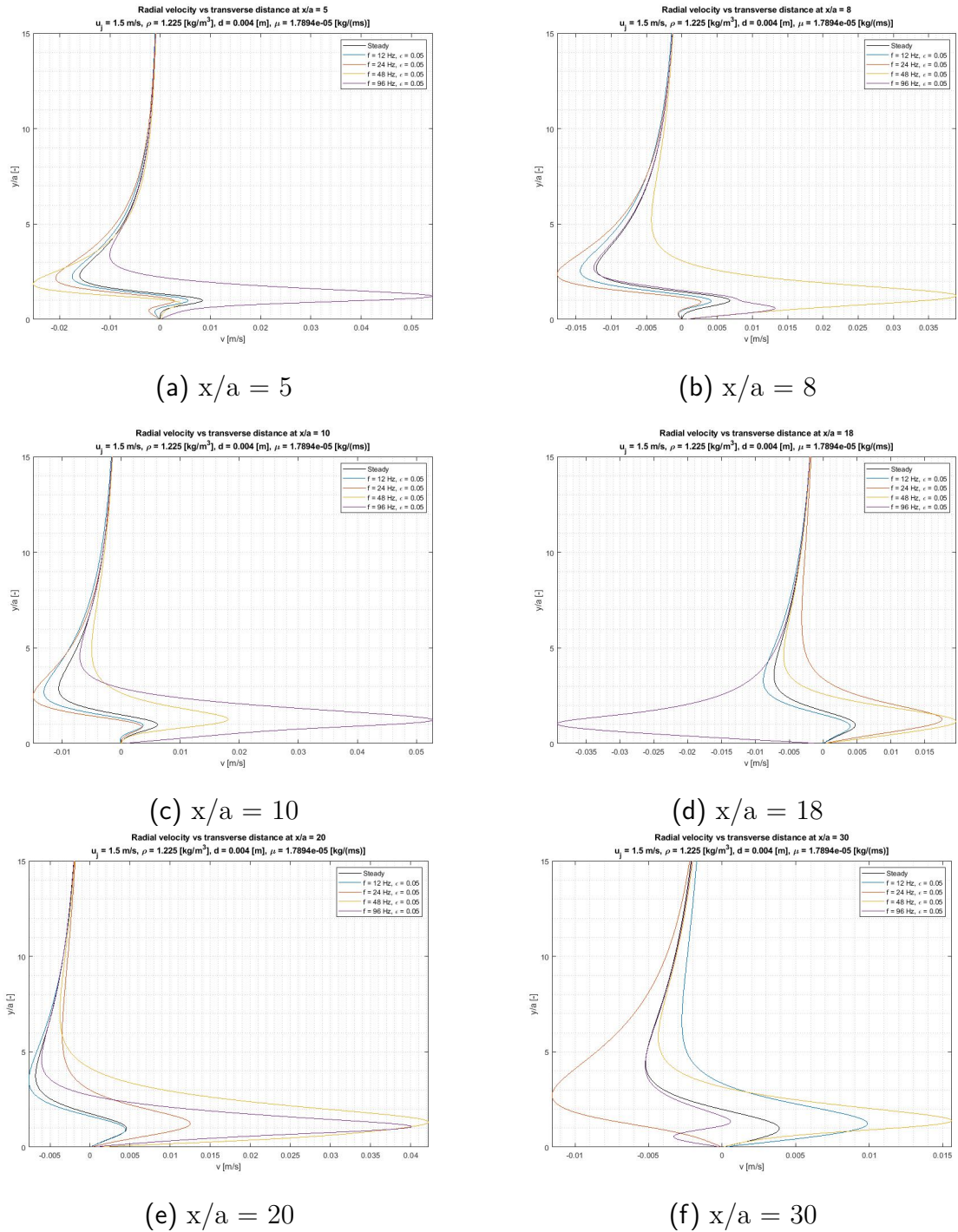


**Figure 9.7:** Radial velocity evolution at different distances from inlet.

In order to compare entrainments, the rate of change in mass with respect to change in longitudinal distance was introduced. This change can be determined from the continuity equation as follow

$$m = \int_0^{\infty} \rho \cdot u \, dy, \quad (9.1)$$

$$\int_0^{\infty} \left( \frac{\partial}{\partial x}(\rho \cdot u) + \frac{\partial}{\partial y}(\rho \cdot v) \right) dy = 0, \quad (9.2)$$

$$\int_0^{\infty} \frac{\partial}{\partial x}(\rho \cdot u) \, dy + \int_0^{\infty} \frac{\partial}{\partial y}(\rho \cdot v) \, dy = 0, \quad (9.3)$$

$$\frac{\partial}{\partial x} \int_{y=0}^{y=\infty} \rho \cdot u \, dy = - \rho \cdot v \Big|_{y=\infty}, \quad (9.4)$$

$$\boxed{\frac{\partial m}{\partial x} = - \rho \cdot v \Big|_{y=\infty}}. \quad (9.5)$$

This means that in order to assess the overall entrainment, the radial velocities along the whole domain<sup>2</sup> have to be retrieved and the average value at each longitudinal distance has to be calculated. In Ansys Fluent, there is not a straight forward method to retrieve velocity averages, therefore 30 transverse lines along the x-axis have been created in the interval  $x/a \in \langle 0, 50 \rangle$  so the radial velocities necessary for the calculation of entrainment can be exported to ASCII and further processed in MATLAB. The graph of jet entrainment based on interpolated data is shown in Figure 9.8. In this Figure, steady case is compared to pulsatile jets of  $S = 0.8$  and  $S = 1.6$ .

It is obvious that the entrainment of the jet is modified significantly in the area where the jet velocity oscillates. However sufficiently far from the jet inlet, where the pulsation decays and the jet yields the classical Schlichting jet, the entrainment approaches the steady case. Also, the results suggests that the entrainment fluctuation increases with the frequency increase. On the other hand, the region where the entrainment is changed

---

<sup>2</sup>The radial velocity was determined in each node of computational mesh in transverse direction to the jet axial velocity.

## 9. Results of unsteady case

decreases as the frequency increases. This is due to more rapid decay of the unsteady velocity component as was explained in previous section.

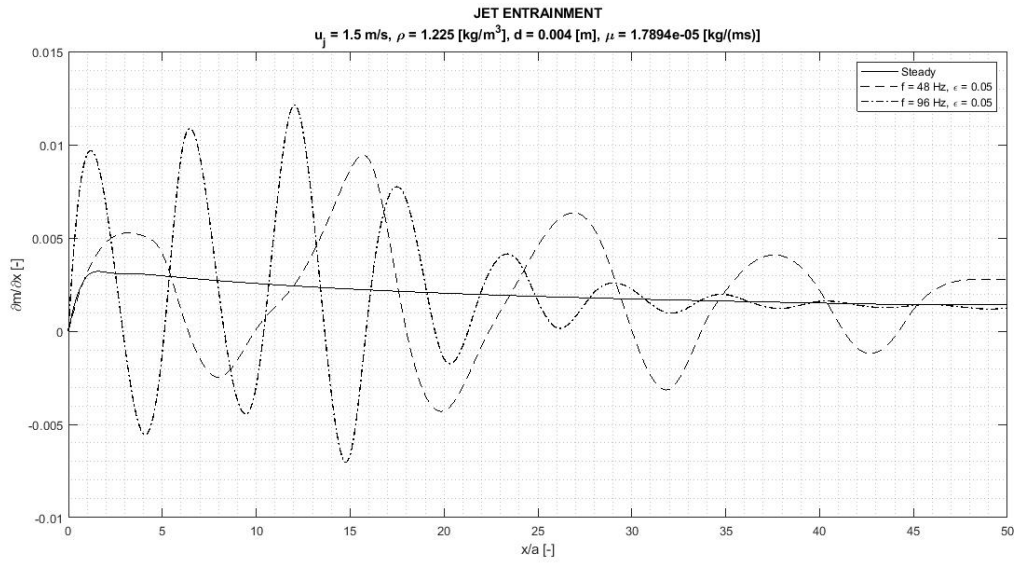


**Figure 9.8:** Jet entrainment vs longitudinal distance.

In Figure 9.8, the instantaneous entrainment for which the time-harmonic velocity equals null at the moment was shown. In the following picture, time-averaged jet entrainment can be seen.

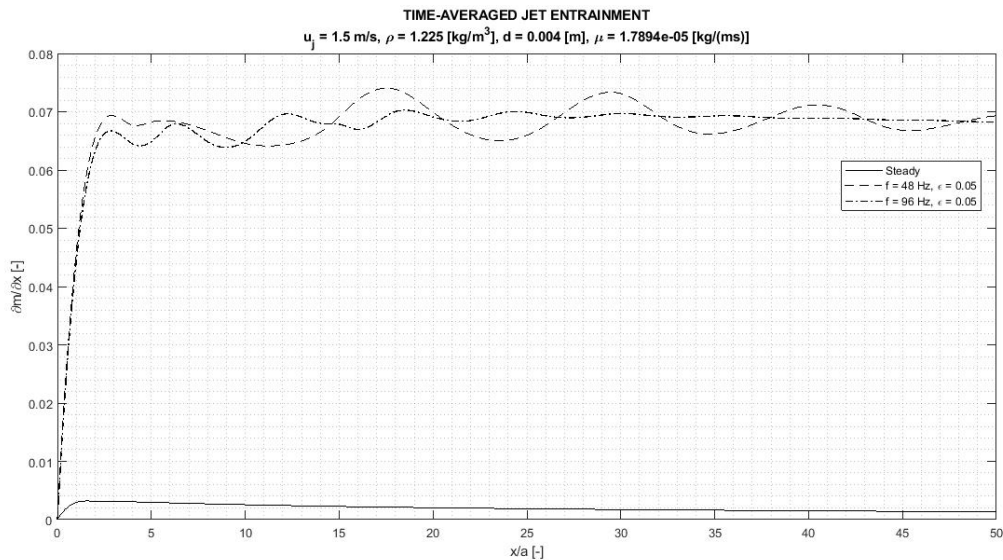


**Figure 9.9:** Time-averaged jet entrainment vs longitudinal distance.

In closing, it is clear that the pulsation has an impact on the jet entrainment and the Strouhal number of the pulsation can affect both the magnitude of the entrainment as

well as the longitudinal distance on which the entrainment is modified. This means that for each particular application, the appropriate Strouhal number has to be determined in order to achieve desired enhancement.

# 10. Conclusion

This thesis is focused on axisymmetric pulsatile jets and their physics that has not been fully comprehended so far. The main aim of the thesis was to create a numerical simulation of laminar pulsatile jet, using time-accurate integration of full Navier-Stokes equations, also known as Direct Numerical Simulation (DNS) and to investigate influence of the velocity, frequency and fluctuation on the evolution of pulsatile jet. In order to validate the numerical results, also an asymptotic solutions for both cases of steady jets were developed, for an axisymmetric jet known as a Schlichting jet as well as for a planar jet that is known as the Bickley jet. MATLAB codes of both asymptotic solutions can be found in appendix. The numerical solution was set up using Ansys Fluent 18.1. In case of pulsatile flow, the governing equations for incompressible flow were solved in their full form, including time while in case of steady jet flow, the governing equation were integrated in steady form, without considering a change in time. The transient simulations are very time-consuming therefore an enormous computational time has been dedicated to obtain results summarized herein. In addition, a great amount of the data has been processed and evaluated in order to draw conclusion.

The numerical solution herein presented was verified by all means available and the results are in agreement with studies performed by Marzouk [25] and Riley et al. [39] as well as with suggestions previously made by Marinnet [24]. The primary results of the present numerical study are following:

1. The axisymmetric laminar pulsatile jet develops into the steady Schlichting jet in a sufficient distance from the orifice.
2. Strouhal number is a critical parameter for the downstream evolution of the jet. The higher the Strouhal number, the faster the time-harmonic component of the velocity decays and the pulsatile jet reaches a steady state.
3. The results do not suggest that fluctuation magnitude triggers laminar-turbulent transition of the jet if the sum of the unsteady and steady velocity components is kept below the velocity that triggers instabilities in the flow even in steady case. On the other hand, the fluctuation magnitude slightly modifies the jet evolution.
4. Pulsation causes contraction of the jet, thus a local increase in axial velocity, which location depends on the frequency.
5. The entrainment of the pulsatile jet is also dependent on the Strouhal number and can be modified by changing the Strouhal number.

As previously suggested, the pulsation jets could find their application in combustion process since they can affect the jet entrainment and flame length. Moreover, as suggested by Sanchez-Sanz et al. [42], the flames are much more sensitive to the oscillation frequency than cold flows. The equivalent frequency variations lead to much sharper changes in flame behaviour which is caused by more significant viscosity variation induced

by the combustion. This also means that even though the results presented herein suggest that the pulsation could be used to enhance the jet entrainment in the combustion chambers, decrease flame length and consequently eliminate pollutants emerging during the combustion process, it is necessary to keep in mind that each application requires different parameters and the study should be performed for particular case of application, considering properties of the fluid that is to be used, in order to determine correct parameters of pulsation and to assess to what extent introducing pulsation will be beneficial.

Finally, an investigation of an influence of the pulsation on the flames could be one possible extensions to the work contained in this thesis. Moreover, the results presented in this study were verified numerically only, the experimental verification has not been done. This gives a room for further verification using experimental approach and attempting to simulate axisymmetric jet under laboratory conditions. Last but not least, this study could be extended to turbulent flows. Solving turbulent flows by DNS requires development of an in-house code designed solely for this purpose. Previous studies suggest that the most efficient approach to solving partial differential equation describing turbulent flows might be a spectral method. DNS of turbulent flows requires solving full unsteady Navier-Stokes equation of much higher Reynolds numbers on enormously fine mesh, therefore the solver must be able to solve PDEs very efficiently in order to make the simulation feasible. This is due to the fact that the finest scales of turbulence, also known as Kolmogorov scales, have to be resolved, which requires tremendous computational power and time. Nevertheless, such a study could bring a significant breakthrough in the field of laminar-turbulent transition and combustion process hence it is worth the effort. The laminar-turbulent transition in the jets still remains to be veiled in mystery and not even the exact critical Reynolds number of transition is known for the time being.

# Bibliography

- [1] ANDRADE, C. DA N. E. and TSIEN, C.L. The velocity-distribution in a liquid-into-liquid jet. *Proceedings of the Physical Society* [online]. 1937, 49(4), 381-391. DOI: 10.1088/0959-5309/49/4/309. ISSN 0959-5309.
- [2] *ANSYS FLUENT 6.3 Documentation*, 2006 [online]. ANSYS. <https://www.sharcnet.ca/Software/Fluent6/index.htm>
- [3] *ANSYS FLUENT 12.0 User's Guide*, 2009 [online]. ANSYS. [http://www.afs.enea.it/project/neptunius/docs/fluent/html/ug/main\\_pre.htm](http://www.afs.enea.it/project/neptunius/docs/fluent/html/ug/main_pre.htm)
- [4] BATCHELOR, K. G. and GILL, E. A. Analysis of the stability of axisymmetric jets. *Journal of Fluid Mechanics* [online]. 1962, 14(4), 529-551. <https://doi.org/10.1017/S0022112062001421>
- [5] BENDER M.C. and ORSZAG, A. S. *Advanced Mathematical Methods for Scientists and Engineers I: Asymptotic Methods and Perturbation Theory* Springer, New York, NY. 1999. p. 593. ISBN: 978-1-4757-3069-2. <https://doi.org/10.1007/978-1-4757-3069-2>
- [6] BICKLEY, W. G. The plane jet. *The London, Edinburgh, and Dublin Philosophical Magazine and Journal of Science*. Elsevier, 2009 23(156), 727-731. <https://doi.org/10.1080/14786443708561847>
- [7] BINDER, G. and FAVRE-MARINET, M. Some Characteristics of Pulsating or Flapping Jets, *Unsteady Turbulent Shear Flows, Symposium Toulouse, France* [online]. Berlin Heidelberg New York: Springer-Verlag, 1981, 370-378. DOI: 10.1007/978-3-642-81732-8\_31.
- [8] CANTWELL, J. B. Transition in the axisymmetric jet. *Journal of Fluid Mechanics* [online]. 1981, 104, 369-386. DOI: 10.1017/S0022112081002954.
- [9] CARPENTER, P. W. and HOUGHTON, E. L. *Aerodynamics for Engineering Students*. 5th ed. Oxford: Butterworth-Heinemann, 2003. p. 590. ISBN 0-7506-5111-3.
- [10] CASTELVECCHI, D. On the trail of turbulence. *Nature*. [online]. London: Nature Publishing Group, 2017, 548(7668), 382-383. ISSN 00280836. <http://search.proquest.com/docview/1932293963/>
- [11] EL-SAYED, F. A. *Fundamentals of Aircraft and Rocket Propulsion*. 1th ed. London: Springer, 2016. p. 1010. DOI: 10.1007/978-1-4471-6796-9. ISBN 978-1-4471-6796-9.
- [12] FALLE, S. SELF-SIMILAR JETS. *Monthly Notices Of The Royal Astronomical Society* [online]. OXFORD UNIV PRESS, 1991, 250(3), 581-596 [cit. 2019-02-02]. DOI: 10.1093/mnras/250.3.581. ISSN 0035-8711.
- [13] *Federal Aviation Administration - Aviation Emissions, Impacts & Mitigation: A Primer*, 2015 [online]. FAA. [https://www.faa.gov/regulations\\_policies/policy\\_guidance/envir\\_policy/media/Primer\\_Jan2015.pdf](https://www.faa.gov/regulations_policies/policy_guidance/envir_policy/media/Primer_Jan2015.pdf)

- [14] FAROKHI, S. *Aircraft Propulsion*. 2nd. Chichester: John Wiley & Sons, 2014. p. 1011. ISBN 978-1-118-80677-7.
- [15] GEORGE, K. W. *Lectures in Turbulence for the 21st Century*. [online] Release Date: January 16, 2013. p. 353. [http://www.turbulence-online.com/Publications/Lecture\\_Notes/Turbulence\\_Lille/TB\\_16January2013.pdf](http://www.turbulence-online.com/Publications/Lecture_Notes/Turbulence_Lille/TB_16January2013.pdf)
- [16] GRATTON, J. Similarity and Self Similarity in Fluid Dynamics. *Fundamentals of Cosmic Physics*. Gordon and Breach Science Publishers, Inc., United Kingdom, 1991, 15, 1-106. ISSN 0009-7330.
- [17] HEWIT, E. R. and DUCK, W.P. Pulsatile jets. *Journal of Fluid Mechanics*. [online]. Cambridge University Press, 2011, 670, 240-259 DOI: 10.1017/S00221120100052277
- [18] HOSSEINI, S.M. et al. Direct numerical simulation of the flow around a wing section at moderate Reynolds number. *International Journal of Heat and Fluid Flow* [online]. Elsevier, 2016, 61(PA), 117-128. DOI: 10.1016/j.ijheatfluidflow.2016.02.001. ISSN 0142-727X.
- [19] JAYANTI, S. *Computational Fluid Dynamics for Engineers and Scientists*. Dordrecht: Springer, 2018. 402 p. DOI: 10.1007/978-94-024-1217-8. ISBN 978-94-024-1217-8.
- [20] KENTFIELD, J.A.C. Fundamentals of Idealized Airbreathing Pulse-Detonation Engines. *Journal of Propulsion and Power*. Elsevier, 2002 18, 77-83. <https://doi.org/10.2514/2.5900>
- [21] KRUEGER, P. S. *The significance of vortex ring formation and nozzle exit over-pressure to pulsatile jet propulsion*. Pasadena USA, 2001 Dissertation (Ph.D.), California Institute of Technology. <http://resolver.caltech.edu/CaltechETD:etd-09142005-111030>
- [22] LESIEUR, Marcel. *Turbulence in Fluids*. 4th. Dordrecht: Springer, 2008. p. 592. ISBN 978-1-4020-6435-7.
- [23] MALMGREN, A. and RILEY, G. Biomass Power Generation, *Reference Module in Earth Systems and Environmental Sciences*. [online]. Elsevier, 2012, 5, 27-53. DOI: 10.1016/B978-0-08-087872-0.00505-9. ISBN 9780124095489.
- [24] FAVRE-MARINET, M., BINDER, G. and HAC, V. TE. Generation of Oscillating Jets, *Journal of Fluids Engineering* [online]. 1981, 103(4), 609-614. DOI: 10.1115/1.3241780.
- [25] MARZOUK, S. et al. Numerical study of a heated pulsed axisymmetric jet in laminar mode. *Numerical Heat Transfer, Part A: Applications* [online]. Informa UK, 2003, 43(4), 409-429. DOI: 10.1080/10407780307360. ISSN 1040-7782.
- [26] MCLEAN, Doug. *UNDERSTANDING AERODYNAMICS Arguing from the Real Physics*. Chichester: John Wiley & Sons, 2013. p. 550. ISBN 978-1-1199-6751-4.

- [27] MOIN, P. and KRISHNAN, M. DIRECT NUMERICAL SIMULATION: A Tool in Turbulence Research. *Annual Review of Fluid Mechanics*, 30, 1998, p.539-578. <https://doi.org/10.1146/annurev.fluid.30.1.539>.
- [28] NASA Global Climate Change - Vital Signs of the planet 2019 [online]. NASA. [https://climate.nasa.gov/climate\\_resources/24/graphic-the-relentless-rise-of-carbon-dioxide/](https://climate.nasa.gov/climate_resources/24/graphic-the-relentless-rise-of-carbon-dioxide/)
- [29] NASA Langley Research Center - Turbulence Modeling Resource, 2015 [online]. NASA. [https://turbmodels.larc.nasa.gov/jetsubsonic\\_val.html](https://turbmodels.larc.nasa.gov/jetsubsonic_val.html)
- [30] O'MALLEY E, R. Singular Perturbation Theory: A Viscous Flow out of Göttingen. *Annual Review of Fluid Mechanics* [online]. Annual Reviews, 2009, 42. 1-17. DOI: 10.1146/annurev.fluid.060909.133212.
- [31] POPE, S. B. *Turbulent flows*. Cambridge; New York: Cambridge University Press, 2000, xxxiv, 771 p. ISBN 978-0-521-59886-6.
- [32] POVINELLI, L. and YUNGSTER, S. Airbreathing Pulse Detonation Engine Performance - NASA/TM-2002-211575. *Combustion, Airbreathing Propulsion, Propulsion Systems Hazards, and Modelling and Simulation Subcommittees Joint Meeting* [online]. 2002. <http://hdl.handle.net/2060/20020063440>
- [33] POVINELLI, L. Pulse Detonation Engines for High Speed Flight - NASA/TM-2002-211908. *11th International American Inst. of Aeronautics and Astronautics and Association Aeronautique et Astronautique de France Conference* [online]. 2002. <http://hdl.handle.net/2060/20020082902>
- [34] POZRIKIDIS, C. *Fluid Dynamics: Theory, Computation, and Numerical Simulation*. 3rd ed. 2017. Boston, MA: Springer US, 2017. 901 p. DOI: 10.1007/978-1-4899-7991-9. ISBN 9781489979902.
- [35] RANKIN, W. G. et al. An experimental investigation of laminar axisymmetric submerged jets. *Journal of Fluid Mechanics* [online]. 1983, 133, 217-231. <https://doi.org/10.1017/S0022112083001871>
- [36] REVUELTA, A., SÁNCHEZ L. and LIÑAN, A.: The virtual origin as a first-order correction for the far-field description of laminar jets. *Physics of Fluids* [online]. American Institute of Physics, 2002, 14(6), 1821-1824 [cit. 2019-02-13]. DOI: 10.1063/1.1473650. ISSN 1070-6631.
- [37] REYNOLDS, J. A. Observation of a liquid-into-liquid jet. *Journal of Fluid Mechanics* [online]. Cambridge University Press, 1962, 14(4), 552-556. DOI:10.1017/S0022112062001433
- [38] RILEY, N. and DRAZIN, P. *The Navier–Stokes equations: a classification of flows and exact solutions*. 1th ed. Cambridge University Press: Cambridge, 2006. p. 196. ISBN 978-0-521-68162-9.
- [39] RILEY, N., SANCHEZ-SANZ, M. and WATSON, E. J.: A planar pulsating jet. *Journal of Fluid Mechanics* [online]. Cambridge University Press, 2009, 638, 161-172. DOI: 10.1017/S0022112009991261. ISSN 0022-1120.

- [40] Rolls-Royce plc. *The jet engine* 5th ed. Birmingham: Renault Printing Co Ltd, 1996. 278 p. ISBN 0902121 235.
- [41] ROSENHEAD, L. *Laminar Boundary Layers*. Mineola, N.Y.: Dover Publications Inc., 1988. 687 p. ISBN 0-486-65646-2.
- [42] SANCHEZ-SANZ, M. et al. Influence of Strouhal number on pulsating methane–air coflow jet diffusion flames. *Combustion Theory and Modelling*. [online]. 2010, 14(3), 453-478,. DOI: 10.1080/13647830.2010.490048. ISSN: 1364-7830.
- [43] SÁNCHEZ–SANZ, M., ROSALES, M. and SÁNCHEZ, L. A. The hydrogen laminar jet. *International Journal of Hydrogen Energy* [online]. Elsevier, 2010, 35(8), 3919-3927. DOI: 10.1016/j.ijhydene.2010.01.081. ISSN 0360-3199.
- [44] SCHLICHTING, H. *Boundary-Layer Theory*. 7th ed. New York: McGraw-Hill, 1979, 817 p. ISBN 0-07-055334-3.
- [45] SCHLICHTING, H. Laminare Strahlausbreitung. *ZAMM - Journal of Applied Mathematics and Mechanics / Zeitschrift für Angewandte Mathematik und Mechanik* [online]. Berlin: WILEY-VCH Verlag, 1933, 13(4), 260-263. DOI: 10.1002/zamm.19330130403. ISSN 0044-2267.
- [46] SPALART, P. and VENKATAKRISHNAN, V. On the role and challenges of CFD in the aerospace industry. *The Aeronautical Journal* [online]. 2016 120(1223), 209-232. DOI: 10.1017/aer.2015.10. ISSN 00019240. <http://search.proquest.com/docview/1963547764/>
- [47] SPURK J. and AKSEL, N. *Fluid Mechanics*. 2nd ed. Berlin Heidelberg New York: Springer-Verlag, 2008. 531 p. DOI: 10.1007/978-3-540-73537-3. ISBN 978-3-540-73537-3.
- [48] TENNEKES, H. and LUMLEY, L. J. *A First Course in Turbulence*. Cambridge, Massachusetts: MIT Press, 1972. p. 300. ISBN 0-262-20019-8.
- [49] The Economist. *Negative Emission. What they don't tell you about climate change*. London: The Economist Group. 2017. <https://www.economist.com/leaders/2017/11/16/what-they-dont-tell-you-about-climate-change>.
- [50] *US Environmental Protection Agency - Sources of Greenhouse Gas Emissions 2016* [online]. EPA. <https://www.epa.gov/ghgemissions/sources-greenhouse-gas-emissions#transportation>
- [51] WANG, Z. et al. Direct Numerical Simulation of Subsonic Round Turbulent Jet. *Flow, Turbulence and Combustion* [online]. Dordrecht: Springer Netherlands, 2010, 84(4), 669-686 [cit. 2019-02-03]. DOI: 10.1007/s10494-010-9248-5. ISSN 1386-6184.
- [52] YELLIN, L. Laminar-Turbulent Transition Process in Pulsatile Flow. *Circulation Research* [online]. American Heart Association, 1966, 19(4), 791-804. DOI: 10.1161/01.RES.19.4.791. ISSN 0009-7330.

# 11. Symbols and abbreviations

$A$	nozzle area
$a$	nozzle radius
$b_{1/2}$	width of the turbulent jet
$d$	nozzle diameter
$g$	body accelerations acting on the continuum due to gravity or other potential field
$K$	kinematic momentum ( $M/\rho$ )
$M$	momentum flux
$\dot{m}$	mass flow rate
$N$	number of molecules
$Q, \dot{V}$	volume flow rate
$p$	total pressure
$r_{1/2}$	jet half width
$Re$	Reynolds number
$t$	time
$u$	longitudinal velocity
$\mathbf{u}$	velocity vector
$U_j$	inlet velocity
$v$	transverse velocity
$\bar{v}$	vector form of mean-velocity
$x$	coordinate in flow direction
$x_0^p$	virtual origin coordinate for parabolic velocity profile
$x_0^r$	virtual origin coordinate for rectangular velocity profile
$y$	coordinate perpendicular to flow direction
$\alpha$	constant (in equation 2.13)

$\delta_0$	characteristic width of the jet
$\nabla$	divergence
$\eta, \xi$	similarity variables
$\epsilon$	magnitude of fluctuation of the inlet velocity
$\epsilon_0$	virtual kinematic viscosity
$\gamma$	integration constant
$\omega$	pulsation frequency
$\nu$	kinematic viscosity
$\psi$	stream function
$\rho$	density
DNS	Direct Numerical Simulation
LE	Left Edge
O	Outflow
ODE	Ordinary Differential Equations
PDE	Partial Differential Equations
PISO	Pressure-Implicit with Splitting of Operators
P-O	Pressure-Outlet
RE	Right Edge
UDF	User-Defined Function
UE	Upper Edge
V-I	Velocity-Inlet
SIMPLE	Semi-Implicit Method for Pressure Linked Equations
SIMPLEC	Semi-Implicit Method for Pressure Linked Equations-Consistent

# 12. List of Figures and Tables

## List of Figures

1.1	The rise of carbon dioxide in the atmosphere [28]. . . . .	11
2.1	Pratt & Whitney F119 thrust-vectoring jet aircraft engine that powers F-22 Raptor fighter aircraft during a operational test and evaluation run up. . .	12
2.2	Perturbation theory and boundary layer problem. . . . .	14
2.3	Stream-lines and velocity profile of the laminar plane jet [6]. . . . .	18
2.4	Exhaust of rocket engine [15]. . . . .	19
2.5	Wake behind the airfoil [9]. . . . .	20
2.6	Plane turbulent wake [48]. . . . .	21
2.7	Plane turbulent mixing layer [48]. . . . .	21
3.1	A sketch of a axisymmetric jet with polar-cylindrical coordinate system [31]	22
3.2	Streamline pattern for a circular laminar jet [44]. . . . .	25
3.3	Comparison of decay speed of Schlichting jet and Bickley jet issuing from the orifice with similar characteristic dimension. . . . .	27
4.1	Expansion, rotation and deformation of small discoidal fluid parcel that occurs during infinitesimal period of time in a two-dimensional flow [34]. .	29
4.2	Plane turbulent jet [48] and its velocity profile that has the same shape as the laminar case. . . . .	31
4.3	Development of a turbulent plane jet [48] with the plug velocity profile at the orifice. . . . .	32
4.4	DNS of a two-dimensional spatially growing Bickley jet [22]. . . . .	34
6.1	Humphrey cycle [11] . . . . .	39
6.2	Valved pulsejet [11] . . . . .	39
6.3	Valveless pulsejet [11] . . . . .	40
6.4	Pressure contours showing the growth of the detonation wave [32] . . . . .	42
7.1	Domain. . . . .	43
7.2	Mesh refinement. . . . .	43
7.3	Residuals of calculation. . . . .	51
8.1	Comparison of boundary condition outflow and pressure-outlet. . . . .	53
8.2	Development of centreline velocity with respect to inlet velocity. . . . .	54
8.3	Transverse velocity profiles for an inlet velocity $u_j = 1 \text{ m/s}$ . . . . .	55
8.4	Transverse velocity profiles for an inlet velocity $u_j = 1.5 \text{ m/s}$ . . . . .	55
8.5	Development of centreline velocity with respect to inlet velocity. . . . .	56
8.6	Frequency and time-step size dependency. . . . .	58
8.7	Validation of the time-step size. . . . .	58
8.8	Evolution of time-harmonic component of the velocity. . . . .	59
8.9	Numerical solution of the axisymmetric jet showing the self-similarity. . . .	60

8.10	Comparison of transverse velocity profiles at different distances from the inlet. . . . .	61
9.1	Jet evolution for Strouhal numbers 0.075 and 0.15, time-step = 0.001. . . .	63
9.2	Results obtained for $S = 0.075$ and 0.15 using mesh 3 (Tab 7.1) . . . . .	63
9.3	Evolution of the time harmonic component for different frequencies of pulsation. . . . .	64
9.4	Evolution of the time harmonic component for $f = 12$ Hz and $f = 96$ Hz. . .	65
9.5	Influence of the steady velocity component on the disturbance propagation. .	65
9.6	Influence of the fluctuation magnitude $\epsilon$ on the jet evolution. . . . .	66
9.7	Radial velocity evolution at different distances from inlet. . . . .	67
9.8	Jet entrainment vs longitudinal distance. . . . .	69
9.9	Time-averaged jet entrainment vs longitudinal distance. . . . .	69
D.1	Axial velocity contours for inlet velocity $u = 1.5$ m/s . . . . .	97
D.2	Axial velocity contours for inlet velocity $u = 1.5$ m/s at near-nozzle region. .	97
D.3	Axial velocity contours for inlet velocity $u = 2$ m/s. . . . .	98
D.4	Axial velocity contours for inlet velocity $u = 2$ m/s at near-nozzle region. .	98

## List of Tables

7.1	Mesh dimensions and number of nodes. . . . .	44
8.1	Boundary conditions combinations that have been tested. . . . .	52
9.1	Parameters of simulated pulsatile jets. . . . .	62

# List of Codes

7.1	User Defined Function modulating the steady jet by imposing time-harmonic fluctuation on the jet. . . . .	50
A.1	Analytical solution of Bickley jet. . . . .	83
B.1	Analytical solution of Schlichting jet. . . . .	89

# Appendices

# A. Bickley jet MATLAB code

In this appendix, the MATLAB code of analytical solution for Bickley jet is attached. This solution does not include the first-order correction.

```
1  %%%%%%%%%%%%%%%%%%%%%%%%%%%%%%%%%%%%%%%%%%%%%%%%%%%%%%%%%%%%%%%%%%%%%%%%%%
2  %%%%%%%%%%          ANALYTICAL SOLUTION OF BICKLEY JET          %%%%%%%%%%
3  %%%%%%%%%%          JIRI DOLINSKY          %%%%%%%%%%
4  %%%%%%%%%%%%%%%%%%%%%%%%%%%%%%%%%%%%%%%%%%%%%%%%%%%%%%%%%%%%%%%%%%%%%%%%%%
5
6  % This solution is based on the analytical solution firstly introduced
7  % by W. G. Bickley in 1937.
8
9  clc, clear all, close all
10
11 %% INPUT DATA
12
13 prompt = {'Fluid density [kg/m^3]', 'Nozzle diameter [m]', ...
14          'Dynamic viscosity [kg/(ms)]', 'Velocity at the inlet [m/s]', ...
15          'Location in which axial velocity profile will be determined [m]', ...
16          'Define the x-coordinate of monitoring point for Fluent', ...
17          'x-coordinate of inlet in Fluent (must be defined for comparison)'};
18 input_dlg_name = 'INPUT VALUES';
19 dims = [1 70];
20 definput = {'1.225', '0.004', '1.7894e-05', '0.5', '0.3', '0.3', '0.05'};
21 inputdata = inputdlg(prompt, input_dlg_name, dims, definput);
22
23 size_inputdata = size(inputdata);
24 if size_inputdata == 0
25     return
26 end
27
28 rho = str2double(inputdata(1));           % fluid density [kg/m^3]
29 d = str2double(inputdata(2));             % nozzle diameter [m]
30 mu = str2double(inputdata(3));           % dynamic viscosity [kg/(ms)]
31 u_j = str2double(inputdata(4));          % velocity at the inlet [m/s]
32 % location in which the axial velocity profile is determined [m]
33 x_uprofil = str2double(inputdata(5));
34 % define the x-coordinate of monitoring point [m]
35 x = str2double(inputdata(6));
36 % define the inlet position in fluent
37 x_orifice_fluent = str2double(inputdata(7));
38
39 nu = mu/rho;                             % kinematic viscosity [m^2/s]
40 a = d/2;                                  % half of the nozzle diameter [m]
41 Re = u_j*2*a/nu;                          % Reynolds number [-]
42
43 %% LONGITUDINAL VELOCITY DISTRIBUTION
44
45 % Centreline definition
46 step = 0.01;
47 x_max = 10 * Re * a;
```

```

48 y_lvd = 0;
49
50 answer = questdlg(sprintf(['Maximum value for x is set by default',...
51     ' as 10 * Re * a.\n Do you want to change this value?']));
52 % Handle response
53 switch answer
54     case 'Yes'
55         str_x_value = 'Y';
56     case 'No'
57         str_x_value = 'N';
58     case 'Cancel'
59         str_x_value = 'C';
60 end
61
62 if str_x_value == 'N'
63     x_lvd = 0 : step : round(x_max,2);
64 elseif str_x_value == 'Y'
65     user_defined_xmax = inputdlg('Define your new x max.',...
66         'Fluent data file', [1 50]);
67     sz_user_defined_xmax = size(user_defined_xmax);
68     if sz_user_defined_xmax(1) == 0
69         return
70     elseif isnan(str2double(user_defined_xmax{1}))
71         disp('INTERRUPTED: x max not defined')
72         return
73     else
74         x_max = str2double(user_defined_xmax(1));
75         x_lvd = 0 : step : round(x_max,2);
76     end
77 else
78     return
79 end
80
81 %% CALCULATION
82
83 % Momentum of plug velocity profile
84 M = 4 * rho * u_j^2 * a;
85
86 % Calculation of similarity
87 eta_lvd = y_lvd * x_lvd.^(-2/3);
88 xi_lvd = 0.5 * (M ./ (6*nu^2 * rho .* x_lvd.^2)).^(1/3) * y_lvd;
89
90 % Calculation of longitudinal velocity
91
92 u_lvd = 0.25 * ((6 * M^2) ./ (nu * rho^2 .* x_lvd)).^(1/3)...
93     .* (sech(xi_lvd)).^2;
94
95 %% NOTE
96
97 % Calculation of transverse velocity
98 % v = ((M * nu) ./ (6 * rho .* x^2)).^(1/3) * (2 * xi * (sech(xi)).^2...
99 % - tanh(xi))
100
101 %% LONGITUDINAL VELOCITY PROFILE AT DISTANCE X
102
103 u_uprofil = 1;

```

```

104 y_loc = 0;
105
106 while u_uprofil > 0.001
107     xi = 0.5 * (M./(6 * nu^2 * rho .* x_uprofil.^2)).^(1/3) .* y_loc;
108     u_uprofil = 0.25 * ((6 * M^2)./(nu * rho^2 .* x_uprofil)).^(1/3)...
109         .* (sech(xi)).^2;
110     y_loc = y_loc + 0.001;
111
112 end
113
114 y_uprofil = linspace(-y_loc,y_loc,1000);
115
116 eta = y_uprofil .* x_uprofil.^(-2/3);
117
118 xi = 0.5 * (M./(6 * nu^2 * rho .* x_uprofil.^2)).^(1/3) .* y_uprofil;
119
120 u_uprofil = 0.25 * ((6 * M^2)./(nu * rho^2 .* x_uprofil)).^(1/3)...
121     .* (sech(xi)).^2;
122
123 %% MASS FLOW RATE
124
125 Q = (36 * M* nu * rho^2 .* x_lvd).^(1/3);
126
127 %% PLOT
128
129 % plot centreline velocity
130 figure
131 plot(x_lvd,u_lvd)
132 xlabel('x [m]')
133 ylabel('u [m/s]')
134 title({'BICKELY (PLANAR) JET';...
135     'Centreline velocity on longitudinal distance.'})
136 grid minor
137 axis([0 x_max 0 1.1*u_j])
138
139 % plot axial velocity profil across the jet
140 figure
141 plot(u_uprofil,y_uprofil)
142 xlabel('u [m/s]')
143 ylabel('y [m]')
144 title({'BICKELY (PLANAR) JET';...
145     'Transverse velocity profil at distance x.'})
146 grid minor
147 axis([0 max(u_uprofil)*1.05 -y_loc y_loc])
148
149 % plot volume flow rate
150 figure
151 plot(x_lvd,Q)
152 xlabel('x [m]')
153 ylabel('m [kg/s]')
154 title('Mass flow rate on longitudinal distance.')
155 grid minor
156 axis([0 x_max 0 inf])

```

```

160
161 %% CENTRILNE VELOCITY AT MONITORING POINT IN FLUENT
162 % this value is used in fluent to verify convergence of the solution
163 % the transverse coordinate has to be y = 0 (centreline velocity)
164
165 % retrieves the centreline velocity at the location
166
167 if x <= max(x_lvd)
168
169 % defining tolerance for finding float number
170 tolerance = step * 10^-1;
171 % finding first value that meets the condition
172 P = find(abs(x_lvd - x) < tolerance, 1, 'first');
173 u_x = u_lvd(P);
174 % printing the value to the command window
175 disp('VALUE FOR MONITORIG POINT IN FLUENT')
176 disp(['The centreline velocity at the location ', num2str(x),...
177      ' is ', num2str(u_x),'.'])
178 else
179
180 % displaying warning when the requested x-coordinate exceeds
181 % the solution vector
182     disp(['WARNING: Centreline velocity was not calculated for ', ...
183          'requested x-coordinate.'])
184     disp(['Please increase the maximum value of "x_lvd_sch" variable',...
185          ' - line 24.'])
186
187 end
188
189 %% COMPARISON WITH NUMERICAL SOLUTION
190
191 % loading data from fluent, skipping first row which contains column
192 % designation
193 answer = questdlg(['Do you want to compare analytical solution',...
194                  ' with your numerical solution?']);
195 % Handle response
196 switch answer
197     case 'Yes'
198         str = 'Y';
199     case 'No'
200         str = 'N';
201     case 'Cancel'
202         str = 'N';
203 end
204
205 if str == 'Y'
206
207     prompt = {sprintf(['Enter fluent data file names. '...
208                      'Do not include file format.\n(DATA FROM FLUENT MUST BE',...
209                      ' EXPORTED IN ASCII FORMAT)\n\n'...
210                      'Centreline velocity']), 'Transverse velocity'};
211     input_dlg_name = 'INPUT VALUES';
212     dims = [1 70];
213     definput = {'xvelocity_fluent', ''};
214     inputdata = inputdlg(prompt, input_dlg_name, dims, definput);
215

```

```

216     centreline = char(inputdata(1,1));
217     transverse = char(inputdata(2,1));
218
219     sz_cent = size(centreline);
220     sz_trans = size(transverse);
221
222     if sz_cent(1,2) < 1
223         fprintf(1, '\n');
224         disp('You did not input the file name for centreline.')
225     else
226         centreline_fluent = dlmread(centreline,',', 1, 0);
227
228 % plotting comparison of numerical and analytical solution
229 % it is necessary to export data from fluent in ASCII format with
230 % comma as the delimiter
231     centreline_fluent_size = size(centreline_fluent);
232     if centreline_fluent_size(1,2) == 4
233         x_fluent = centreline_fluent(:,2)-x_orifice_fluent;
234         u_fluent = centreline_fluent(:,4);
235         figure
236         plot(x_lvd,u_lvd, 'r-.')
237         xlabel('x [m]')
238         ylabel('u [m/s]')
239         title({'BICKLEY JET',...
240             'Centreline velocity vs longitudinal distance.'})
241         grid minor
242         hold on
243         %plot(x_lvd,u_lvd_corrected, 'b--')
244         plot(x_fluent,u_fluent, 'k')
245         legend('Analytical solution', 'Fluent')
246         axis([0 max(x_lvd) 0 u_j * 1.1])
247     else
248         fprintf(1, '\n'); % just to leave an empty line
249         disp('WARNING: SOLUTION DATA HAS TO BE EXPORTED IN',...
250             ' ASCII FORMAT')
251         disp(['File -> Export -> Solution -> File type:',...
252             ' ASCII -> Delimiter: Comma -> Quantities: Axial',...
253             ' Velocity -> Surface: Axis/Symmetry'])
254     end
255 end
256 if sz_trans(1,2) < 1
257     fprintf(1, '\n');
258     disp('You did not input data file for transverse.')
259 else
260     transverse_fluent = dlmread(transverse,',', 1, 0);
261
262 % transverse velocity profile
263
264     transverse_fluent_size = size(transverse_fluent);
265     if transverse_fluent_size(1,2) == 4
266         y_fluent = transverse_fluent(:,3);
267         y_fluent1 = -y_fluent;
268         u_profile_fluent = transverse_fluent(:,4);
269
270         figure
271         % plot(u_uprofil_corrected,y_uprofil, 'b--')

```

```

272     xlabel('x [m]')
273     ylabel('u [m/s]')
274     title({'BICKLEY JET',...
275           'Longitudinal velocity profile.'})
276     grid minor
277     hold on
278     plot(u_uprofil,y_uprofil, 'r-.')
279     plot(u_profile_fluent,y_fluent, 'k')
280     plot(u_profile_fluent,y_fluent1, 'k')
281     legend('Analytical solution with first-order correction',...
282           'Analytical solution without correction','Fluent')
283     axis([0 max(u_uprofil)*1.05 -y_loc y_loc])
284 else
285     fprintf(1, '\n'); % just to leave an empty line
286     disp('WARNING: SOLUTION DATA HAS TO BE EXPORTED IN',...
287         ' ASCII FORMAT')
288     disp(['File -> Export -> Solution -> File type:',...
289         ' ASCII -> Delimiter: Comma -> Quantities: Axial',...
290         ' Velocity -> Surface: Axis/Symmetry'])
291     end
292 end
293 else
294     return
295 end

```

**Code A.1:** Analytical solution of Bickley jet.

## B. Schlichting jet MATLAB code

This MATLAB code includes also first-order correction based on observations of Andrade [1] and it has been used as a benchmark for the numerical solution.

```
1  %%%%%%%%%%%%%%%%%%%%%%%%%%%%%%%%%%%%%%%%%%%%%%%%%%%%%%%%%%%%%%%%%%%%%%%%%%
2  %%%%%%%%%%          ANALYTICAL SOLUTION OF SCHLICHTING JET          %%%%%%%%%%
3  %%%%%%%%%%          JIRI DOLINSKY          %%%%%%%%%%
4  %%%%%%%%%%%%%%%%%%%%%%%%%%%%%%%%%%%%%%%%%%%%%%%%%%%%%%%%%%%%%%%%%%%%%%%%%%
5
6  % This solution is based on the analytical solution firstly introduced
7  % by Herman Schlichting in 1933.
8
9  clc, clear all, close all
10
11 %% INPUT DATA
12
13 prompt = {'Fluid density [kg/m^3]', 'Nozzle diameter [m]', ...
14          'Dynamic viscosity [kg/(ms)]', 'Velocity at the inlet [m/s]', ...
15          'Location in which axial velocity profile will be determined [m]', ...
16          'Define the x-coordinate of monitoring point for Fluent', ...
17          'x-coordinate of inlet in Fluent (must be defined for comparison)'};
18 input_dlg_name = 'INPUT VALUES';
19 dims = [1 70];
20 definput = {'1.225', '0.004', '1.7894e-05', '0.5', '0.3', '0.3', '0.05'};
21 inputdata = inputdlg(prompt, input_dlg_name, dims, definput);
22
23 size_inputdata = size(inputdata);
24 if size_inputdata == 0
25     return
26 end
27
28 rho = str2double(inputdata(1));           % fluid density [kg/m^3]
29 d = str2double(inputdata(2));           % nozzle diameter [m]
30 mu = str2double(inputdata(3));         % dynamic viscosity [kg/(ms)]
31 u_j = str2double(inputdata(4));       % velocity at the inlet [m/s]
32 % location in which the axial velocity profile is determined [m]
33 x_uprofil_sch = str2double(inputdata(5));
34 % define the x-coordinate of monitoring point [m]
35 x = str2double(inputdata(6));
36 % define the inlet position in fluent
37 x_orifice_fluent = str2double(inputdata(7));
38
39 nu = mu/rho;                           % kinematic viscosity [m^2/s]
40 a = d/2;                               % half of the nozzle diameter [m]
41 Re = u_j*2*a/nu;                       % Reynolds number [-]
42
43 %% LONGITUDINAL VELOCITY DISTRIBUTION
44
45 % Centreline definition
46 step = 0.001;
47 x_max = 3 * Re * a;
```

```

48 y_lvd_sch = 0;
49
50 answer = questdlg(sprintf(['Maximum value for x is set by default',...
51     ' as 3 * Re * a.\n Do you want to change this value?']));
52 % Handle response
53 switch answer
54     case 'Yes'
55         str_x_value = 'Y';
56     case 'No'
57         str_x_value = 'N';
58     case 'Cancel'
59         str_x_value = 'C';
60 end
61
62 if str_x_value == 'N'
63     x_lvd_sch = 0 : step : round(x_max,2);
64 elseif str_x_value == 'Y'
65     user_defined_xmax = inputdlg('Define your new x max.',...
66         'Fluent data file', [1 50]);
67     sz_user_defined_xmax = size(user_defined_xmax);
68     if sz_user_defined_xmax(1) == 0
69         return
70     elseif isnan(str2double(user_defined_xmax{1}))
71         disp('INTERRUPTED: x max not defined')
72         return
73     else
74         x_max = str2double(user_defined_xmax(1));
75         x_lvd_sch = 0 : step : round(x_max,2);
76     end
77 else
78     return
79 end
80
81 %% CALCULATION
82
83 % Momentum of plug velocity profile
84 M = pi * rho * u_j^2 * a^2;
85
86 % Constant of integration
87 gamma_sch = sqrt((3 * M) / (16 * pi * rho * nu^2));
88
89 % Calculation of similarity
90 xi_lvd_sch = sqrt(3 / (16 * pi)) * (sqrt(M / rho) / nu) .* (y_lvd_sch ...
91     ./ x_lvd_sch);
92
93 % Calculation of longitudinal velocity
94
95 u_lvd_sch = (3 / (8 * pi)) * ((M / rho) ./ (nu .* x_lvd_sch)) .* (1 ...
96     ./ (1 + (0.25 .* xi_lvd_sch.^2)).^2);
97
98 % First-order correction (virtual orifice)
99
100 % Determination of virtual orifice
101 x0 = (9/(40*pi*nu))*pi*(d^2/4)*u_j;
102
103 % Calculation of similarity variable and longitudinal velocity

```

```

104
105 xi_lvd_sch_corrected = sqrt(3 / (16 * pi)) * (sqrt(M / rho) / nu)...
106     .* (y_lvd_sch ./ (x_lvd_sch + x0));
107
108 u_lvd_sch_corrected = (3 / (8 * pi)) * ((M / rho) ./ (nu .*...
109     (x_lvd_sch + x0))) .* (1 ./ (1 + (0.25 .* xi_lvd_sch.^2)).^2);
110
111 %% NOTE
112
113 % Calculation of transverse velocity
114 % v = 0.25 * sqrt(3 / pi) .* (sqrt(M / rho) ./ x) .* ((xi - 0.25...
115 % .* xi.^3) ./ (1 + 0.25 .* xi.^2).^2)
116
117 % Corrected
118 % v = 0.25 * sqrt(3 / pi) .* (sqrt(M / rho) ./ (x - x0)) .* ((xi - 0.25...
119 % .* xi.^3) ./ (1 + 0.25 .* xi.^2).^2)
120
121 %% AXIAL VELOCITY PROFILE AT DISTANCE X
122
123 u_uprofil_sch = 1;
124 y_loc = 0;
125
126 while u_uprofil_sch > 0.001
127
128     xi_uprofil_sch = sqrt(3 / (16 * pi)) * (sqrt(M / rho) / nu)...
129         .* (y_loc / x_uprofil_sch);
130
131     u_uprofil_sch = (3 / (8 * pi)) * ((M / rho) ./ (nu .*...
132         x_uprofil_sch)) .* (1 ./ (1 + (0.25 .* xi_uprofil_sch.^2)).^2);
133
134     y_loc = y_loc + 0.001;
135
136 end
137
138 y_uprofil_sch = linspace(-y_loc,y_loc,1000);
139
140 xi_uprofil_sch = sqrt(3 / (16 * pi)) * (sqrt(M / rho) / nu)...
141     .* (y_uprofil_sch / x_uprofil_sch);
142
143 u_uprofil_sch = (3 / (8 * pi)) * ((M / rho) ./ (nu .* x_uprofil_sch))...
144     .* (1 ./ (1 + (0.25 .* xi_uprofil_sch.^2)).^2);
145
146 % First-order correction (virtual orifice)
147
148 xi_uprofil_sch_corrected = sqrt(3 / (16 * pi)) * (sqrt(M / rho) / nu)...
149     .* (y_uprofil_sch / (x_uprofil_sch + x0));
150
151 u_uprofil_sch_corrected = (3 / (8 * pi)) * ((M / rho) ./ (nu .*...
152     (x_uprofil_sch + x0))) .* (1 ./ (1 + (0.25 .* xi_uprofil_sch.^2))...
153     .^2);
154
155 %% VOLUME FLOW RATE
156
157 Q_sch = 8 * pi * nu .* x_lvd_sch;
158 Q_sch_corrected = 8 * pi * nu .* (x_lvd_sch + x0);
159

```

```

160 %% PLOT
161
162 % plot centreline velocity
163 figure
164 plot(x_lvd_sch,u_lvd_sch)
165 hold on
166 plot(x_lvd_sch,u_lvd_sch_corrected)
167 xlabel('x [m]')
168 ylabel('u [m/s]')
169 title({'SCHLICHTING (ROUND) JET';...
170       'Centreline velocity on longitudinal distance.'})
171 grid minor
172 legend('Without correction', 'First-order correction')
173 axis([0 max(x_lvd_sch) 0 1.1*u_j])
174
175 % plot axial velocity profil across the jet
176 figure
177 plot(u_uprofil_sch,y_uprofil_sch)
178 hold on
179 plot(u_uprofil_sch_corrected,y_uprofil_sch)
180 xlabel('u [m/s]')
181 ylabel('y [m]')
182 title({'SCHLICHTING (ROUND) JET';...
183       'Transverse velocity profil at distance x.'})
184 grid minor
185 legend('Without correction', 'First-order correction')
186 axis([0 max(u_uprofil_sch)*1.05 -y_loc y_loc])
187
188 % plot volume flow rate
189 figure
190 plot(x_lvd_sch,Q_sch)
191 hold on
192 plot(x_lvd_sch, Q_sch_corrected)
193 xlabel('x [m]')
194 ylabel('Q [m^3/s]')
195 title('Volume flow rate vs longitudinal distance.')
196 legend('Without correction', 'First-order correction')
197 grid minor
198 axis([0 max(x_lvd_sch) 0 inf])
199
200 %% CENTRILNE VELOCITY AT MONITORING POINT IN FLUENT
201 % this value is used in fluent to verify convergence of the solution
202 % the transverse coordinate has to be y = 0 (centreline velocity)
203
204 % retrieves the centreline velocity at the location
205
206 if x <= max(x_lvd_sch)
207
208 % defining tolerance for finding float number
209 tolerance = step * 10^-1;
210 % finding first value that meets the condition
211 P = find(abs(x_lvd_sch - x) < tolerance, 1, 'first');
212 u_x = u_lvd_sch(P);
213 u_x_corrected = u_lvd_sch_corrected(P);
214 % printing the value to the command window
215 disp('VALUE FOR MONITORIG POINT IN FLUENT')

```

```

216 disp(['The centreline velocity at the location ', num2str(x),...
217       ' is ', num2str(u_x),'. The corrected values is ',...
218       num2str(u_x_corrected),'.'])
219 else
220
221 % displaying warning when the requested x-coordinate exceeds
222 % the solution vector
223     disp(['WARNING: Centreline velocity was not calculated for ', ...
224           'requested x-coordinate.'])
225     disp(['Please increase the maximum value of "x_lvd_sch" variable',...
226           ' - line 24.'])
227
228 end
229
230 %% COMPARISON WITH NUMERICAL SOLUTION
231
232 % loading data from fluent, skipping first row which contains column
233 % designation
234 answer = questdlg(['Do you want to compare analytical solution',...
235                   ' with your numerical solution?']);
236 % Handle response
237 switch answer
238     case 'Yes'
239         str = 'Y';
240     case 'No'
241         str = 'N';
242     case 'Cancel'
243         str = 'N';
244 end
245
246 if str == 'Y'
247
248     prompt = {sprintf(['Enter fluent data file names. '...
249                       'Do not include file format.\n(DATA FROM FLUENT MUST BE',...
250                       ' EXPORTED IN ASCII FORMAT)\n \n'...
251                       'Centreline velocity']), 'Transverse velocity'};
252     input_dlg_name = 'INPUT VALUES';
253     dims = [1 70];
254     definput = {'xvelocity_fluent', ''};
255     inputdata = inputdlg(prompt, input_dlg_name, dims, definput);
256
257     centreline = char(inputdata(1,1));
258     transverse = char(inputdata(2,1));
259
260     sz_cent = size(centreline);
261     sz_trans = size(transverse);
262
263     if sz_cent(1,2) < 1
264         fprintf(1, '\n');
265         disp('You did not input the file name for centreline.')
266     else
267         centreline_fluent = dlmread(centreline, ',', 1, 0);
268
269 % plotting comparison of numerical and analytical solution
270 % it is necessary to export data from fluent in ASCII format with
271 % comma as the delimiter

```

```

272
273 % longitudinal velocity development
274     centreline_fluent_size = size(centreline_fluent);
275     if centreline_fluent_size(1,2) == 4
276         x_fluent = centreline_fluent(:,2)-x_orifice_fluent;
277         u_fluent = centreline_fluent(:,4);
278         figure
279         plot(x_lvd_sch,u_lvd_sch_corrected, 'b--')
280         xlabel('x [m]')
281         ylabel('u [m/s]')
282         title({'SCHLICHTING JET',...
283             'Centreline velocity vs longitudinal distance.'})
284         grid minor
285         hold on
286         plot(x_lvd_sch,u_lvd_sch, 'r-.')
287         plot(x_fluent,u_fluent, 'k')
288         legend('Analytical solution with first-order correction',...
289             'Analytical solution without correction','Fluent')
290         axis([0 max(x_lvd_sch) 0 u_j * 1.1])
291     else
292         fprintf(1, '\n'); % just to leave an empty line
293         disp('WARNING: SOLUTION DATA HAS TO BE EXPORTED IN',...
294             ' ASCII FORMAT')
295         disp(['File -> Export -> Solution -> File type:',...
296             ' ASCII -> Delimiter: Comma -> Quantities: Axial',...
297             ' Velocity -> Surface: Axis/Symmetry'])
298     end
299 end
300
301 if sz_trans(1,2) < 1
302     fprintf(1, '\n');
303     disp('You did not input data file for transverse.')
304 else
305     transverse_fluent = dlmread(transverse,',', 1, 0);
306
307 % transverse velocity profile
308
309     transverse_fluent_size = size(transverse_fluent);
310     if transverse_fluent_size(1,2) == 4
311         y_fluent = transverse_fluent(:,3);
312         y_fluent1 = -y_fluent;
313         u_profile_fluent = transverse_fluent(:,4);
314
315         figure
316         plot(u_uprofil_sch_corrected,y_uprofil_sch, 'b--')
317         xlabel('x [m]')
318         ylabel('u [m/s]')
319         title({'SCHLICHTING JET',...
320             'Longitudinal velocity profile.'})
321         grid minor
322         hold on
323         plot(u_uprofil_sch,y_uprofil_sch, 'r-.')
324         plot(u_profile_fluent,y_fluent, 'k')
325         plot(u_profile_fluent,y_fluent1, 'k')
326         legend('Analytical solution with first-order correction',...
327             'Analytical solution without correction','Fluent')

```

```

328         axis([0 max(u_uprofil_sch)*1.05 -y_loc y_loc])
329     else
330         fprintf(1, '\n'); % just to leave an empty line
331         disp('WARNING: SOLUTION DATA HAS TO BE EXPORTED IN',...
332             ' ASCII FORMAT')
333         disp(['File -> Export -> Solution -> File type:',...
334             ' ASCII -> Delimiter: Comma -> Quantities: Axial',...
335             ' Velocity -> Surface: Axis/Symmetry'])
336     end
337 end
338 else
339     return
340 end

```

**Code B.1:** Analytical solution of Schlichting jet.

# C. Ansys Fluent settings overview

In this appendix, a brief setting overview of the numerical solution in Ansys Fluent is shown.

## Setup

### Solver

Type: Pressure-based  
Velocity Formulation: Absolute  
2D Space: Axisymmetric  
Time:  
Steady case: Steady  
Unsteady case: Transient

### Models

Multiphase: Off  
Energy: On  
Viscous: Laminar  
Radiation: Off  
Species: Off  
Discrete Phase: Off  
Solidification & Melting: Off  
Acoustics: Off  
Electric Potential: Off

### Material

Density: incompressible-ideal-gas  
Viscosity: 1.7894e-05 kg/(ms)

### Boundary Conditions

Operating Pressure (pascal): 101325

### Reference Values

Density 1.225 kg/m<sup>3</sup>  
Pressure (pascal): 0  
Temperature 288.16 K

## Solution

### Solution Methods

Pressure-Velocity Coupling

Steady case  
Scheme: SIMPLEC  
Skewness Correction: 0  
Gradient: Least Squares Cell Based  
Pressure: Second order  
Momentum: Second Order Upwind

Unsteady case  
Scheme: PISO  
Skewness Correction: 0  
Neighbor Correction: 0  
Skewness-Neighbor Coupling: YES  
Gradient: Least Squares Cell Based  
Pressure: Second order  
Momentum: Second Order Upwind  
Transient Formulation: First Order Implicit

# D. Axial velocity contours

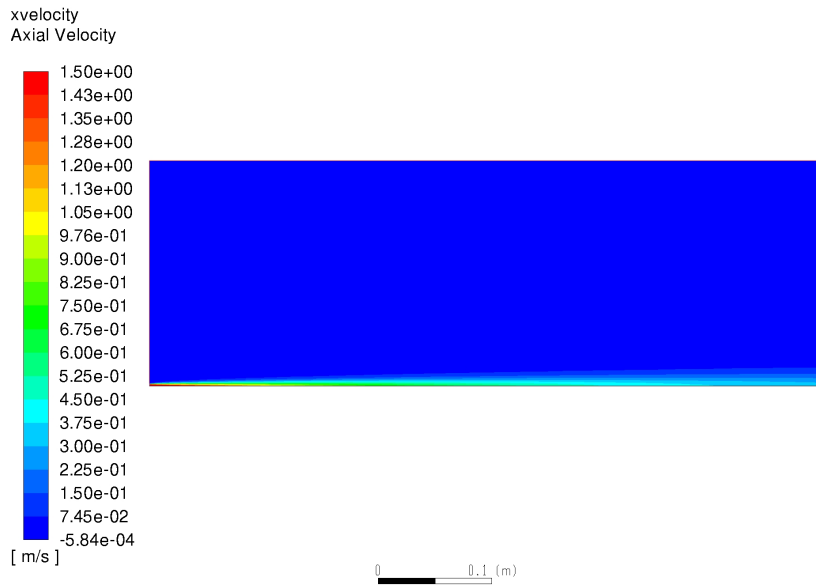


**Figure D.1:** Axial velocity contours for inlet velocity  $u = 1.5$  m/s

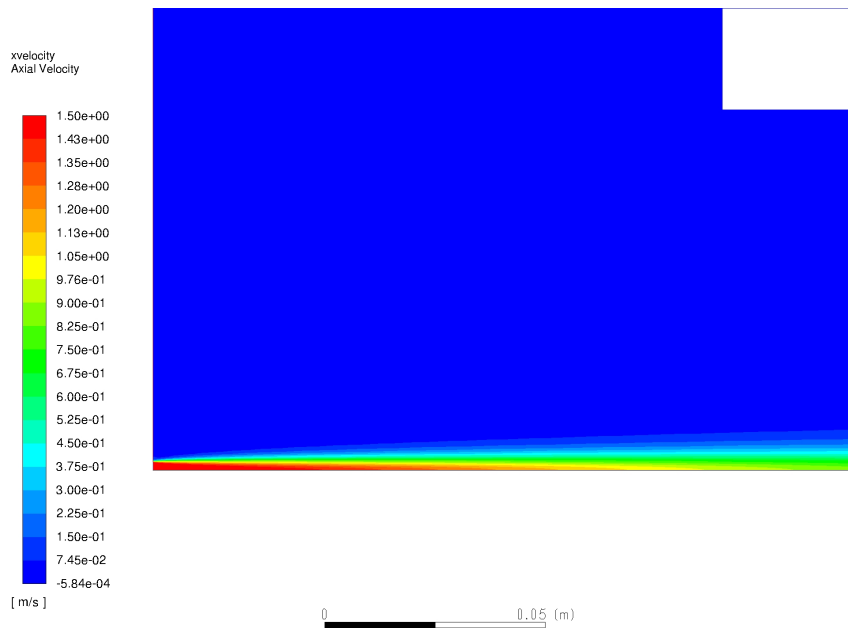


**Figure D.2:** Axial velocity contours for inlet velocity  $u = 1.5$  m/s at near-nozzle region.

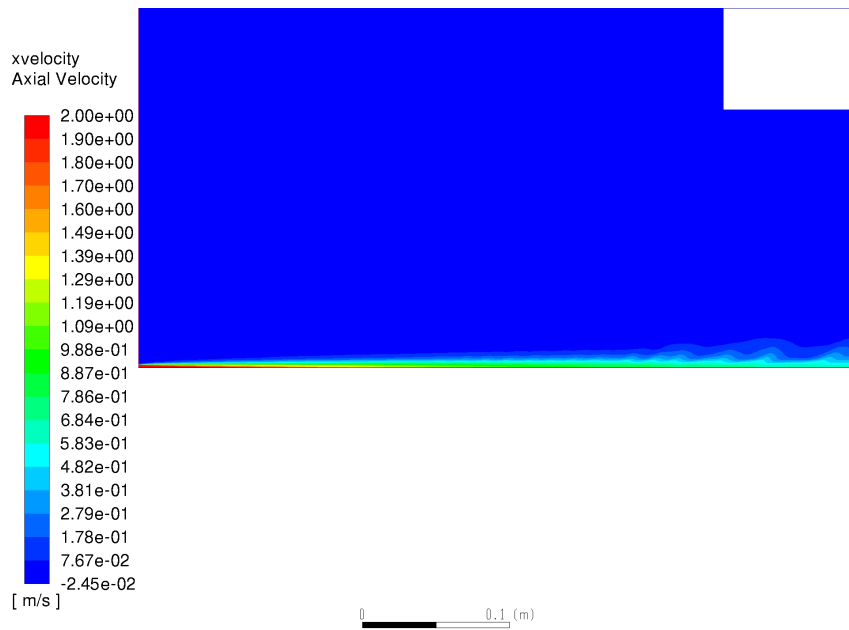


**Figure D.3:** Axial velocity contours for inlet velocity  $u = 2$  m/s.

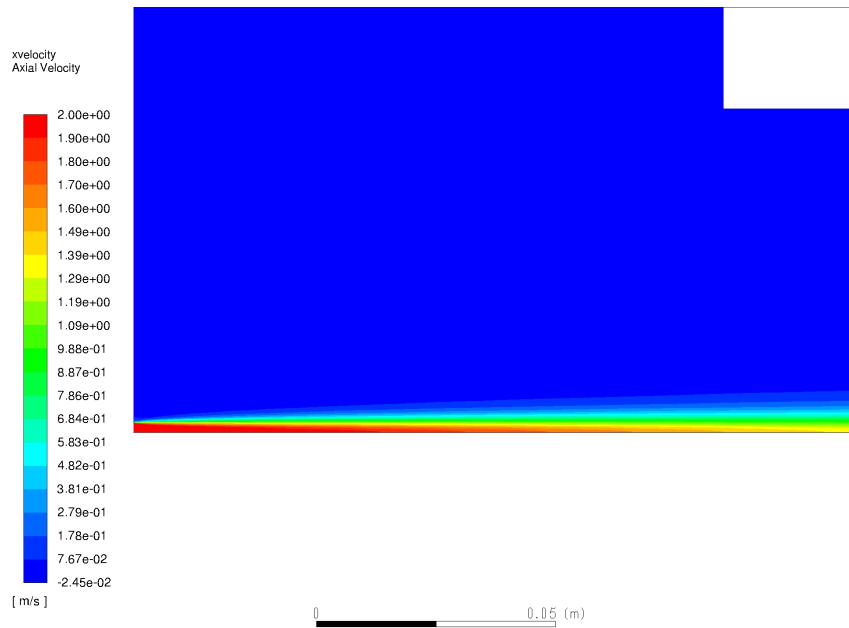


**Figure D.4:** Axial velocity contours for inlet velocity  $u = 2$  m/s at near-nozzle region.